University of Southampton

Faculty of Engineering, Science and Mathematics

School of Electronics and Computer Science

Impact of Dispersion of Interfaces on the Rheology of Polymeric Nanocomposites

by

Toby Matheson

A thesis submitted for the degree of

Master of Philosophy

October 2009

UNIVERSITY OF SOUTHAMPTON

ABSTRACT

FACULTY OF ENGINEERING, SCIENCE AND MATHEMATICS

SCHOOL OF ELECTRONICS AND COMPUTER SCIENCE

Master of Philosophy

IMPACT OF DISPERSION OF INTERPHASES ON THE RHEOLOGY OF POLYMERIC NANOCOMPOSITES

by Toby Nicholas Matheson

This work focuses on the rheological properties of polymeric nanocomposites. A model system based on aqueous surfactant dispersions is explored to define the limitations of a concentric cylinder rheometer and its software. Following on from this, hydropolymeric/silicate clay dispersions are studied to assess if dispersion can be quantified. To this end, a reliable methodology of data processing is described, which incorporates the use of the De Kee equation for a variety of sample compositions. The effects caused by the presence of silicate particulates on the crystallisation properties are studied using optical microscopy techniques.

Electrical characterisation using standard AC breakdown techniques is applied to study the effects rheological dispersion has on an epoxy composites insulation properties. Two types of filler are used; silicates and hydroxides of alumina in the form of montmorillonite and functionalised and unfunctionalised boehmite. Raman spectroscopy is used to identify the surface chemistry of the functionalised boehmite.

Lastly, the Raman technique is employed in developing a methodology to organically modify inorganic particulates in the form of nano sized silicon dioxide. Functionalised silicon dioxide nanocomposites are manufactured using a combination of sonication and rheology to promote dispersion. Samples are then electrically tested using a standard AC electrical break down procedure.

Contents

List of Figures

List of Tables

DECLARATION OF AUTHORSHIP

I, …….,
declare that the thesis entitled

……..……
……

and the work presented in the thesis are both my own, and have been generated by me as the result of my own original research. I confirm that:

- this work was done wholly or mainly while in candidature for a research degree at this University;
- where any part of this thesis has previously been submitted for a degree or any other qualification at this University or any other institution, this has been clearly stated;
- where I have consulted the published work of others, this is always clearly attributed;
- where I have quoted from the work of others, the source is always given. With the exception of such quotations, this thesis is entirely my own work;
- I have acknowledged all main sources of help;
- where the thesis is based on work done by myself jointly with others, I have made clear exactly what was done by others and what I have contributed myself;
- parts of this work have been published as:

T. N. Matheson; A. S. Vaughan, S. J. Sutton, A. Minigher. Electrical Characteristics of Epoxy/Nanoclay Nanodielectric Systems. IEEE, ICSD, 2007, pp 326-329

T. N. Matheson, A. S. Vaughan, A. S. Cooper, J. Minigher. Impact of Sonication on the Electrical Properties of Epoxy-Clay Composites. IEEE, ISEI, 2008, pp 219-222

Signed: ……..
Date:…….

Acknowledgements

I would like to thank the following:

My partner Charmaine for her love, support and strength,

Paul Lewin for his advice and patience,

Mike Smith, Brian Rodgers and Niel Palmer, for their technical support and friendship,

Lastly I would like to thank EPSRC and National Grid for their sponsorship, without which, none of this would have been possible.

List of Abbreviations

AlOOH (boehmite)	Aluminium oxide hydroxide
APES	Aliphatic polyester
ASTM	American society for testing and materials
CEC	Cation exchange capacity
CMC	Critical micelle concentration
CNT	Carbon nanotube
D. E. R.	Dow epoxy resin
DGEBA	Diglycidyl ether of bisphenol A
DM	Direct mixing
DMA	Dynamic mechanical analysis
DSC	Differential scanning calorimetry
EVA	Ethylene(vinyl acetate)
FT-IR	Fourier transform infrared
GIS	Gas insulated switch gear
HDT	Heat distortion temperature
HRR	Heat release rate
i-PP	Isotactic polypropylene
IUPAC	International union of pure and applied chemistry

KD	Krieger-Dougherty
LL	Liquid-liquid
MMT	Montmorillonite
N6	Nylon-6
NaOA	Sodium olate
ODA	Octadecylamine
OMLS	Organically modified layered silicate
o-PCL	Oligo (ε-caprolactone)
PCL	Poly(ε-caprolactone)
PDMS	Polydimethylsiloxane
PE	Polyethylene
PEO	Poly(ethylene oxide)
PLA	Polylactide
PLACN	Polylactide clay nanocomposite
PMMA	Poly(methyl methacrylate)
PP	Polypropylene
PPO	Poly(propylene oxide)
PS	Polystyrene
PTHC	P-toluidine hydrochloride
PVA	Poly(vinyl acetate)
QA	Quaternized ammonium

SDS	Dodecyl sulfate
SEM	Scanning electron microscopy
Tg	Glass transition temperature
TGA	Thermogravimetric analysis

CHAPTER 1: - Introduction; Polymers

In its essence, the word polymer means 'many parts' when translated from its Greek origins. For a more scientific definition courtesy of IUPAC (Metanomski 1991)[1].

"*A polymer is a substance composed of molecules characterized by the multiple repetition of one or more species of atoms or groups of atoms (constitutional repeating units) linked to each other in amounts sufficient to provide a set of properties that do not vary markedly with the addition of one or a few of the constitutional repeating units*."

The 'repeating units' are linked together by covalent bonds – as are the atoms that make up these units. The repeating units are referred to as monomers, which in the case of the industrially important polymer that is polypropylene is propylene (see Figure 1.1). The process by which a monomer is converted into a polymer is known as polymerization.

A homopolymer is a polymer made up from a single type of monomer, where a copolymer is made up from two different monomers.

Unorientated amorphous polymers are isotropic and polymer crystals are highly

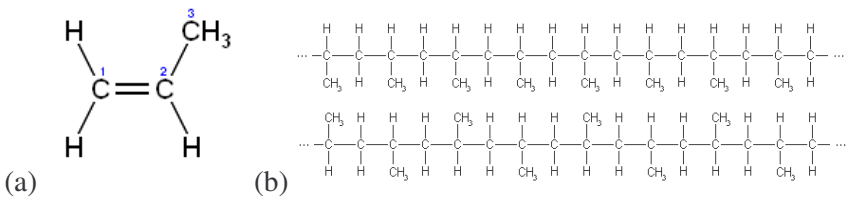

Figure 1.1: Chemical structure of (a) a propylene monomer and (b) its polymer (polypropylene)

anisotropic. The anisotropy originates from the variation in bonds between the monomers that make up the polymer in a single chain (strong - covalent) and the bonds between adjacent chains (weak - Van der Waals).

Polymers can exist in three phases, liquid crystal, crystalline and amorphous. Semi-crystalline polymers consist of a combination of crystalline and amorphous phases. The crystalline lamellae and amorphous interlamellar layers that make up its morphology can form spherical aggregates known as spherulites, which are formed when a polymer is crystallized from the melt. Light scattering from a non-absorbing medium is primarily associated with the changes in local refractive index that are associated with phase boundaries or particular structural features, when these have dimensions that are comparable to the wavelength of light[2]. In semi-crystalline polymers, spherulitic development is therefore particularly important and, for this reason, increases in optical clarity are often associated with enhanced nucleation and a corresponding reduction in spherulite size[3].

1.1 Polymer Matrices

Thermoplastics. A thermoplastic is a polymer that becomes either a liquid above or a solid below its glass transition temperature (Tg). Most thermoplastics are high molecular weight polymers whose chains associate through weak Van der Waals forces (polyethylene); stronger dipole-dipole interactions and hydrogen bonds (nylon); or even stacking of aromatic rings (polystyrene). Thermoplastic polymers differ from thermosetting (epoxy) as they can be re-melted and re-molded[4].

Thermosetting resins. The most commonly used resins are epoxy, unsaturated polyester and vinyl ester. In thermosetting polymers, the liquid resin is converted into a hard rigid solid by chemical cross-linking, which leads to the formation of a tightly bound three-dimensional network. The mechanical properties depend on the molecular units making up the network and on the length and density of the cross links. The length and density of the cross-links is controlled during the curing process. Curing can be achieved at room temperature, or by following a cure schedule that involves

heating at one or more temperatures for predetermined times for optimal cross-linking and hence optimum properties. The main distinction between if a polymer is a thermoset or thermoplastic is based on their response to temperature. A thermoplastic behaves like a liquid above a certain temperature, whereas the heating of a thermoset leads to its degradation without it going through the fluid state.

Epoxy resin is one of the most important thermosetting polymers used in electrical insulation today. Its use as an insulator extends to the encapsulation of integrated circuits and for the fabrication of printed circuit boards[5]. Epoxy resin also has a good balance mechanical properties allowing it to also find application in environments such as dry type transformers, coil insulators within rotating machines[6] and as spacers within gas insulating switchgear (GIS)[7]. Epoxy resins add further advantages in its low cost and ease of processing.

1.2 Composites

A composite is a product made with a minimum of two materials – one being a solid material (often in elongated form) and the other being a binding material (or matrix). For example, wood is made up of fibrous chains of cellulose molecules in a matrix of lignin, while bone and teeth are essentially composed of hard inorganic crystals in a matrix of a tough organic constituent called collagen[4]. Composites of these sorts feature anisotropy e.g. their properties vary significantly when measured in different directions. This feature is a consequence of the harder constituent being in a fibrous form, with the fibre axis preferentially aligned in particular directions, or because one or more of the constituents have inherent anisotropy as a result of their crystal structure. In natural materials, such anisotropy of mechanical properties is often exploited within the structure. For example, wood is much stronger in the direction of the fibre tracheids, which are usually aligned parallel to the axis of the trunk or branch, than it is in the transverse direction. This is an important property of the tree considering it has to sustain high stresses along its length, due to its weight, and wind which is effectively loading it like a cantilevered beam[4].

Composite materials combine the properties of two or more components that are carefully selected to maximize mechanical performances like hardness, toughness, stiffness, strength and damage tolerance. Material classes used in composites include metals, ceramics, glasses, elastomers and polymers. Most composites in industrial use are based on polymeric matrices; thermosets and thermoplastics. These are usually reinforced with aligned fibres, such as glass or carbon. They commonly exhibit marked anisotropy, since the matrix is much weaker and less stiff than the fibres. The most common example of a composite is fibreglass, in which glass fibres are mixed with a polymeric resin.

1.3 Surface Modifications

Polymer composites are two-phase materials usually made by combining a low-density polymeric matrix with a high-modulus filler/reinforcement. Although each of the main phases maintains its identity in the composite, the final properties achieved by this combination cannot be obtained by the components acting alone. This improved performance depends, to a large extent, on the interactions generated between the two main components, that is, the adhesion between the polymer matrix and the filler, and therefore on the nature of the interface/interphase developed. Interface is defined as the surface boundary between matrix and reinforcement, which maintains the bond between the two components. Although it is common to believe an interface to be of negligible thickness, when looking at the process at a molecular level, the thickness of the interfacial region is significant and definitely non-zero. The term interphase includes the interface concept, but it is also the region (volume) altered during the consolidation process, with properties that can vary progressively or stepwise from those of the filler to those corresponding to the bulk matrix.

The reduction in the size domains of the filler component leads to what are known as micro composites and nano composites. These smaller size domains of the phases enhance the contribution of the interfacial region to the overall composite behaviour. The overall behaviour of the composites depend on the filler characteristics, such as geometry, size, orientation, and volume fraction, and on the matrix characteristics, e.g.

degree of polymerization, crystallinity, or cross-linking density. However, the mechanical and fracture behaviours are also strongly affected by the strength of the bond between the matrix and the filler, which is responsible for the stress transfer across the interface. Concentrations of stresses around the filler also occur because of the different thermal expansion coeffecients of the two main phases of the material – which is likely to be encountered when one is dealing with a polymer from the melt or epoxy resin systems that are being cured at high temperatures. This complex situation generated by the presence of fillers can generate voids or micro-cracks in the material that will act as points where failure of the material can initiate.

Thermodynamic wetting of the fillers by the matrix during the mixing stages of composite production is a necessary condition to achieve matrix-filler adhesion; it is determined by the surface energies of these two components. The spreading of a liquid over a solid depends on the components of the interfacial tensions acting parallel to the solid surface at the line of contact. The triple interface (matrix, filler, air) will move in a direction until thermodynamic equilibrium is reached. If such a position is not possible, the matrix spreads completely over the filler interface. 'Good' wetting of the filler by the matrix takes place if the matrix phase has a surface free energy lower than that of the reinforcement. Thus, an epoxy resin, with a surface tension of 39 mJ/m^2 wets a sized carbon fibre or a glass fibre with surface energies of 40-60 mJ/m^2. When this condition is fulfilled, the liquid matrix flows over the filler, following every imperfection of its surface, and displaces any trapped air, thus reducing the number of points where fracture can be initiated.

The chief factor affecting the surface tension of a pure liquid is the temperature. Experimentally it is found that the surface tension of a pure liquid decreases nearly linearly with temperature[8]. Therefore, upon mechanical mixing, elevated temperatures can assure wetting of the fillers within a polymer matrix.

The effect of wetting on [9,10,11,12] the final properties of the composites has been the subject of many publications Increased surface energies of the filler have been seen to give increases in tensile modulus[12] and interlaminar shear strength.

Besides wetting, a necessary but not sufficient condition for the formation of a strong interface, is the adhesion of the matrix to the fibre. Adhesion conditions the bond of the two main phases (matrix and reinforcement), so that stresses can be transmitted between them. The nature of the bond can differ from system to system, and the mechanisms of adhesion that can be active in a given composite interface are

1) Mechanical adhesion, which can occur through mechanical interlocking between two given surfaces.
2) Electrostatic bonding, which includes ionic, acidbase, and hydrogen bonding, dipole-dipole and polar interactions, and van der Waals forces. The strength of the bonds generated by these mechanisms varies considerably from very weak (Van der Waals forces) to very strong (hydrogen, ionic, or acid-base bonds).
3) Chemical bonding, which exists when there are covalent bonds between specific chemical groups on the surface of the fibres and reactive groups in the matrix.
4) Interdiffusion, where the bond is formed by entangled molecules attached to two different surfaces or belonging to two different phases. The bond strength depends on the amount of molecular entanglements.

The dispersion of a filler in a liquid polymer is a process that involves wetting of the particles and their further separation by mechanical shear during mixing, followed by stabilization of that dispersion. The stabilization is necessary to avoid re-aggregation of the filler as aggregates could act as weak points causing material failure. Treated fillers are usually easier to disperse because the adsorbed water that acts as an adhesive in most inorganic fillers is replaced or coated with the modifier (usually an amphilic molecule, such as silane). The improved dispersion can result in lower viscosity of the filled resins than those obtained using the untreated fillers. This effect has been described for a wide range of different materials, from reinforced elastomers to woodflour-filled thermoset resins[13,14]. To summarise, the advantages of surface modifying a filler is three-fold:

1) To avoid re-aggregation of the filler by preventing water molecules from bonding to the fillers surface.
2) To give improved filler-matrix adhesion through chemical bonds

3) To provide a coating to the particulate that has higher surface energies than that of the untreated surface to allow for easier thermodynamic wetting. This third point is not crucial, as surface energy of the polymer can be lowered by heating.

As previously mentioned, a coupling agent is used when surface modifying a particulate. Coupling agents are comprised of an amphilic molecule. The most common form of amphilic molecule encountered in everyday life is that of soap, i.e. a hydrophilic head and a lipophilic tail. These molecules are often called surface active agents or surfactants in that the polar and non polar nature of the molecule can act upon a wide variety of interfaces.

1.4 Dispersion

Dispersion is an important aspect regarding sample production of isodimensional nanocomposite materials. In the context of this work, 'good' dispersion is the process of delaminating or exfoliating aggregates or the breaking apart micron sized filler clusters and spreading them evenly as nanosized particulates in a polymer matrix.

There are various tools used to aid dispersion. Mechanical mixers such as homogenizers and rheometers that rely on a rotating blade or a shear force - as well as more subtle forms such as ultra sonication which relies on acoustic pressure changes to break up the large aggregates.

The advantage of rheology over other forms of mixing is that a physical quantity – the viscosity, is measured. This implies that dispersion could potentially be quantified prior to sample production, whereas the standard techniques for gauging dispersion require microscopic techniques on a finished material.

1.5 Nanocomposites

Nanocomposites are a new class of composites that are particle-filled polymers for which at least one dimension of the dispersed particles is in the nanometre range[15]. There are three variations of nanocomposites that depend upon how many dimensions of the dispersed particle are within the nanometre range. When the three dimensions are in the order of nanometres, we are dealing with isodimensional nanoparticles, such as spherical silica nanoparticles[16,17] and semiconductor nanoclusters[18]. When two dimensions are in the nanometre scale and the third is larger, forming an elongated structure, we have nanotubes e.g. carbon nanotubes[19]. The third type of nanocomposites is characterized by only one dimension in the nanometre range. In this case the filler (the material that is placed into a matrix) is present in the form of sheets a few nanometres in thickness and hundreds to thousands of nanometres in lateral extent[15].

The field of nanocomposites has grown considerably in the last decade. A literature search on nanocomposites will result in a large number of research papers ranging from material production and methodology to chemical surface treatment of nanoparticles to the various physiochemical properties nanocomposites can be tailored for. This is the subject of the next chapter, where a literature review based on nanocomposite physiochemical properties is presented. Papers were chosen from the public domain in such a way that a variety of properties could be reviewed.

1.6 Thesis overview

The second chapter presents a literature view on the subject of nanodielectrics. The areas of research reviewed contain mechanical, thermal, electric, dielectric, rheological, optical, biodegradability and gas permeability. There exists a wealth of literature on each, and this review only skims the surface on each area.

In the third chapter of this thesis, the rheology of a model aqueous surfactant system based on soap and water is studied. This system was chosen as it provides an easy and

accessible route into the chemistry of surfactants that allows firsthand experience in the techniques of rheology, especially in the context of instrumental limitations.

The fourth chapter of this thesis is mainly concerned with experience using rheology as a means of dispersion. This is carried out using a hydropolymer in the form of poly(ethylene oxide) and water and the layered silicate, montmorillonite. The short comings of the data handling of third chapter are addressed and the rheological detection limit of filler loaded matrices discussed.

The fifth chapter utilises the procedures developed from Chapters 3 and 4 in making epoxy based nanocomposites using rheology. The rheological properties of un-modified montmorillonite, un-modified boehmite and surface modified boehmite is reported along with the impact of the interfacial surface chemistry and dispersion on its electrical breakdown characteristics. Raman spectroscopy is demonstrated as a useful tool in identifying the nature of the functionalised boehmite.

The subject of surface chemistry is continued with the sixth chapter. A technique is developed using Raman spectroscopy by which one can surface modify an inorganic filler. To this end, a silane coupling agent is used to modify nano silicon dioxide. The impact of the surface chemistry on its rheological and electrical characteristics is reported. As a reference, the rheology of untreated micro and nano silicon dioxide is reported so a means of comparison between surface chemistry and size can be made.

The research presented in this thesis is concluded in chapter seven. This section summarises the work carried out and the contributions made to production and characterisation of polymeric nanocomposites.

CHAPTER 2: Nanocomposites; a review

In 1993, the Toyota research group in Japan successfully synthesized organoclay/polyamide 6 nanocomposites[20] that showed great improvement in the mechanical properties and thermal stability when only 4% wt clay was introduced into the polymer matrix[21]. Since then, many researchers have applied the use of organoclays to a variety of polymer matrixs including epoxy, polypropylene, polystyrene, polyimide, polyurethane and dendritic polymers. Due to the nanometre sized particles obtained by dispersion, these nanocomposites can exhibit vastly improved mechanical, thermal, optical and physico chemical properties when compared with the pure polymer or conventional (microscale) composites, as firstly demonstrated by Kojima and coworkers[21] for nylon-clay nanocomposites. Improvements can include increased moduli, strength and heat resistance, decreased gas permeability and flammability.

2.1 Mechanical Properties

Dynamic mechanical analysis (DMA) measures the response of a given material to an oscillatory deformation as a function of temperature. DMA results consist of three vital parameters.

1) The storage modulus (*G'*)
2) The loss modulus (*G''*)
3) The ratio of *G''*/*G'*, tan δ

These parameters can be used for measuring the occurrence of molecular mobility transitions, such as glass transition temperature Tg [22].

Roh and Lee studied the temperature dependence of storage modulus upon the formation of an intercalated polystyrene (PS)/montmorillonite (MMT) nanocomposite[23]. No Significant difference was seen in the storage modulus over the investigated temperature range (40 °C–130 °C) which gives the indication that

intercalated nanocomposites do not strongly affect the elastic properties of the matrix. However there was a shift in the tan δ peak towards higher temperatures for the nanocomposite, which gives an indication of superior Tg properties together with some broadening of this transition. This behaviour has been attributed to restricted segmental motions at the filler/matrix interface regions of intercalated compositions.

DMA has been used to study the temperature dependence of the storage modulus of poly (methyl methacrylate) (PMMA)/lipopilized smectite clay nanocomposites polymerized with various comonomers[24]. Comparisons were made between PMMA, PMMA copolymer blend, PMMA/clay copolymer blend which had been organically modified with quaternized ammonium salt (QA+).and the PMMA/QA+ copolymer blend which has an absence of the clay. No temperature dependence was seen in the tan δ and storage modulus for the blends with and without the clay (PMMA/clay and PMMA/QA+). Upon the addition of the monomers to the neat PMMA a strong increment in the storage modulus was seen was seen to develop at all temperatures as the copolymer matrix forms. This indicates that the copolymer has a strong influence on the elastic properties of the matrices. The tan δ peaks for the nanocomposites were seen to shift to lower temperatures than for the corresponding clay-free blends.

Polypropylene-clay-nanocomposites (PPNCs) and corresponding polypropylene maleic anhydride (PP-MA) have been investigated by DMA[25]. The filler loadings used were 2%, 4% and 7.5%. For all of the PPNCs there was a strong enhancement of the moduli over the investigated temperature range, which indicates the plastic and elastic responses of PP towards deformation are strongly influenced in the presence of organically modified layered silicates (OMLS).

The dynamic mechanical properties of PP and PPNCs with dispersed epoxypropyl methacrylate (EM) intercalated MMT have been seen to shown to yield significant increases in stiffness and a decrease in tan δ [26]. The nanocomposites also displayed improved thermal-mechanical properties that were shown by the behaviour of the improved storage modulus at high temperatures. The Tg values of PPCNs was not seen to decrease further after a filler loading of 3%.

The significant improvement in storage modulus which is related to the dimensions of the OMLS has been further demonstrated in polylactide clay nanocomposites (PLACN)[27]. In order to understand the impact the compatibilizers had on the mechanical properties, the authors also prepared PLACNs with small quantities of oligo (ε-caprolactone) (*o*-PCL). For all of the PLACNs the storage modulus was seen to be enhanced across the temperature range, indicating that the organically modified MMT had a strong effect on the elastic properties of neat PLA. Below the Tg, the enhanced storage modulus is clear, however, above the Tg one sees a greater increase in storage modulus with respect to the pure PLA, even though it has decreased relative to values below the Tg. This has been attributed to mechanical reinforcement by the clay particles and extended intercalation at high temperatures[28]. Above Tg, when the material becomes soft, the reinforcement effect of the clay particles becomes prominent due to the restrictive movement of the polymer chains, which is characterised by the increase in storage modulus relative to the pure PLA.

DMA has been used to measure the mechanical properties of epoxy/clay nanocomposites[29]. Compared to the pure epoxy resin system, the storage moduli of the nanocomposites only slightly increased. The glass transition temperature, of the epoxy/clay nanocomposite system, which can be determined by taking the temperature of the most drastic decrease in the storage modulus, increased with increasing clay content. This increase in Tg was attributed to the dispersive nature of the clays hindering the mobility of molecular chains and network junctions.

The fracture behaviour of epoxy filled nano and micro sized aluminium composites have been studied by Zunjarrao and Singh[30]. The diameters for the nano and micro particles were 20-100 nm and 3-4.5 μm respectively. Results for fracture tests were recorded by measuring the length of a crack caused by their 'specially designed crack tap' and were only considered valid if they satisfied the ASTM 5045 standard. Results were taken for the pure epoxy, untreated and treated aluminium micro/nano composites with a particle volume fraction of 2%. It was observed that fracture toughness of untreated nanocomposites was larger than its microcomposite counterpart. This was further enhanced upon silane treatment; however, the improvement for fracture initiation toughness was greater for the micro composites

than for the nanocomposites. The fracture surfaces of the nanocomposites showed a higher degree of surface roughness than for microcomposites, which when quantified, gave results that correlated with 'work of fracture' observations. Overall, it was observed that the addition of aluminium particles toughened the epoxy especially for the treated systems where bonding between filler and matrix was promoted. Unfortunately, the fracture toughness was not optimised for some of the treated systems, as agglomeration of the aluminium was evident for the particles that were treated purely during sample processing. A second method of coating was also utilised which seemed to address the issue of agglomeration, this involved modifying the particles prior to being added to the resin.

The storage moduli of epoxy/nano-(untreated) silica composites has been found to be higher than that of pure epoxy resin[31]. The increased modulus was justified as a reinforcement effect and was seen to increase with filler loading- 1%, 2%, 3%. However, after 3%, a decrease was reported, which was attributed to aggregation.

Nigam et al. studied the mechanical properties of epoxy-montmorillonite nanocomposites[32]. This study included samples filled with 0, 1.5, 3, 4.5 and 6% loadings of inorganic and organic MMT samples. Tensile strength modulus was measured for organo samples where an increase in clay content from 0% to 6% filled epoxy yielded a 100% increase in tensile modulus, 20% increase in ultimate tensile strength, and 80% decrease in elongation at break values. It was seen that organoclay composites yield superior mechanical properties than that of inorganic clay composites up to 6%, beyond which agglomeration of the fillers causes a severe weakening.

2.2 Heat Distortion

Heat distortion temperature (HDT) of a polymeric material is an index of heat resistance towards applied load. It is usual for HDT measurements to be reported as a function of clay content, characterised by the procedure in ASTM-D648. Kojima et al.[21] first showed that the HDT of pure nylon-6 (N6) increases up to 90 °C after nanocomposite preparation with OMLS. In their further work[33] they reported the clay

content dependence of HDT of N6/MMT nanocomposites. In N6/MMT nanocomposites there is a marked increase in HDT from 65 °C for the neat N6 to 152 °C for 4.7% wt nanocomposite. Beyond that weight of MMT, the HDT levels off. They also conducted HDT on various N6 nanocomposites prepared with varying lengths of clay and found that the HDT also depends on the aspect ratio of dispersed clay particles. The HDT of N6 nanocomposites is due to the presence of strong hydrogen bonds between the matrix and silicate surface.

The nanodispersion of octdecyltrimethylammonium modified MMT in neat PLA also promotes a higher HDT[34]. Ray et al. examined the HDT of PLA and various PLACNs at different load conditions. There was seen to be a marked increase in intermediate load of 0.98 MPa, from 76 °C for neat PLA to 93 °C with the addition of 4% MMT. This value was seen to increase with clay content up until their final loading of 7%, which yielded a HDT of 111 °C.

2.3 Thermal Stability

The thermal stability of polymeric materials is usually studied by thermogravimetric analysis (TGA). The weight loss due to the formation of volatile products after degradation at high temperature is monitored as a function of temperature. When the heating occurs under an inert gas flow, a non-oxidative degradation occurs, while the use of air or oxygen allows oxidative degradation of the samples. The incorporation of clay into the polymer matrix has generally been found to enhance the thermal stability by acting as a superior insulator and mass transport barrier to the volatile products generated during decomposition.

The improved thermal stability of a polymer clay nanocomposite that combined PMMA and MMT clay was first reported by Blumstein in 1965[35] . He reported that PMMA inserted between the lamellae of MMT resisted thermal degradation under conditions that would otherwise completely degrade pure PMMA. X-ray analysis showed an increase of 0.76 nm of the basal spacing. Thermogravimetric analysis (TGA) showed that both PMMA and cross linked PMMA intercalated into Na MMT

have a 40 °C to 50 °C higher decomposition temperature (as measured at a point of 50% mass loss). These nanocomposites had been prepared by free radical polymerization of methyl methacrylate (MMA) intercalated in the clay. Blumstein found that after polymerization in the clay had taken place, the PMMA upon extraction showed superior thermal stability than that of the PMMA made from solution. He hypothesised that this be due to a decrease in the relative number of macromolecules terminated with double bonds for the PMMA polymerized in the confined environment inside the clay lamellae, as compared to the PMMA made in solution. This PMMA was not as stable as when intercalated in the nanocomposite which led to his conclusion that the stability of the PMMA nanocomposite is due not only to its different structure, but also due to restricted thermal motion of the PMMA in the spacing between the lamella layers.

Burnside and Giannelis in 1995 studied the thermal stability of polydimethylsiloxane (PDMS) clay nanocomposite[36]. Their results showed similar findings to that of Blumstein[35], however, instead of in-situ polymerization, they sonicated ion exchanged MMT in a silanol terminated PDMS that had been cross linked into an elastomer. The nanocomposite had featureless X-ray patterns indicating a disordered delaminated nanostructure. The nanocomposite showed more than a 140 °C higher decomposition temperature that the pure PDMS elastomer (measured at 50% mass loss). Burnside attributed the increased thermal stability to hindered diffusion of volatile decomposition products from the nanocomposite, in view of the improved barrier properties observed for other nanocomposites.

Other reports concerned with the improved thermal stability of OMLS and polymer matrices were written by Zhu et al.[37] They investigated the thermal properties of polystyrene-MMT nanocomposites modified with either phosphonium or ammonium salts. The phosphonium clays exhibited greater thermal stability than the ammonium types. TGA demonstrated that the nanocomposites possessed a greater resistance to thermal degradation with a 50 °C difference between the composite and pure material. Cone calorimetry showed that the rate of heat release was significantly reduced by the formation of the nanocomposite. The fact that there is a difference in TGA between phosponium and ammonium means that the chemical used in surface modifications is

crucial when it comes to the materials performance at high temperatures. This trend has also been shown by Zanetti et al., who showed that fluorohectorite and MMT modified with octadecylammonium cations produces strongly acidic sites[38]. These acidic sites act as a catalyst for deacylation. This, they reasoned, could cause the nanocomposite to thermally degrade at lower temperatures than that of the pure polymer

TGA results of polysulfone dodecylammonium exchanged MMT have been taken at 1%, 3% and 5% loadings by Sur et al.[39] The approximate decomposition temperatures of pure polysulfone, 1% and 5% polysulfone nanocomposite were 494 °C, 498 °C and 513 °C respectively. These were considered significant increases, which were attributed to the exfoliated platelets retarding diffusion of oxygen into the host matrix.

TGA has also been conducted on poly(ε-caprolactone) (PCL)-MMT nanocomposites modified with dimethyl 2-ethylhexyl ammonium[40]. The temperature which saw a 50% weight loss was shifted upwards by 60 °C at 1% filler loading compared to that of pure PCL. Higher loadings resulted in a lower increase, with 10% giving a 30 °C upwards shift.

Epoxy/clay nanocomposites have been thermally studied using TGA[41]. Filler loadings up to 14 phr were investigated, with each sample showed improved thermal stability over that of the neat epoxy. The greatest benefit the organo-clay had on the D.E.R 331 resin was at filler loadings lower than 8 phr. The sample that showed the greatest thermal stability, that is, the lowest rate of weight loss as a function of temperature was at 6 phr.

Sun et al. studied the effect of micro and nano sized fillers on the glass transition temperature of epoxy composites[42]. They used the fillers; silica (nano-100 nm, micro 3 µm), silver (nano-65 nm, micro 1-2 µm), aluminium (nano-100 nm, micro 1-2 µm) and carbon black (30 nm). Silica composites showed no change in their Tg characteristics when loaded with the micro sized filler whereas the nanofiller showed a slight increase in Tg with filler loading of 5% and 10%. After which a rapid linear decrease was recorded for loadings of 20-50%. Similar behaviour was reported for the other composites where samples with nano sized fillers having a lower Tg than their

micro sized counterparts. The reduction of Tg for the composites was reasoned to be due to the increase of surface area of the nano sized fillers influencing chain mobility. The interfacial area of the filler was confirmed to be the contribution to the reduction of Tg using carbon black samples at low filler loadings (<5%). Poorly dispersed carbon black exists as large aggregates made up of many small 1-50 nm primary particles. It was seen that over a period of varying sonication time (0–60 min) a steady decrease in Tg was observed.

TGA was conducted on both micro and nano silica composites up to a temperature of 800 °C. Micro sized silica was stable over the temperature range whereas the nano sized samples underwent weight loss that totalled 8% by 800 °C. The weight loss was attributed to chemically bonded water and residual organics (ethanol or methanol brought about by the sol-gel process during silica synthesis) bonded to the surface of the particles.

Differential Scanning Calorimetry (DSC) was carried out on epoxy/silica composites to investigate whether the presence of the silica hindered the ability of the epoxy to cure. No change was seen in the thermal scans for any of the composites so it was concluded that the filler did not affect the cross linking of the epoxy resin. A more in-depth study of the curing kinetics of epoxy silica composites has been carried out by Zheng et al.[31] where they report lower activation energies needed to initiate the curing reaction due to the presence of –OH groups on the surfaces of the filler. It has been reported that the curing rate of epoxy has been slightly increased with the addition of MMT[29].

Nigam et al.[32] studied the thermal properties of epoxy-MMT nanocomposites. This study included samples filled with 0, 1.5, 3, 4.5 and 6% loadings of inorganic and organic MMT samples. Cure rates were seen to increase with filler loadings of organo samples. TGA for samples at 6% loadings showed that the organo clay composites were unstable due to it incurring a weight loss of 50% at 440 °C as opposed to 480 °C for its inorgano counterpart. This was attributed to the organic species used to modify the clay; octyldecalammonium ions.

2.4 Flame Retardant

The Cone Calorimeter is the most effective method for studying the fire retardant properties of polymeric materials. It can gather data regarding the ignition time, mass loss, combustion products, heat release rate (HRR) and other parameters associated with its burning properties. Fire relevant properties such as HRR, heat peak, smoke production and CO_2 yield are vital parameters to be measured when testing the fire safety of materials.

Gilman has utilised the Cone Calorimeter for studying the flammability properties of nanocomposites[43]. In a review paper, Gilman gives an overview of the work that he and his co-workers among others have done in researching the flammability properties of nanocomposites[44]. The nanocomposites that Gilman et al. manufactured consisted of delaminated nylon-6 and nylon-12 nanocomposites and intercalated PS and PP clay nanocomposites. What was seen was that the HRR was reduced significantly (50%-75%) for intercalated and delaminated nanocomposites with low silicate mass fraction (2%-5%). Similar results were shown for thermoset polymer nanocomposites made from vinyl esters and epoxies. According to the authors, the MMT must be nanodispersed for it to affect the flammability of the nanocomposites. However, the clay need not be completely delaminated. In general, the nanocomposites flame retardant mechanism involves a high performance carbonaceous silicate char, which builds up on the surface during burning. This insulates the underlying material and slows the mass loss rate of decomposition products.

Zhu has investigated the HRR of polystyerene-MMT nanocomposites, which were modified using three different surfactants[37]. These consisted of two varieties of ammonium salts and one phosphonium salt. They initially used phosphonium salt for the modification of clay and then examined the differences of organo ammonium and phosphonium salt treatments of clay fillers in nanocomposites towards thermal stability. A 50% reduction in HRR was seen for all three nanocomposites at 3% loadings. The suggested mechanism by which clay nanocompsoites function involves the formation of a char that serves as a barrier to both mass and energy transport. As the fraction of clay increases so too does the amount of char formed which causes a

decrease in the amount of heat released. It has been suggested that an intercalated material is more effective than an exfoliated material when it comes to fire retardancy. This claim is supported in Zhu's work where the nanocomposite that gives the lowest HRR has a majority of MMT that is intercalated. The decrease in the rate of heat release corresponds to

1) A decrease in mass loss rate and the amount of energy released by the time the polystyrene has ceased burning.

2) A modest increase in the time it takes for the peak heat release to be reached.

The production of a char barrier retains some of the polystyrene which causes the decrease in the energy released/mass loss. It was observed that the formation of the nanocomposites reduces smoke production but presence of additional clay does not continue this smoke reduction.

2.5 Gas Barrier

Composite materials are believed to have improved gas barrier properties. This is based on the model that the fillers themselves act as barriers that bring about a maze like structure that retards the progress of a gas molecules in the matrix. The benefits of such a structure have been observed in polyimide-clay nanocomposites[45] where layered silicates dramatically improved barrier properties in conjunction with a decrease in thermal expansion coefficient. The polyimide-layered silicate nanocomposite with a small fraction of organically modified layered silicate showed reductions in the permeability of small gases, e.g. O_2, H_2O, He, CO_2. Yano et al.[45] found that a 2% loading of synthetic mica and MMT gave drastic decreases in the coefficient of permeability. By looking at the dependence of filler length on permeability coefficient, it was seen that as the length of the clay increases the permeability coefficient decreases dramatically. With 2% mica bringing the permeability coefficient of water vapour to a value that is less than one tenth of that of pure polyimide. In other words, the permeability is seen to decrease with increasing aspect ratio.

Oxygen gas permeability has been measured for polylactide (PLA)/organically modified synthetic fluorine mica nanocomposites[46]. The relative permeability coefficient was seen to decrease when plotted as a function of filler loading from 0%-10%. The greatest change in O_2 permeability came between 0 and 4% which resulted in over a 50% drop in relative permeability. Subsequent loadings showed lower and lower decreases.

The H_2O permeability of poly (urethane urea)/organically modified silicate nanocomposites showed dramatic decreases in relative permeability as a function of silicate volume fraction[47]. Deviation of experimental results from theoretical results using the tortuosity model (at aspect ratios 300 and 1000) suggested that there was a gradual change in effective aspect ratio of the filler as the volume fraction of silicate increased, suggesting aggregation.

Bharadwaj has built upon the tortuosity arguments described by Nielsen by modelling the barrier properties of polymer layered silicate nanocomposites[48]. It is by understanding these processes of sheet length, relative orientation, state of aggregation etc that greater guidance can be used to help design superior materials.

2.6 Ionic Conductivity

Solvent free electrolytes are of much interest because of their charge transport mechanism and their potential application in electrochemical devices. Vaia et al. has attempted to modify poly (ethylene oxide) (PEO) in order to adjust its ionic conducting characteristics[49]. An intercalated nanocomposite prepared by melt intercalation of PEO (40% wt) into Li MMT (60% wt) was shown to enhance the stability of the ionic conductance at lower temperatures when compared to the more conventional PEO/LiBF4 mixture. The improvement in conductivity is due to the absence of the non conducting crystallites that usually form during nucleation in the absence of silicates. The silicates upon intercalation disrupt the nucleation process and hence prevent crystalline structures forming. The higher conductivity at room temperature makes these nanocomposites appealing for future electrolytes. Similar behaviour has

been seen by Hutchison who used poly [bis(methoxyethoxy) ethoxyphosphazene] / Na+ MMT nanocomposites[50].

2.7 Optical Properties

Although layered silicates are microns in lateral size, they are just 1 nm thick. Stawhecker and Manias have demonstrated that the optical properties of poly(vinyl acetate) PVA remain unchanged with well dispersed 4% and 10% filler loadings of organically modified MMT[51]. For ultraviolet (UV) wavelengths there was strong scattering, which is due to the lateral size of MMT being of the order of 50-1000 nm.

2.8 Biodegradability

Another aspect of nanocomposite material is the significant improvement (increased biodegradability times) of biodegradability with the use of OMLS. Tetto et al. first reported results on biodegradability on PCL/OMLS nanocomposites[52] where they found increased biodegradability with use of the OMLS. Lee et al. has reported on the biodegradability of aliphatic polyester (APES)/MMT based nanocomposites. Two variations of organo MMT were used in their study. Measurements were taken by burying the composites beneath compost at a neutral pH at 60 °C and weighing the samples periodically. They found that all the nanocomposites showed a lower wt% loss than that of the pure system over a total of 30 days. Cloisite A (modified with dimethylbenzyl hydrogenated tallow ammonium) showed a weight loss of 30% at 3% loading as opposed to 80% weight loss of the pure system. Increasing loadings up to 30% yielded non-linear lower wt% losses. Cloisite B (modified with methyl tallow bis-2-hydroxyethyl ammonium) gave greater wt% losses, with 3% loading yielding a 70% loss. Increasing the filler loading post 10% did not seem to greatly affect the already 35% weight loss. They assumed that the retardation of biodegradation was due to the improvement of barrier properties of the layered silicates. Unfortunately no permeability data was presented that could support this claim.

2.9 Rheology

One of the problems associated with the production of nanocomposites is the matter of dispersion[53,54]. In order to aid this, fillers or clay particulates as is the case here, are functionalized in order to make them organophilic and thus readily bond with the host matrix where it can promote intercalation/exfoliation[55] which can account for substantially improved reinforcement of the polymer.

The method of mixing also plays a crucial role that determines the state of dispersion within the host matrix. Wang et al. studied two different methods of mixing clay with an epoxy resin[56]. The direct mixing method, in which organoclay is mechanically mixed with epoxy with or without solvents, is the most common method in clay/epoxy nanocomposites.

The production of epoxy nanocomposites using a direct mixing method (DM) consists of 3 simple steps:

1) Mixing the desired amount of organoclay with epoxy resin under mechanical stirring and heating.
2) Adding the curing agent to the previous mixture and degassing in a vacuum oven.
3) Pouring the mixture into the mold and curing it at an elevated temperature.

The problem reported with this technique is that the dispersion of the organoclay is quite poor with particles above 10 μm remaining after processesing. The reason for this is that the dry organoclay exist as an agglomerate, such that the epoxy molecules cannot easily diffuse into the interlayer galleries the layers because of the existence of Van der Waals force between the layers and particles.

A solvent is usually used to improve the direct mixing process. The solvent can lower the force between the layers and facilitate the movement of epoxy molecules into the clay galleries. The solvents used generally need to have a low boiling point e.g. acetone, ethanol, isopropyl alcohol, such that they are easily removed by evacuation.

This means that an extra degassing step needs to be added to the direct mixing method prior to the addition of the curing agent.

The agglomeration of clays during mixing can be combated using an extremely high shear force that can effectively break the layers apart and the solvent prevents the small size particles from agglomerating again. For these reasons Wang et al.[56] used a spindle rheometer. Wang et al.[56] carried out research on the rheology of organoclay prepared by both direct mixing (DM) and a second technique using a solvent that they named the liquid-liquid (LL) method. The filler loadings they used in their study were 1%, 3% and 5% and what they found was the LL method gave a huge increase in viscosity compared to that of the DM method. This difference was seen to increase as the filler loadings increased. Shear thinning was observed in their rheology, where their shear rates were reported to be of the order of 1000 s^{-1}. After experiments that disproved the notion that the intercalating agent and residual solvent within the system played a part in significantly affecting the systems viscosity, they concluded that the increased viscosity for the LL system was due to an increase in interactions between the clay and epoxy molecules and an increase in clay-clay friction.

They also looked at their composite mixtures at low shear rates (<700 s^{-1}). They observed Newtonian flow for the pure epoxy system and an arguably slight shear thinning (33-100 s^{-1}) for their 5% DM sample. A great deal of shear thinning could be seen from their LL processed sample at 5% loading. At 33 s^{-1} the sample had a viscosity 18 times greater than that of the pure resin, and 7 times greater than that prepared by the DM method.

They finished their rheological investigation by computing the parameters of a model that describes the viscosity of polymers filled with particulates. The model they used is the Krieger-Dougherty (KD) model which relies upon the parameter termed the intrinsic viscosity.

$$\frac{\eta}{\eta_0} = \left(1 - \frac{\phi}{\phi_m}\right)^{-[\eta]\phi_m} \tag{2.1}$$

Where η is the viscosity of the composite, η_0 is the viscosity of the matrix, Φ is the volume fraction of the filler within the matrix, Φ_m is the maximum volume packing

fraction (63% for random close packing) and [η] is the intrinsic viscosity (2.5 for spheres). This equation predicts that the viscosity of a sample increases with increasing particle loading especially when the maximum packing fraction is reached.

This parameter is determined by the shape of the particle and clay-clay and clay-matrix interactions. The intrinsic viscosity parameter is known to be 2.5 for spheres which they compare to their own calculated paranetsr of 22 and 3 for the LL and DM mixtures respectively. This implied that the DM mixture showed large aggregates that could be approximated by a sphere whereas the LL value was much larger meaning that the dispersion was improved. Unfortunately they did not have any transmission electron microscopy (TEM) images to support or discredit the implications of this result, it could have huge benefits in the manufacture of composites using rheology – and would enable composites to be characterised in the initial stages of material processing whereas TEM is a procedure usually given to characterising dispersion post material production.

Luckham and Ukeje have investigated the impact of particle size distributions of polystyrene latex spheres on the rheology of dispersed systems[57]. Very high loadings were investigated, ranging from 25% to 60% wt. In order to stabilize the latex, a stabilizing polymer was added, namely a triblock copolymer of PEO and poly(propylene oxide) (PPO) in a combination PEO-PPO-PEO. As PEO is hydrophilic it will orientate itself into the aqueous medium, while the hydrophobic PPO will anchor itself onto the surface of the polystyrene latex. By plotting the relative viscosity at a shear rate of 921 s^{-1}, as a function of volume fraction for three different particle size distributions (narrow, moderately and very broad) they showed that the relative viscosity decreased as the size distribution increased. There was a 2- to 20-fold reduction in the viscosity, yield value, elastic moduli, and loss moduli when a very polydisperse system was compared to a monodisperse one. The KD equation gave a good fit to experimental data especially when consideration was given to the total volume fraction of the adsorbed polymer layer onto the latex spheres.

Mohan et al. have carried out a comprehensive study on the rheological and curing properties of epoxy-MMT nanocomposites[58]. Rheology was performed on organo modified and unmodified MMT at loadings between 0 -10% at room temperature and

at 120 °C. At room temperature it was seen that the increasing clay content of both modified and unmodified particles within the resin gave an increase in the systems viscosity. 10% organo clay gave a 93% increase in viscosity compared to that of the base resin, whereas unmodified clay gave a 91% increase. At 120 °C the viscosity of the base resin fell by 94% relative to the viscosity at room temperature. The presence of 10% organo modified clay again gave a 93% increase in viscosity whereas the unmodified clay gave only 84%. The increase in viscosity due to the organo clay was claimed to be due to the homopolymerization of epoxy and also due to increase in clay size due to increased separation of clay layers.

Krishnamoorti et al. has studied the rheological properties of a siloxane copolymer filled with an organically modified mica-type layered silicate[59]. Rheological studies were carried out in the melt for two types of nanocomposite systems, namely, mica type layered silicates intercalated with polystyrene and delaminated hybrids. At 8% and 15% loadings they saw a considerable increase in viscosity (100%+) at low shear rates. At low shear rates the pure polymer system was seen to exhibit Newtonian behaviour whereas the intercalated systems showed slight shear thinning. At high shear rates ($> 20\ s^{-1}$) both the pure polymer and the intercalated system at 8% loadings with viscosity values comparable to the polymer itself. The 15% loaded intercalated system showed far greater shear thinning at high shear rates. Solomon et al. also investigated the rheological properties of polypropylene/clay hybrid materials[60] has also observed similar trends in that increasing the concentration of clay in the hybrid contributes to a large increase in the low- shear rate steady viscosity of the hybrids. At high (4.8%) loadings no evidence of a low shear plateau is exhibited – instead shear thinning is seen at the onset.

Galgali et al. studied the rheological properties of polypropylene (from the melt) MMT nanocomposites[61]. Again the same trends of increasing zero shear viscosity with filler loadings were reported. These trends were significantly greater for loadings post 3% for their compatibilized clays.

Krishnamoorti et al.[59] showed that their delaminated hybrids again showed viscosity increases with loading at low shear rates. Their polymer in this study was just poly(dimethylsiloxane) which showed Newtonian behaviour even in the presence of

filler at 6% and 13% loadings at low shear rates (<7 s^{-1}). At shear rates post 10 s^{-1}, large amounts of shear thinning was seen for all samples.

Le Pluart et al. investigated the rheological effects of three organo clays on a DGEBA epoxy resin[62]. The functionality of the three clays was the only difference between them. Rheological experiments were carried out at 80 °C with a filler loading of 5 phr. Their results showed that on the ramp up (up to a stress of 100 Pa) phase of their experiment, each sample exhibited a yield stress. This meant that they only included data from their systems on the ramp down. Each one gave a yield stress during the ramp up during the rheological tests – as the mechanical stress broke down the physical networks within the resin - so only their ramp downs were included. The pure epoxy system was observed to be Newtonian. The suspensions forming weak gels showed a strongly marked shear thinning behaviour, whereas those forming strong gels presented almost Newtonian flow behaviour during the shear stress ramp down. They justified these effects on the basis that strong gels would not reform when shear stress is decreased, or if it did, it would at a much slower rate than that of the weak gels.

2.10 Dielectric Properties

When a dielectric material is placed within an electric field it becomes polarised. Polarisation is a process where the dipoles respond to an electric field by redistributing its component charges e.g. negative charges orientating themselves so that they are closer to the positive electrode and positive charges towards the negative electrode. The polarisation of a dielectric can be used mathematically in conjunction with electric field to determine the permittivity (ε') of the material.

If the dielectric material is in an alternating field, such as one produced by a capacitor supplied with an AC voltage, then – depending on the frequency - there may not be enough time between periodic cycles for a molecule to respond. The polarisation effects that contribute to the permittivity will therefore be dominated by lower mass components of the charges that can respond in time i.e. electronic. Therefore the permittivity of a material can be said to depend on the frequency (over particular ranges); a phenomena known as dispersion, (see Figure 2.1[63]).

If the frequency of the field is too high, so as not to allow enough time for the molecule to reach equilibrium, there will exist a phase lag between molecular orientation and electric field. This lag means that throughout further cycles, the field will be partly working against the orientation of the molecule, a property that is now called the dielectric loss (ε'').

ε' and ε'' can be linked via the expression:

$$\frac{\varepsilon''}{\varepsilon'} = \tan\delta \qquad (2.2)$$

Dielectric constant and loss have been measured over a variety of frequencies and temperatures for silica composites at 20% loading[42]. The dielectric permittivity and

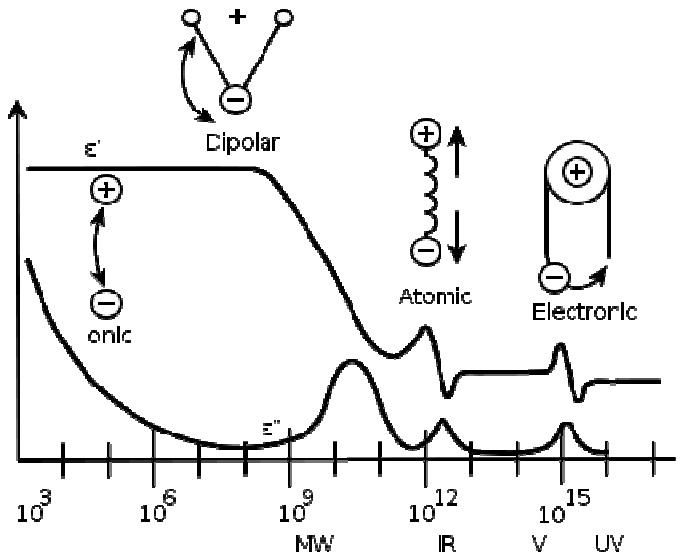

Figure 2.1: Dispersion of polarisation in a dielectric

loss were seen to be much greater than the pure epoxy sample at low frequencies. Over the entire frequency range the nanocomposite possessed a much higher loss factor than the pure epoxy/micro composite. In the low frequency range (<100 Hz) the loss factor of the micro composite was higher than the pure epoxy sample but lower than the nanocomposite. The loss peaks in the scans were seen to be at lower frequencies for the pure epoxy/micro composite and higher for the nanocomposite. The dielectric loss of silica filled composites has been attributed to absorbed water on the silica surface. This study, while providing interesting results in terms of how change in interfacial area immediately affects the thermal and dielectric properties of composite materials, the conclusion is intuitively obvious. That is the surface chemistry of the nano fillers and the study of the interfacial science between the filler and the matrix are essential for understanding the processes involved in modifying a composite materials properties.

The dielectric constant of epoxy-titanium dioxide (TiO_2) composites has been measured by Nelson et al.[64] Room temperature measurements at 1 kHz were taken on samples with 10% loadings of micro (1.5 μm) and nano (23 nm) sized particulates. The nanocomposite samples were seen to exhibit a lower dielectric constant of 4.5 compared to 6.01 for microcomposites. The base resin was measured to be at 5.68.

Sarathi studied the dielectric properties of MMT nanocomposites[65]. Over the frequency range 100 Hz to 1MHz a decrease in the relative permittivity and an increase in the tan(δ) in the material was shown for all clay loadings. At a fixed frequency, the relative permittivity and tan(δ) were seen to decrease up to 5% clay loadings, after which it began to increase. Imai et al.[66], studied the influence of temperature on permittivity and tan(δ) of epoxy loaded with organo modified silicates. They observed that at high temperature the loss is greatly suppressed for the nanocomposite compared with pure epoxy. The dielectric constant was seen to be also lower for the nanocomposite – which became more significant as the temperature increased.

Singha and Thomas carried out dielectric analysis of nano sized aluminium oxide (Al_2O_3) (45 nm) and TiO_2 (50 nm) at 0.1%, 0.5%, 1% and 5% fillers loadings over the frequency range of 1 MHz to 1 GHz[67]. They showed that the dielectric behaviour of nanocomposites differed from the behaviour of microcomposites made from the same

materials. Their Al_2O_3 composites showed values of lower dielectric constant then that of the pure epoxy resin at filler loadings of 0.1%, 0.5% and 1%. At 5% the dielectric constant was seen to be greater than that of the epoxy resin. Similar behaviour was seen for TiO_2 composites for 0.1% and 0.5% filler loadings. The dielectric constants of both pure Al_2O_3 and TiO_2 are higher than that of the base epoxy resin. Therefore, individual polarization processes within the epoxy resin must account for the lower dielectric constant measured of the composite. The polarization mechanism in Singha's study is due to the orientation of dipolar groups with respect to the electric field (see Figure 2.1). This orientation process can be reduced only if the movements of the contributing dipolar groups are restricted. This mechanism of reduced polymer chain mobility has been reported both experimentally[68] and computationally[69],[70] where mechanical enhancements were seen to be brought about by nanofillers that caused a decrease in polymer chain mobility. Depending on the interaction mechanism of the polymer and the nanoparticle, an interfacial layer is formed on the surface of the nanoparticle. This interfacial area is of course much greater for nano particles then for its micro sized counterpart and when these interfacial areas are extended to include the contributions of all the other particles in the system, it is expected that a large portion of mobility of the polymer segments interacting with the nanoparticle be restricted. These restrictions, in turn, cause the occurrence of a lower measured permittivity in the sample. With increasing filler loadings, agglomeration is expected to take place. This then causes a decrease in surface area to volume ratio which causes the permittivity measurement to become dominated by the intrinsic permittivity of the filler itself, which is why gains are seen after the decline at low filler loadings.

Lewis, in 1994 was the first in the dielectrics and electrical insulation community to propose that the basis of understanding behind the properties of nano dielectrics be related to the interfaces present in the materials[71]. Tanaka et al. have taken Lewis's work[72] and developed their dielectric multi core model that not only takes into account the behaviour of the particle, but includes the whole interfacial area between filler and particulate that encompasses it[73]. The interface consists of the following four states:

1) bonded layer
2) bound layer

3) loose layer
4) An electric double layer overlapping the above three layers (Gouy-Chapman)

The first one can be defined as a particle that is bonded to the polymer matrix. The second layer is an interfacial region consisting of polymer chains strongly bound and/or interacted to the first layer and the surface of the inorganic particle. Values of its thickness cited are in the range of 2 to 9 nm. These values depend on the strength of the polymer-particle interaction in a large polymer bound fraction. The third layer is a region loosely coupling and interacting to the second layer. It is characterised by having a variation in chain conformation, chain mobility, and even free volume or crystallinity from the polymer matrix.

Chain mobility is generally attributed to the second state; bound layer and directly effects glass transition temperature. Chain conformations are altered in the interface. It includes the orientation of specific established radical groups or parts of a polymer chain stuck to a nanostructured surface, the local density of the interfaces, the degree of chain folding etc. Crystallinity is also strongly affected by interfacial interactions. When a curing agent is mainly absorbed onto the nano filler, the region surrounding the nano particle consists of a layer of stoichiometrically crosslinked thermoset with excess curing agent, surrounded by a layer of depleted curing agent and thus less than stoichemetric cross linking. The third layer; loose layer, is considered to be a region affected chemically by the second layer, and electrically by the diffuse Gouy-Chapman layer.

The Gouy-Chapman diffuse layer is a consequence of charge injection from the particulate filler to the polymer matrix. Charge injection is related to the triboelectric properties of both the matrix and the filler and is based on the electron affinity and the equalization of the Fermi level or electrochemical potential. The triboelectric series indicates that polyolefins tend to attract electrons whereas condensation polymers tend to give them up. This charge distribution over an interface might affect the formation of polymer morphology.

Permittivity usually increases, if polymers are filled with inorganic fillers of micrometer size by several tens wt%[74]. This is because fillers naturally have a higher

permittivity than unfilled polymers. Nano sized fillers can have interesting effects on the permittivity of its host matrix as a whole. The permittivity is found to decrease if polymers are filled with nano sized fillers by several wt% as was shown by Fothergill et al.[75] These reductions in permittivity have been used to define what is now known as nanostruturation. Alternatively, increases have been reported for materials referred to as nanocomposites, which could be brought about during material production due to an accidental inclusion of the imperfection of nanocomposites such as inhomogeneous dispersion and agglomeration or impurities present during processing that could lead to such a contradictory result

This reduction in permittivity has been attributed to the restriction of polymer chain mobility by the nano particles. Some impairment of dipole moment takes place at the interfaces, perhaps resulting from surface hydroxyl group bonding (first layer) for the case of unmodified fillers. This bonding would affect the surrounding morphology to form an extended interface (second and third layers) e.g. epoxy titania nanocomposite, the second layer corresponds to a layer of stoichiometrically cross linked thermoset with excess curing agent, while the third layer corresponds to a layer of depleted curing agent and as a consequence – less stoichiometric cross linking.

Free volume is another mechanism which could describe the permittivity reduction. Nano-fillers with high surface energy and/or other species are present that could otherwise disrupt contact between filler and matrix resulting in an interfacial region with a low density. This layer would have to be fairly thick when compared to the inner layers to explain a reasonable reduction in sample permittivity. In the context of the multi core model this layer would be ascribed to the less stoichiometrically cross linked layer.

Dielectric tan(δ) is also seen to change with nanostructuration[66,75]. Strong suppression is seen in epoxy-organically modified layered silicate nanocomposites than in base epoxy[66]. Fothergil et al.[75] showed that at room temperature, nanocomposites typically showed higher loss tan(δ) at low frequencies (0.001 to 0.1 Hz) and lower tan(δ) at higher frequencies (1 to 1 MHz) than that of the pure epoxy. This was attributed to nanostructuration.

Permittivity measurements have been used to investigate the effects of curing agents and nano clay dispersion on epoxy nanocomposites.[76] The epoxy cured with the amine curing agent had a permittivity that was seen to be much greater than that with the acid anhydride. This was reasoned to be due to the extra polar –OH groups present for the amine curing agent. The effect of nanostructuration on the permittivity was also seen to be more significant for the amine cured samples. The permittivity of the amine cured nanocomposite was lower than that of the pure amine cured epoxy. This was attributed to the hydrogen bonds between –OH groups of the hardener/particle which restrict orientation processes in the presence of an electric field as proposed by the multi core model.[73]

Zheng et al. investigated the dielectric (50 Hz) properties of epoxy-nanosilica (20 nm) nanocomposites at 0, 1, 2, 3, 4 and 5% filler loadings[31]. They found that the introduction of increasing amounts of untreated nano silica caused a increase in DC conductivity and dielectric loss. This was attributed to the increased amounts of –OH groups present on the surfaces of the nano silica, which is believed to act as a source of ions at post Tg temperatures.

2.11 Electrical Breakdown

Iami et al. have conducted research on 5 % wt loaded organo clay/epoxy nanocomposites using a needle plate geometry with a needle-ground gap of 3 mm[77]. They have shown that epoxy resin with functionalised layered silicate fillers yielded a superior insulation breakdown time at constant AC voltage (10 kV, 1kHz) than epoxy resin without fillers in needle plate geometry. This was particularly the case at high temperatures, e.g. at 145 °C, their nanocomposite had a breakdown time of more than 20,000 min while the base epoxy resin had a breakdown time of 280 min.

Generally, as the temperature of an insulating material rises, the insulating properties due to a reduction in volume resistivity - decline. Iami and co-workers' result mentioned above led them to monitor the propagation of electrical treeing. At room temperature, the electrical tree was seen to propagate with several branches yet

comparatively straight compared to that of the filled epoxy. More branches are seen to grow for the filled epoxy as the tree propagates. At room temperature, the average propagation speed of the electrical treeing was 0.06 mm/min in the nanocomposite, whereas it was 0.11 mm/min in the base epoxy resin. It was this delay of tree initiation time and the tree propagation controlled at slow speed which enables the nanocomposite to have a longer insulation breakdown time than the base epoxy resin. At 145 °C, spherical trees were formed in both the base epoxy resin and the nanocomposite. The electrical energy concentration at the needle tip is said then to be relaxed by the spherical shape, implying that the electrical stress is spread over a wider area. It was stated that this phenomenon was the reason for the increase in breakdown times at high temperatures.

Sarathi et al. carried out a thorough investigation into the electrical properties of MMT/epoxy nanocomposites[65]. Electrically they studied the impact of organophilic MMT using a range of loadings up to 10% under AC and DC voltages. The AC breakdown voltage is less than the DC breakdown voltage. This was explained as follows: "Under AC voltages, the charges injected in one half cycle gets swamped out in the next half cycle. Constant injection and extraction of charges in the medium causes local temperature variation which aids the process of breakdown. Under DC voltages, the charge inhibits the breakdown process due to charge accumulation near the defect site counteract the applied electric field, thereby requires higher voltages to cause breakdown."

It has been shown that increasing the clay content of nanocomposites up to 5% resulted in an increase in breakdowns strength under both AC and DC voltages. Zilg et al. carried out DC electrical breakdown tests on organo layered silicate ethylene(vinyl acetate) (EVA) and isotactic polypropylene (i-PP) nanocomposites[78]. All tests were taken at 20 °C under a ramp rate of 5 kVs^{-1} and analysed using Weibull statistics. They found that the presence of nanofiller at 6% loading slightly decreased the time to breakdown for EVA nanocomposites while the PP nanocomposites gave an increase over that of the pure systems. Positive effects have been reported by Montanari et al. for i-PP using organo modified silicates at 6% filler loadings[79]. Negligible differences were seen in the EVA nanocomposites. In both Montanari's and Zilg's study the same

modifications were applied to the silicates (octadecylamine (ODA)) and the tests were carried out in an identical manner. An interesting aspect in these studies is the dramatic increase in shape parameter (β) for the nanocomposites when compared to their pure matrix counterparts which Montanari and co-workers believed was indicative of a more homogenous material with fewer micro-voids.

Nelson and Hu electrically tested epoxy/TiO_2 micro/nano composites under DC with a voltage ramp rate of 500 Vs^{-1} [80]. They showed that micro composites were electrically weaker than nanocomposites at all loadings up to 40%. The nanocomposites showed constant breakdown strength up to 10% after which it decreased rapidly. This finding demonstrates that nanocomposites have a positive effect on breakdown strength as compared to microcomposites.

Kozako et al. investigated the breakdown properties of organo alumina nano-composites using the needle-plane electrode geometry[81]. Tests were carried out on samples using 0%, 3%, 5%, 7% and 10% filler loadings. They showed – using Weibull statistics - that the presence of 5% filler extended the time to breakdown by 265%. Again at 5% loadings, the permittivity was seen to increase from 3.7 to 4, mechanical properties showed an increase in flexural strength and modulus by 5% and 8% respectively and no change was seen in the glass-transition temperature.

Sarathi et al. attribute the breakdown voltage for nano-filled epoxy resin material to the following factors[65]:

1) Increase in surface area of the nano particle, which alters polymer behaviour.
2) Changes in space charge distribution in the insulation structure.
3) Scattering mechanism.
4) Dielectric properties especially the volume resistivity, tan(δ) and permittivity of the material.

Nano particles by nature have a larger surface area when compared to their larger counterparts, e.g. micro particles. This larger surface area means there can be more interfacial interactions between particulate and polymer. Also because of high packing density, the accumulated charge is reduced and threshold field at any point is reduced and the space charge distribution is altered. When the material is packed with nano-

materials, the fillers act as scattering sites. The electrons injected from the high voltage electrode or formed by different mechanism in solid insulation get accelerated by the applied field. Due to dispersed nano particles, the electrons transfer energy to the nano-particles and lose momentum. Since the particles are so closely packed, the electrons cannot re-gain momentum to initiate dielectric breakdown. For it to cause damage to the insulation, it requires additional voltage to cause any catastrophic failure of insulation. Thus, the epoxy nanocomposite has improved breakdown strength compared to the normal epoxy, under both AC and DC voltage conditions. When the percentage of clay content is increased above a certain weight percentage, the chance of formation of aggregates/clusters in the matrix is high. These loose clusters or unexfoliated structures in the matrix acts as additional crack initiation sites by splitting up easily under applied electric stress causing a reduction in breakdown voltage.

Tanaka believes nano fillers are too big to be scattering centres for electrons to scatter from and instead proposes a mechanism that incorporates the multi core model[82]. The basis of the discussion was the density changes between the layers, e.g. third layer; low density, second layer; higher density, first layer; bonded layer and lastly, the inorganic particle. The third layer is the main contribution to free volume, where it is believed that the electrons move easiest in these lower density areas – which would imply lower breakdown strength for nanocomposites. This is not the case, as has been seen by many researchers experimentally.

Electric double layers around nano particles can act as sources for Coulombic attraction or repulsion for moving electrons, depending on the polarity of the filler. Polarity is determined by the difference in electron affinity and the Fermi level.

Electrons are supplied from the negative electrode and/or the Gouy-Chapman diffuse layer, and experience acceleration due to the applied field. When electrons move within the Debye shielding length, they will either be scattered or attracted by the Coulombic force, to lose the energy they have gained from the field. When electrons are outside the Debye shielding length, they are accelerated in a polymer matrix and collide with the third layer or enter inside the Debye shield. In any case, electrons are decelerated to increase breakdown voltage.

CHAPTER 3: Rheology of a Model System

3.1 Introduction

Throughout the course of this research, a narrow gap concentric cylinder rheometer is used to conduct rheological analysis on various systems. This chapter focuses on determining the instrumental limitations of the equipment. This was done using an aqueous surfactant solution as a simple model system. To this end, relationships between varying concentrations of tap water and bathfoam are analysed using their stress and strain characteristics. This should ensure that subsequent experiments provide reliable results that will give a good foundation for future research, where the principle aim is to correlate the rheological characteristics with the dispersion of nanoparticulate fillers within polymeric systems.

3.2 Theory

Rheology can be defined as stress and strain in the study of deformation and flow of matter[83]. Consider a fluid that is confined between two parallel plates (See Figure 3.1). The upper plate moves at a constant velocity v while the lower plate is at rest. The force needed to move the upper plate is denoted F and the contact area of the upper plate to the liquid is A [1].

The molecules of the liquid next to the lower plate can be considered to have zero velocity. The molecules in the next layer above slide over these molecules at a slightly faster speed, and so on with each successive layer moving at a slightly faster speed until the molecules just below the upper plate are moving at the same speed as the upper plate. The molecules in a single layer travel at the same velocity and this variation of velocities between the layers is defined as laminar flow. The fluid can be said to be *sheared*, and there is a velocity gradient $\delta v/\delta y$ across it which is often

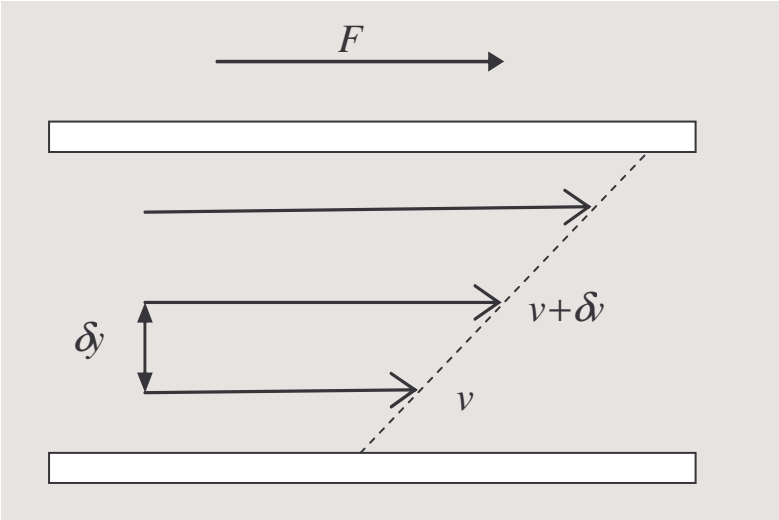

Figure 3.1: Effects of shearing

referred to as the *shear rate*. The sliding between the layers can be thought of as a form of friction: *viscosity*[84].

It was Newton who first suggested that the frictional force F between the layers is proportional to A and to the velocity gradient. With a constant of proportionality we have

$$F = \eta A \frac{\delta v}{\delta y} \tag{3.1}$$

This is sometimes referred to as Newton's law of viscosity. It holds for many gases and liquids. Such liquids are termed Newtonian liquids; water is an example. η is known as the coefficient of viscosity[85]. Re-arranging equation (3.1) gives

$$\eta = \frac{Shear\ stress}{Shear\ rate} = \frac{F/A}{\delta v/\delta y} \tag{3.2}$$

3.3 Model Systems

This section investigates the rheology of a model system. This model system consists of water and common household surface active agents (surfactants) in the form of

bathfoam. With this model system, the measuring limitations of the rheometer are investigated at both high and low shear stress.

3.3.1 The water molecule and mixing

The water molecule consists of two hydrogen atoms covalently bonded to a single oxygen atom, see Figure 3.2. The charges on water molecules and their strong tendency to form hydrogen bonds that control their interactions with not only other water molecules, but with other materials as well. If a material is non-polar, like the backbone of a surfactant, a water molecule is incapable of forming hydrogen bonds with it. Instead the water molecules arrange themselves into a cage-like structure (clathrate) around the molecule in order to utilize all four potential hydrogen bonds per water molecule. This results in a decrease in entropy, as the water molecules are more ordered then in the bulk liquid, an effect that restricts the solubility of the solute[8].

In a polymer-solvent solution there exist forces of attraction between similar (polymer-polymer, solvent-solvent) and non-similar (polymer-solution) molecules. In order to form a solution of a polymer in a solvent, the polymer-solution forces must be greater than or equal to the forces between similar molecules. If not, the molecules with the biggest intermolecular attraction will cohere and fail to mix with dissimilar molecules. There is, therefore an enthalpic driven tendency for the molecules to aggregate.

Solubility occurs where the free energy of mixing, ΔG_m, is negative. This value is related to the enthalpy of mixing, ΔH_m, and the entropy of mixing, ΔS_m, by the Gibbs equation[8]:

$$\Delta G_m = \Delta H_m - T\Delta S_m \tag{3.3}$$

In these model systems, the solvent is the aforementioned water molecule. In order to give the required chemical potential to yield a negative ΔG_m the entropy of mixing must be greater than the enthalpy of mixing. This is done by mechanical stirring or mixing, which in this case is carried out in the rheometer.

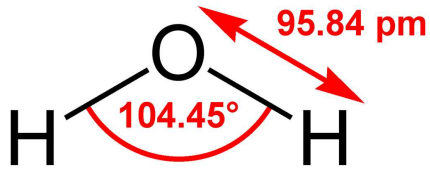

Figure 3.2: Water molecule

In 1942 Flory and Huggins independently developed a lattice model theory which takes into account the dissimilarity in molecule sizes between polymer and solvent. The result obtained by Flory and Huggins is:

$$\Delta G_m = RT\left[n_1 \ln \phi_1 + n_2 \ln \phi_2 + n_1 \phi_2 \chi_{12}\right] \tag{3.4}$$

Where n_1 and ϕ_1 are the number of moles and volume fraction of the solvent and n_2 and ϕ_2 being the equivalent for the polymer. R is the gas constant, T is the absolute temperature and χ is known as the interaction parameter which is associated with the enthalpy of the system. χ can be calculated using Hildebrand solubility parameters which are numerical estimates of the degrees of interaction between solvent and polymer.

3.3.2 Water and surfactants

The first model system comprises of bathfoam and tap water. Like all detergents, bath foam consists of a variety of surfactants. Surfactant molecules are known as amphiphiles which contain water insoluble (hydrophobic) and soluble (hydrophilic) segments[8]. The contents of the bathfoam were listed on the bottle. The first two primary ingredients were water and the anionic surfactant; sodium dodecyl sulfate. This molecule is shown in Figure 3.3; it essentially contains a hydrophobic hydrocarbon back bone attached to a hydrophilic sulfate group.

With respect to surfactant molecules at high concentrations, the tendency is for the molecules to aggregate into spheres to minimize their surface areas, with the hydrophobic backbone pointing inwards and the hydrophilic head on the outside[8,86]. These structures are known as spherical micelles and occur at a critical micelle

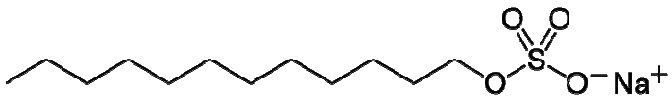

Figure 3.3: Chemical structure of sodium dodecyl sulphate

concentration (cmc). At this concentration, the addition of more surfactants will not decrease the surface tension of the water. Increasing the surfactant concentration yields more complex structures: cylindrical, hexagonal, cubic, lamellar to surfactant crystals[87].

Bathfoam is composed of a range of surfactant molecules and, as a consequence, contains mixed micelles[88] that exist in equilibrium with unassociated surfactant monomers. Their composition depends on the cmc of the single surfactants and the overall composition of the solution.

The presence of electrolyte fillers in bath foam (in this case NaCl) and detergents act as an ionic screen on the surfactant head groups. This lowers the cmc and the repulsion between the head groups. This decrease in head-group repulsion can lead to a change in shape of spherical to cylindrical; this change decreases the effective area per head-group and allows the geometrically preferred structure of lower mean curvature to form[87]. Surfactant chain length also plays a role: the longer the alkyl chain the less soluble are the molecules in water so that micelles tend to form at lower concentrations[8].

3.4 Apparatus

The rheometer used to measure the mechanical properties of all the systems was a RHEOLAB MC1 (Paar Physica) using a Z1 DIN concentric cylinder geometry, see Figure 3.4. The data were received via the rheometer to a standard laboratory PC via a RS 232C Com1 port. The data were interpreted by the software Physica Rheologic RS 100 which also controlled the variables, e.g. shear rate. The viscosity range for the Z1 DIN measuring cup and bob is 0.001 to 1.30 Pa s (Operation Manual Rheolab MC1).

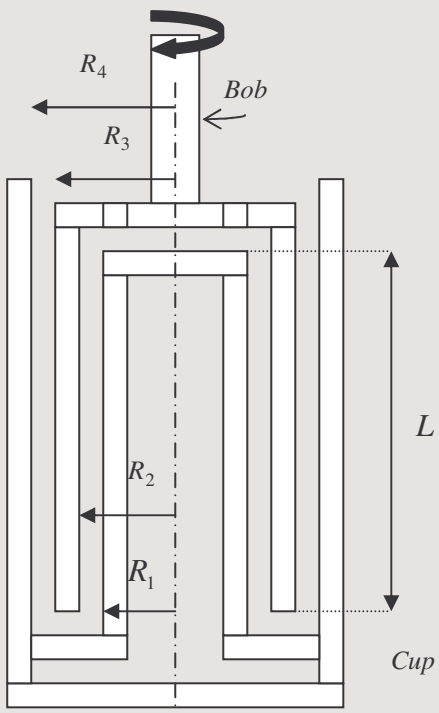

Figure 3.4: Measuring geometry of the cup and bob according to Z1-DIN/O0

The rheometer measures the torque acting on the measuring bob as a result of the viscosity of the sample at a pre-set shear rate. Each experimental run consisted of three phases: ramp up, constant shear rate and ramp down. By using the values in Figure 3.4, the sample volume can be calculated to be 16.13 ml over the length *L*. The data sheet claims that the internal cup length is 113 mm meaning that the gap at the bottom is 2 mm in height. The ratio of the immersion length *L* to the gap between the cylinders is in excess of 100 meaning that end effects created by this gap at the bottom are negligible provided one uses the correct amounts of sample[89]. The total volume of the cup over *L* including the reservoir at the bottom is approximately 16.6 ml.

3.5 Experimental

During ramp up, the bob was subject to a torque that caused it to increase in speed in steps from 0 to 5 Pa (20 Pa for 20 ml bf). During the constant shear phase, the bob was held at 5 Pa for 20 seconds and then the torque on the bob was ramped down to 0 Pa. Each experiment was carried out at room temperature ~ 22 °C. The maximum

amount of sample used in all these experiments was 20 ml. The concentration of the bathfoam was the only variable. The samples used were 20 ml tap water (bfw0/100/22), 15 ml tapwater + 5 ml bathfoam (bfw25/75/22), 10 ml tapwater + 10 ml bathfoam (bfw50/50/22), 5 ml tapwater + 15 ml bathfoam (bfw75/25/22) and 20 ml bathfoam (bfw100/0/22). The measuring bob and cup were washed and dried after every experimental run.

3.6 Results and Discussion

3.6.1 Rheological characteristics

Figure 3.5(a) shows the results obtained for the sample bfw0/100/22. Water is accepted to be a Newtonian fluid[85] i.e. constant viscosity regardless of shear rate. However, this seems to not be the case as is seen by the variations in viscosity with shear rate. It is also known that at 25 ºC it has a viscosity of 1×10^{-3} Pa·s [90]. The coefficients of viscosity are temperature dependent, therefore at room temperature the value would be lower; the viscosities of liquids decrease with increasing temperature, whereas those of gases increase with increasing temperature[85]. Even with a slightly lower viscosity, the results would still be on the borderline viscosity range of the measuring cup. From Figure 3.5 the viscosity can be seen to increase monotonically. At a shear rate of approximately 630 s^{-1} the viscosity levels off for a short period at a value of approximately 0.001 Pa·s. Above a shear rate of approximately 1200 s^{-1}, the system appears to become unstable as seen by the dramatic viscosity increase.

The start of each horizontal linear regime is relatively constant, as is seen clearly from the results taken from Figures 3.5, 3.6 and 3.7 shown in Table 3.1. This gives the lowest stress limit of the torque transducer below which recorded values cannot be accepted as reliable. Not only does the linear regime get progressively longer with increasing bf concentration but the measured viscosity values also increase.

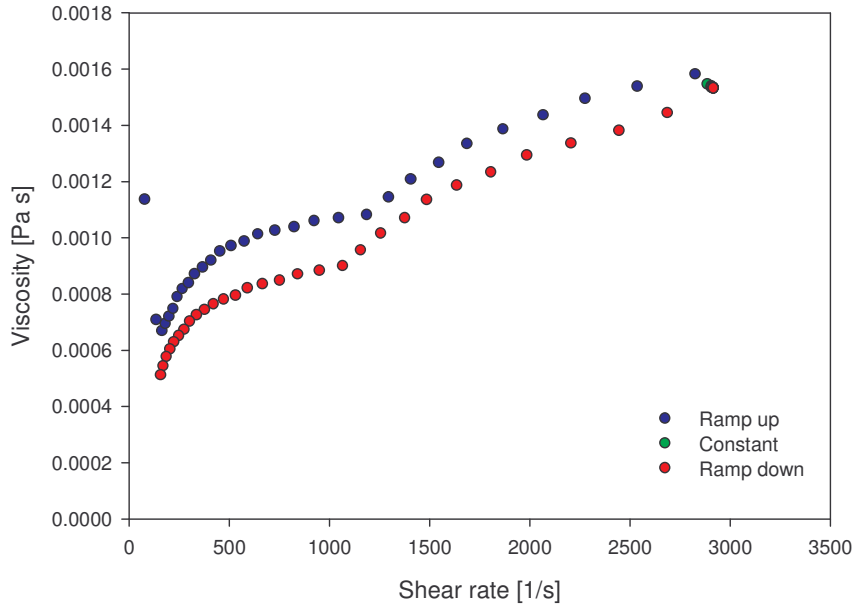

(a)

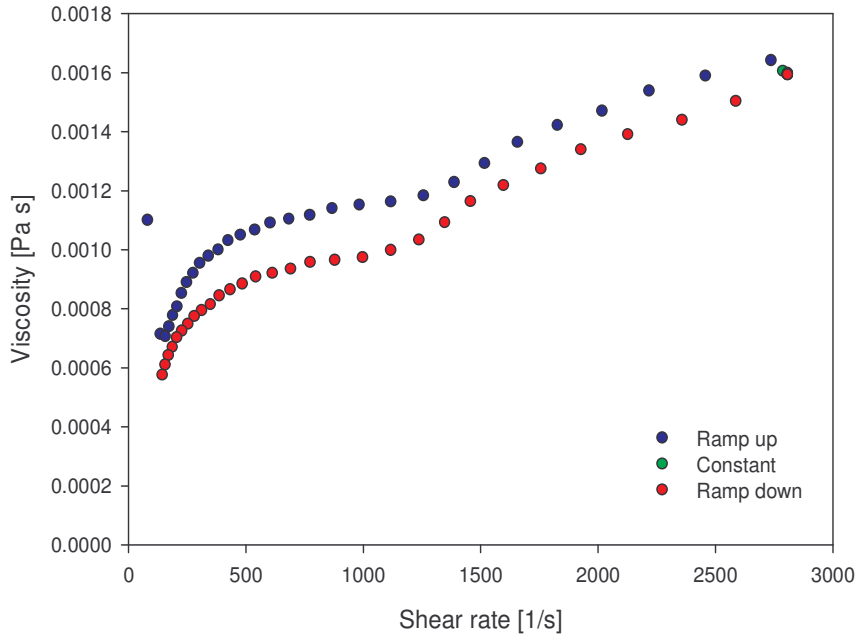

(b)

Figure 3.5: Viscosity as a function of shear rate for (a) bfw0/100/22 and (b) bfw25/75/22

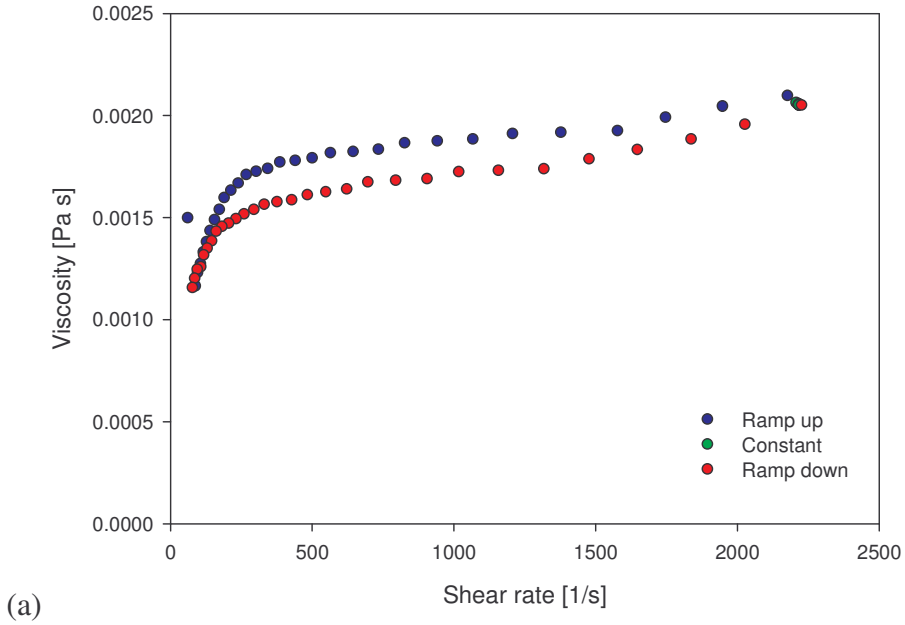

(a)

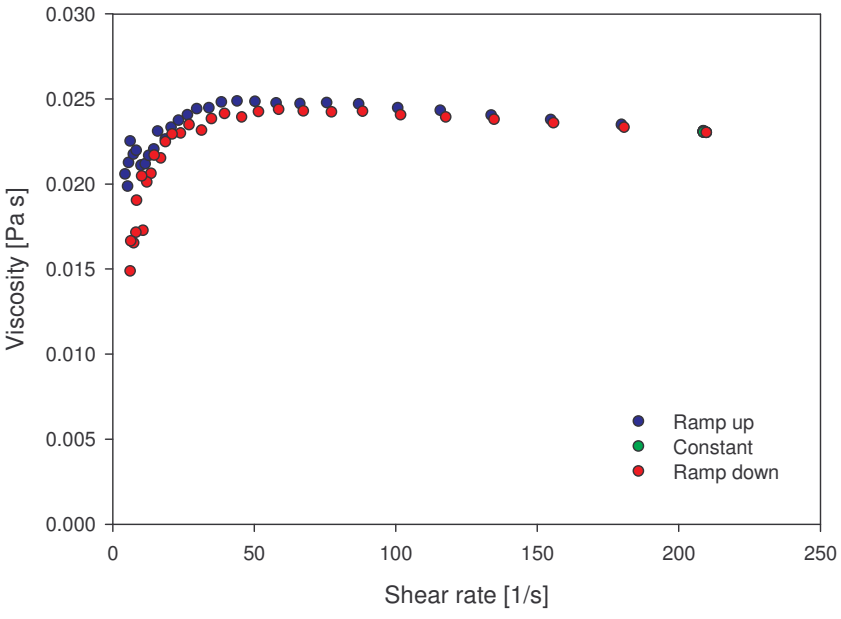

(b)

Figure 3.6: Viscosity as a function of shear rate for (a) bfw50/50/22 and (b) bfw(75/25/22)

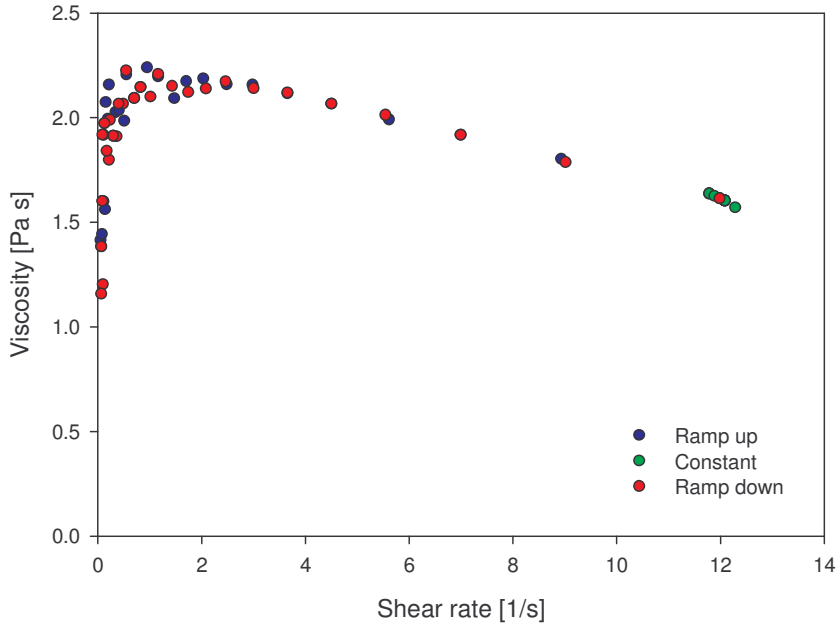

Figure 3.7: Viscosity as a function of shear rate for bfw/100/0/22.

Due to the fact that values of viscosity can change depending on where one believes the linear regime to start makes the system unreliable. Specifically, the viscosity value extracted directly from the instrument control analysis software is questionable, particularly at low shear rates. It can also be seen that due to thixotropic loops in systems containing 50% water and above, the values in Table 3.1 will vary depending on which data points are relied on. It is also cumbersome when it comes to data

Table 3.1: Rheological data for start of horizontal linear regime

System	Shear rate [1/s]	Viscosity [Pa·s]	Shear stress [Pa]
Bfw0/100/22	630	0.001	0.63
Bfw25/75/22	550	0.001	0.55
Bfw50/50/22	350	0.0017	0.60
Bfw75/25/22	28	0.02	0.56
Bfw100/0/22	0.24	2.2	0.53

analysis.

In Figure 3.6(b) the viscosity is seen to decrease with increasing shear rate. This is known as shear thinning[1] and, from Figures 3.6 and 3.7, it can be seen to be increasingly noticeable with higher concentrations of bathfoam. Shear thinning is absent from systems containing 25 and 50% bf (Figure 3.5 (b) and Figure 3.6(a)), instead a monotonic increase is present that is similar to that seen in Figure 3.5(a). As more bf is added to the system, the monotonic increase becomes weaker until it resembles that of a power law (pareto distribution function) function (Figure 3.6 (b)).

The concentration limit where the on-set of shear thinning occurs is found from empirical analysis. This requires a more fundamental format of presenting rheological results; stress as a function of strain (see Figures 3.8, 3.9 and 3.10).

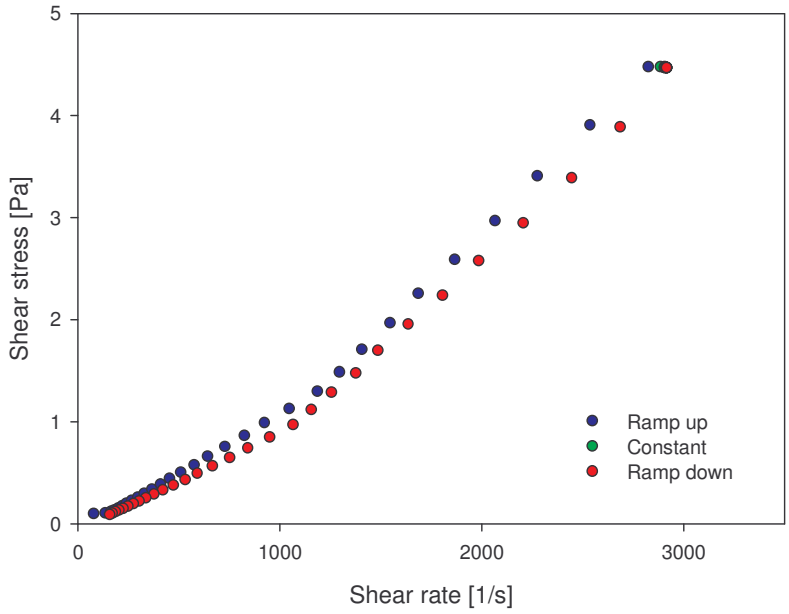

Figure 3.8: Shear stress as a function of shear rate for 20 ml tap water

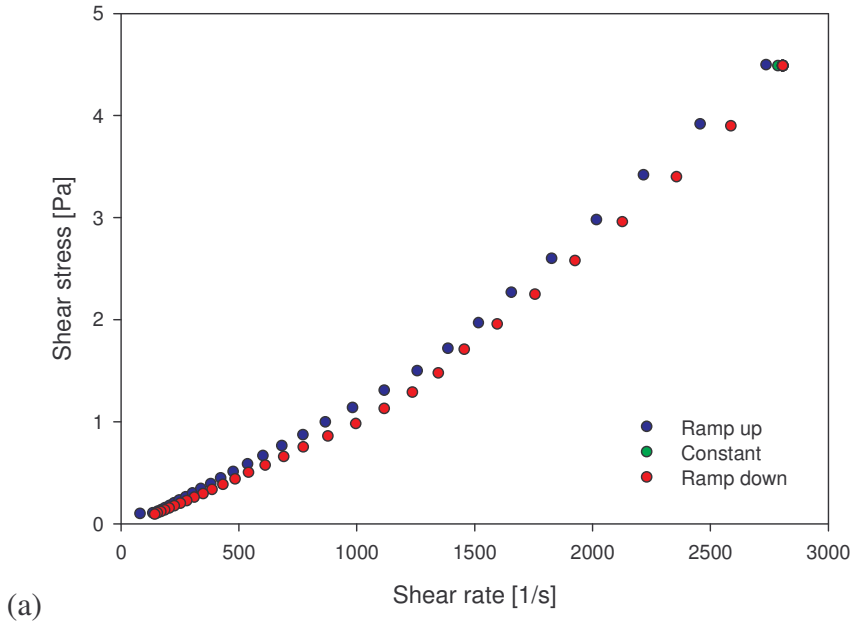

(a)

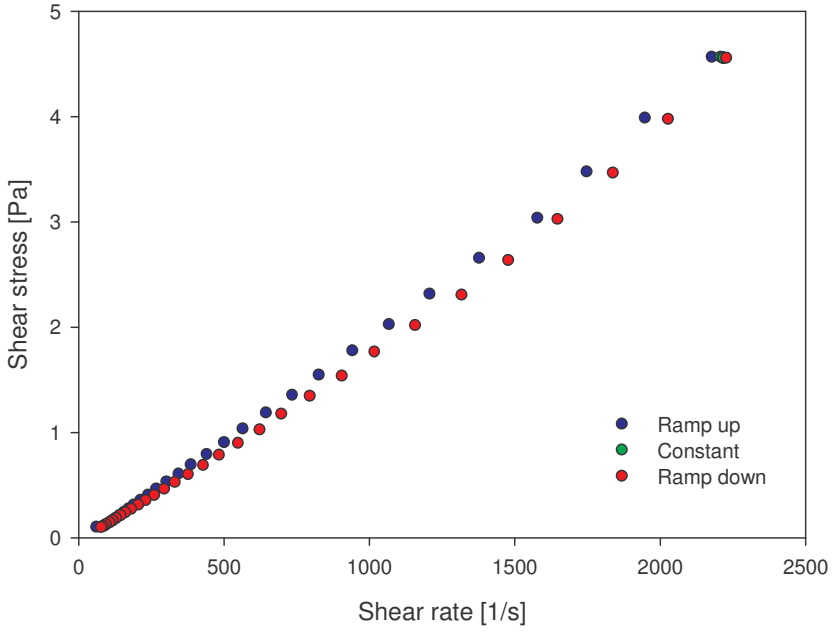

(b)

Figure 3.9: Shear stress as a function of rate for (a) 15 ml tap water + 5ml bath foam (b) 10 ml tap water + 10 ml bath foam

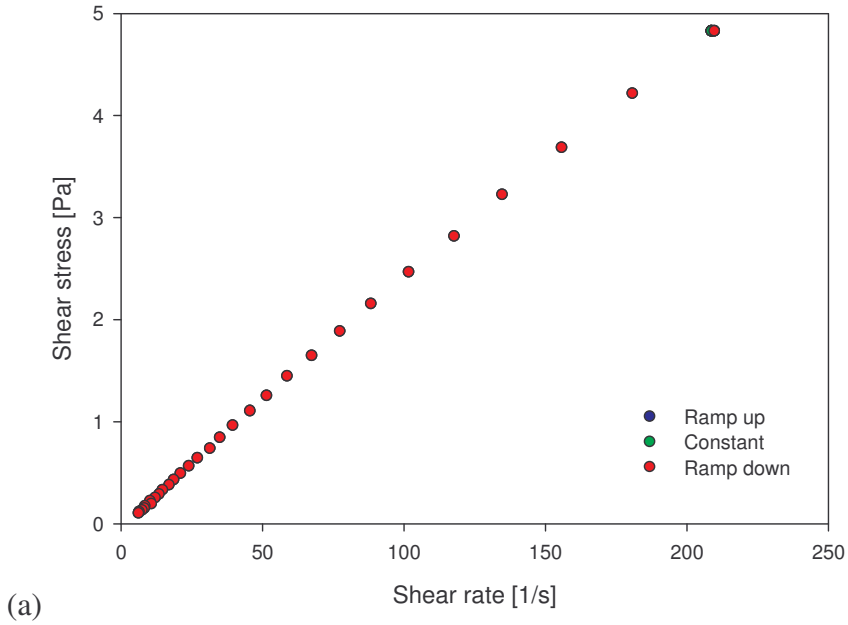

(a)

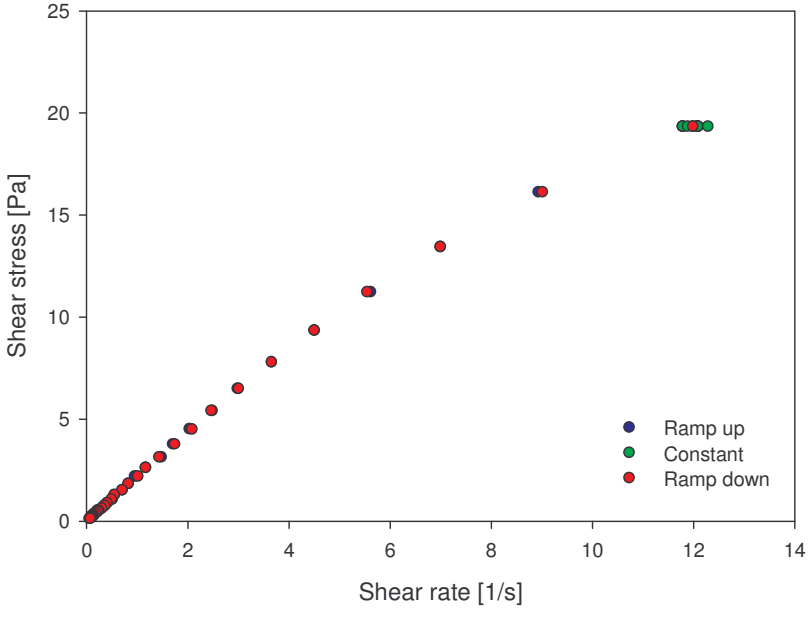

(b)

Figure 3.10: Shear stress as a function of rate for (a) 5 ml tap water and 15 ml bath foam (b) 20 ml bath foam

A two parameter power law function known as the Ostwald-de Waele equation[1] (Eq. (3.5)) was therefore fitted to the raw stress-strain data. This two parameter empirical model was proposed by Ostwald and de Waele in 1929. It is based on experimental observation that by plotting $\ln\eta(\dot{\gamma})$vs.$\ln(\dot{\gamma})$ (where η is the viscosity and $\dot{\gamma}$ the shear rate) , a straight line is obtained in the high shear rate region for many non-Newtonian fluids, including most polymer melts[91].

Curves were fitted using Sigma Plot and the power index values from this empirical equation were plotted as a function of water concentration as shown in Figure 3.11. A quadratic function was then fitted in order to get a concentration limit where the power index is lower than the value 1 (1 being a Newtonian system) which shows the onset of shear thinning. This occurs at approximately 30% water concentration (~ bfw70/30/22). This means that at approximately 22 ºC where the water content is less than 30% shear thinning will occur.

$$\sigma = K\dot{\gamma}^n \tag{3.5}$$

Where σ is the shear stress, $\dot{\gamma}$ is the shear rate and *K* and *n* are constants.

As can be seen from Figure 3.10 (b) the system has been subject to a far greater shear stress than the other systems. At a shear stress of 5 Pa the pure bathfoam system is only just starting to show signs of shear thinning, whereas the other systems have had a high enough stress to show their shear characteristics regarding shear thinning/instabilities. To keep consistency in this regard, the shear stress was increased for this sample. If this had not been done, the power law index would be similar to that of bfw75/25/22.

It is well known that cationic surfactants can self assemble in solution to form wormlike micelles upon the addition of salt. The salt reduces the electrostatic interactions between the cationic headgroups which reduces the effective area per headgroup and thereby promotes the growth of cylindrical aggregates at the expense of spherical ones[92]. The presence of such molecular structures imparts strong viscoelasticity[93] to the solution, and the rheology of these fluids is similar to that of solution of flexible polymers. However, because the micelles are in dynamic

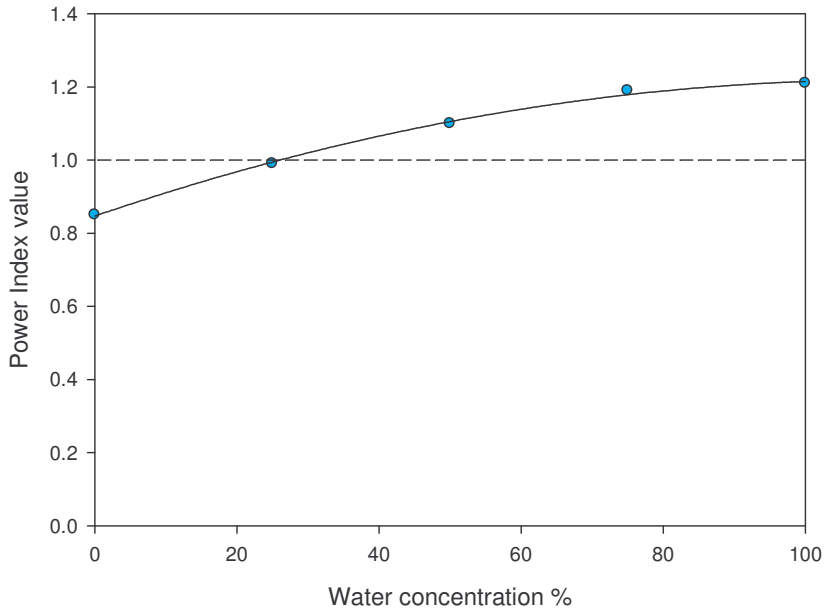

Figure 3.11: Power law function index as a function of tap water concentration

equilibrium with their monomers, they can break and recombine rapidly and thus are called 'living polymers'[92,94]. It is this reason that less and less thixotropic loops are seen as the concentration of bf is increased; the molecular surfactants recombine as the stress to the system decreases, leaving a structurally intact system when the stress reaches zero.

An interesting characteristic can be seen through all the samples regarding their viscosities and thixotropic loops (hysteresis) with bf concentration. The higher the concentration of bf; the higher the viscosity/degree of shear thinning and the smaller the thixotropic loops become. Kalur et al.[92] found that the anionic surfactant in their research - sodium olate (NaOA) in the presence of potassium chloride (KCl) as an electrolyte – displayed similar rheological characteristics regarding shear thinning. They stated that this was due to anionic wormlike micelles becoming entangled into a transient network where they impart a high viscosity and viscoelasticity to the sample. The gradient of their viscosity/shear rate graphs showed a gradient of -1 in the shear thinning regime. This means that the shear stress asymptotes to a plateau in this regime which is a characteristic feature of wormlike micelle rheology. Although the

gradient in Figure 3.7 is not -1, asymptopic behavior can be seen to develop in Figure 3.10(b).

Hassan et al.[95] worked with sodium dodecyl sulfate (SDS) and *p*-toluidine hydrochloride (PTHC) as the salt. They found that even at low concentrations of PTHC to SDS, there was a dramatic increase in viscosity of their solutions due to a transition from spherical to rodlike micelles. Magid et al. in their work in[96] investigated the flexibility of wormlike micelles formed in aqueous NaCl solutions and found that the micelles became more flexible as the ionic strength increased.

To summarise, the above demonstrates:

1) Low shear and low viscosity (≤0.001 Pa s) readings become unreliable.
2) Data processing in software is flawed, in that it calculates viscosity using apparent shear stress/apparent shear rate
3) The system is structurally complex which gives complex behaviour.

In addition to these effects, when the shear rate gets high for low viscous systems (Figure 3.8 and 3.9), the assumption that laminar flow is present is subject to doubt. This is shown by unstable behavior at high shear rates (~1200 s^{-1}) that yields dramatically high viscosity readings. This will be discussed by considering the fluid dynamics of the system.

3.6.2 Fluid Dynamics

The subject of fluid dynamics is vast and its depth is far beyond the scope of this research. Only the relevant basics are included here in a manner that is suitable to gain understanding of the limiting factors within our concentric cylinder (cone and bob) rheometer.

In 1890, Couette and Mallock[97] observed that the torque needed to rotate the outer cylinder in a rotating concentric cylinder system increased linearly with the rotation speed to a point, after which, it increased much more rapidly. This change was due to a transition from stable to unstable flow at a critical rotation speed. In a classic paper, Taylor[98] found that for a gap between cylinders much smaller than the radii and under

a given rotating speed of the outer cylinder, as the rotating speed of the inner cylinder exceeds a certain critical value, rows of cellular patterns are developed[99]. In Taylor's findings, he also discovered that increasing the fluid's viscosity would delay the onset of these instabilities[99]. Taylor's work resulted in what is now known as Taylor vortices, the onset of which can be given by its Taylor number[100]:

$$T_a = \frac{U_i d}{\upsilon}\sqrt{\frac{d}{R_i}} \geq 41.3 \tag{3.6}$$

where d is the gap between the cylinders, R_i is the radius of the inner cylinder (which in this case equates to R_3 in Figure 3.4), U_i is the circumferential velocity of the inner cylinder and υ being the kinematic viscosity. The flow is considered stable below T_a values of 41.3 and unstable above this region (due to the vortices).

Plane Couette flow is the limiting status of Taylor-Couette flow when the radii of the cylinders tend towards infinite dimensions[99]. Plane Couette flow is stable for all Reynolds numbers, while Taylor-Couette flow displays a critical Taylor number from the classical linear stability analysis performed by Taylor[98]. How the linear stability that leads to the formation of Taylor vortices is lost in the case of the plane Couette flow is not known. Other authors have attempted to link these two flows using numerical simulation and experiments[101]. Recent studies show that the instability in shear flows is dominated by the energy gradient in the transverse direction and the energy loss in the streamwise direction for wall-bounded parallel flows[102,103].

Taylor vortices arise in Taylor-Couette flow due to the centripetal force acting on laminar layers at R_3 on the layers at R_4. This results in local circulation, leading to vortices that circulate in opposite directions[98].

At extreme Taylor numbers greater than 1708[100,104], these vortices can lead to turbulent flow. Turbulent flow occurs at a certain critical velocity where molecules or larger particles jump from one layer to another and dissipate a substantial amount of energy in the process[105]. The net result is that a larger energy input is required to maintain turbulent flow than laminar flow at the same velocity. The increased energy input manifests itself as a greater shear stress than would be observed under laminar flow conditions at the same shear rate. This results in an increased viscosity reading.

More detailed experimental study for the flow structure and pattern with the variations of the rotating speeds of the two cylinders has been given in the literature[106],[107].

The bfw/0/100/22 system shall only be considered here. From Figure 3.4, taking the onset of instability to occur at approximately 1200 s^{-1}, and using standard values for the density and viscosity of water, a Taylor number of 44 can be calculated from Eq 3.6.

This is in good agreement with Taylor's finding for the onset of vortices and provides a limiting factor for future work regarding rheology. This is especially important where rheological analysis is done at varying temperatures, i.e. the temperature must not be too high such that it causes the viscosity of the system to drop low enough for Taylor vortices to form.

3.7 Conclusion

The shear characteristics of a model system based on bathfoam and water has been investigated. From this, the limiting characteristics of a Z1 DIN cup and bob geometry system were obtained. To summarise:

1) Values of viscosity calculated using shear stresses below 0.60 Pa are unreliable.
2) The software calculates according to Eq 3.2. This means that a small error in shear rate or shear stress can have large impact on the value of viscosity. Another means of data analysis must be used.
3) At increasing concentrations, bathfoam systems conform more and more to micelle rheology.
4) Low viscosity systems (~ 0.001 Pa·s) at shear rates above 1200s^{-1} are susceptible to laminar instabilities in the form of Taylor vortices that give rise to dramatic increases in viscosity readings

CHAPTER 4: Hydropolymeric/Clay Dispersions

4.1 Introduction

At the end of the last chapter, it was seen that a new method of data processing was required in order to get an accurate interpretation from the raw results given by the rheometer. In this chapter, extra procedures relating to the data processing are introduced in the form of model fits that describe the shearing characteristics of each sample. It is believed that this should act as a means of improving data reliability and to potentially give insight into dispersion phenomena for composite samples.

Although aqueous surfactant dispersions are acceptable for defining the limitations of the equipment, it is not the main focus of interest in this research. The desired material is one that is polymeric and more stable and predictable in nature than micelles that can be created with high concentrations of surfactants. For these reasons a hydropolymer; namely poly(ethylene oxide) (PEO) was selected as the material for this chapter.

Due to the improved stability of a polymeric matrix over that of surfactant micelles, controlled modifications can be made to the system's rheological properties with the addition of inorganic fillers. In this chapter, the addition of montmorillonite (MMT) is added to PEO to form composite samples. MMT was used as the inorganic filler in this chapter due to the large volume of literature that exists on the material.

4.2 Rheology of Poly(ethylene oxide)/Water Systems

Dispersion of fillers is crucial in producing nanocomposites, as it controls the properties of the final product. This has been demonstrated by Song and Youn[108] who

investigated the impact of dispersion on rheological, mechanical, electrical and thermal properties of epoxy/carbon nano tube (CNT) composites. They found that variations in the properties were caused by differing dispersion states of their CNT fillers. The nanocomposites containing poorly dispersed CNTs exhibited higher storage modulus, loss modulus, and complex viscosity than ones with the well dispersed CNTs. This showed rheologically that the poorly dispersed CNTs composite adopt more solid-like characteristics. In contrast to poorly dispersed composites, good CNT dispersion gave an improved tensile strength, electrical and thermal conductivity. Other researchers have also encountered improvements of a material with dispersion, Quercia et al.[109] for their thin film sensors, Lee et al.[110] for their high density poly(ethylene) (PE)/MMT systems and Ramanathan et al.[111] with graphite nanofillers in PMA to name but a few.

Poorly dispersed fillers within a composite system can lead to large aggregates that can cause deterioration in a material's performance[112]. Two factors exist in particulate filled composites. The polymer adheres to the surface of the particles forming an interphase with properties differing from those of the polymer matrix as opposed to the particles interacting with each other forming aggregates. The occurrence and the extent of aggregation depend on the relative magnitudes of adhesion and separation forces[112]. The former depends on the surface tension of the matrix and the particle size and the latter depends on the level of shear forces. Large shear forces and small surface energy favours homogenous distribution, while small particles have a tendency to aggregate.

There consists a large library of research on poly(ethylene oxide). It has been studied theoretically[113,114,115,116,117] often with computational models[118,119,120,] and experimentally. A lot of experimental work has been conducted using dynamic,[121,122,123,124,125] static[122,124,125,126,127,] and Raman[124,128] light scattering. However, it has also been studied with neutron scattering[124] and diffraction[129], nuclear magnetic resonance[124,130], pyrolysis mass spectroscopy[131], Fourier transform infrared spectroscopy[132], differential scanning calorimetry,[132,133] microscopy,[132] viscometry[132,134] isothermal crystallization,[135] thermogravimetric analysis[133] and thermodynamically[136,137].

It is readily soluble in water at room temperature, making simple sample preparation.

PEO with three different molar mass values were studied to this end. The addition of un-modified inorganic clay - montmorillonite (MMT) - was carried out to investigate whether using concentric cylinder rheology could be used to quantify dispersion.

PEO belongs to the polyepoxide group and has a general formula[115] of $\left[\left(CH_2\right)_n O\right]_x$ with n = 2. The solubility of PEO is due to the hydrogen bonding between water molecules and the oxygen on the polymer backbone[115].

PEO is a very fragile material that is easily degraded, which is why in the literature there are many discrepancies regarding its data. It has been reported that PEO degrades at around 225 ºC[131]. It is very sensitive to oxidation which is dependent on its molecular weight. Scheirs et al.[132] investigated the oxidation effects from exposing PEO powder (M_w of 1×10^5 $gmol^{-1}$) exposed to air at 60 ºC. They found that the molecular weight decreased at a slow rate for the first 23 days after which it decreased dramatically.

It was shown by MacLaine and Booth[135] that the crystallinity of PEO reaches a maximum around a molecular weight of 6000 $gmol^{-1}$, and then decreases as the molecular weight increases. Owing to its low crystallinity, low molecular weight PEO is more resistant to oxidation. Mechanical degradation in the bulk system has been reported by Crowley et al.[133] where it was shown that PEO was sensitive to both processing temperature and screw speed during extrusion.

Mechanical shear degradation of PEO in aqueous solution has also been investigated by D' Almeida and Dias[134]. They found that degradation increased with shear stress and hydrodynamic volume. Low concentration solutions were shown to be more susceptible to degradation due to an increase in hydrodynamic volume.

The introduction of nano-sized particulates into the PEO matrix can greatly enhance its inherent properties. H. Geng et al.[138] has shown that the introduction of functionalized CNTs can result in a nano-composite system with greatly increased mechanical properties. The storage modulus and yield strength was shown to increase monotonically with increasing CNT loading.

Regarding PEO, most theoretical[139,140] and experimental work involve the layered silicate MMT [141-156]. The impact of MMT on PEO crystallinity[141,142], adsorption of organic waste water[143], glass transition[144], rheological[145,146], thermal[147,149], mechanical[147,148,149], X-ray diffraction[147,148,149] conduction[149] and nuclear magnetic resonance spectroscopic[150,151] properties have been studied. Other fillers have been used, namely; laponite[152,153,154,155,156] silica[157] and layered double hydroxides[158].

The inspiration for this chapter was based upon the work of Strawhecker and Manias[141]. Their research found that the addition of MMT caused a retardation in crystal growth which resulted in the formation of spherulites with jagged geometries. This crystal growth obstruction due to the presence of MMT allows for more time for many more crystalline nucleation sites to form, which grow to smaller sizes than that of pure PEO spherulites. In the filled systems, a large amount of nucleation sites were observed to initiate in the bulk PEO matrix, far from the silicate surfaces. Despite the different crystal morphologies between neat and filled PEO, no marked change was seen in polymer crystal fraction for small amounts of silicate (<10%). The crystallisation of the filled PEO systems was seen to increase even though the crystal growth was hindered by the MMT. This was a consequence of the increased number of nucleation sites. As the crystallisation rate (as measured by $t_{1/2}$) is the product of nucleation rate and crystal growth rate, it is possible for the overall kinetics to increase despite a slowing down of the crystal growth. Ogata et al.[147] also found that the presence of modified MMT increased the speed of crystallisation.

Rheological analysis has been reported by Hyun et al.[146] They found that the addition of modified MMT led to a sample with higher zero shear viscosity that was more susceptible to shear thinning over that of the pure PEO system. This they claimed was due to the re-orientation of the dispersed clay particles.

The MMT structure (Figure 4.1)[15] consists of a 2:1 ratio of two silica tetrahedral sheets (net negative charge on lamellae surface) and one aluminium octahedral sheet (about 100 nm wide and long) that stack 1 nm thick layers by weak dipolar and Van der Waals forces giving rise to interlayer galleries[142]. The net negative charge present on the lamellar surface of the tetrahedral silicate sheets enables the surface to absorb

cations[146]. The interlayer galleries are normally occupied by cations such as Na^+, Ca^{2+} and Mg^{2+} [142].

The polar nature of MMT makes it highly hydrophilic. When placed into water, swelling occurs as water molecules diffuse into the galleries and cause an increase in interlayer spacing. This process is the prerequisite to intercalation and can lead to exfoliation.

The reaction property of MMT is given by what is known as the cation exchange capacity (CEC). The CEC refers to the total quantity of adsorbed cations (Na^+, Ca^{2+},Mg^{2+}) at a pH value of 7 and its unit of measurement is mmol/100g of layered silicate. The higher the value of a negative charge of a layered silicate, the stronger is the capacity for hydration, swelling and dispersion. The cations within the galleries are exchangeable with other cations such as H^+, multiple nuclei (monomer, inorganic clusters) and organic cations (alkylammonium ion).

When MMT is reacted with an organic reagent, two types of adsorption can occur: ion-exchange adsorption and hydrophobic bonding. If the quantity of organic cation reagent is less than or equal to the CEC value of the MMT, all the organic cations are

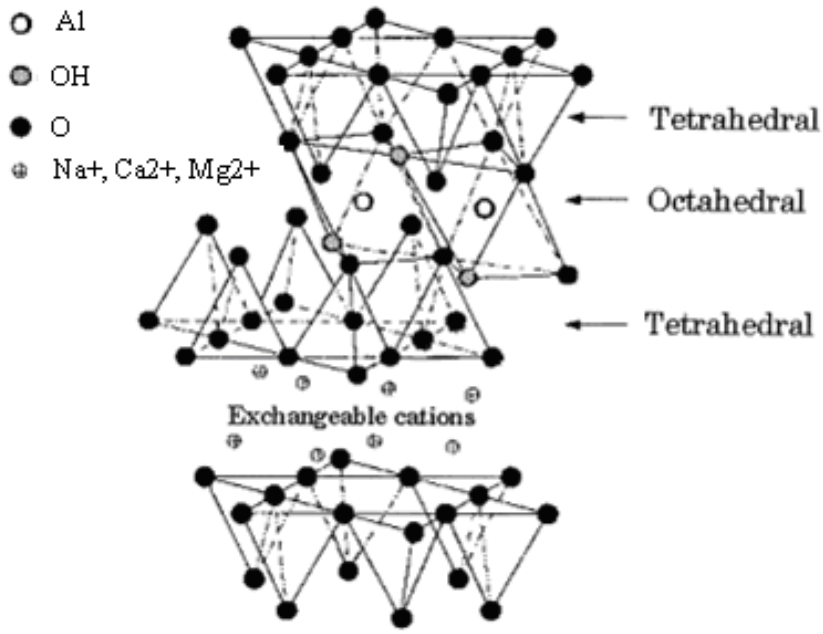

Figure 4.1: Structure of 2:1 smectic clay MMT[15]

absorbed by the MMT by ion exchange, and the ions are not forced out except in high concentration salt solutions. When the quantity is greater than the CEC of the MMT, those already in the layers of MMT will further adsorb organic compounds in the solution by hydrophobic bonds. In practice, the added quantity of organic cation reagent should be less than the CEC value of the MMTs. An overload of surfactant will reduce the stability of the organo-clay. The organic cations are usually cationic surfactants of the quaternary ammonia salt. The cationic headgroup of the alkylammonium molecule normally resides at the layer surface, while the aliphatic tail is away from the surface. The presence of these aliphatic chains in the galleries modifies the original hydrophilic silicate surface to be organophilic[146].

Two terms (intercalated and delaminated/exfoliated) are used to describe the two general classes of nano-morphology. Intercalated structures are well ordered multi-layered structures where the polymer chains are inserted into the gallery space between the individual silicate layers. Exfoliated structures result when the individual silicate layers are no longer close enough to interact with the adjacent layers' gallery cations. Exfoliated structures can therefore be considered well dispersed in the matrix[44]. See Figure 4.2[15].

In general, there are three different approaches to the synthesis of a polymer-clay nanocomposite. These are as follows:

1) Melt intercalation process for thermoplastic polymers: Organic polymer pellets and treated clay directly mixed in an extruder. The shear force from the extruder and the melt process serves to disperse the clay in the matrix[159,160].
2) Solution method: Both organoclay and polymer precursor are dissolved in a polar organic solvent (chloroform). This causes the clay to swell to promote intercalation[141,145,146].
3) *In-situ* polymerization: This method requires that the initial mixing of the monomer with the organo-clay. During this process, the monomer is able to diffuse into the interlayer spacings. Upon polymerization using the correct reaction conditions exfoliation should take place[161].

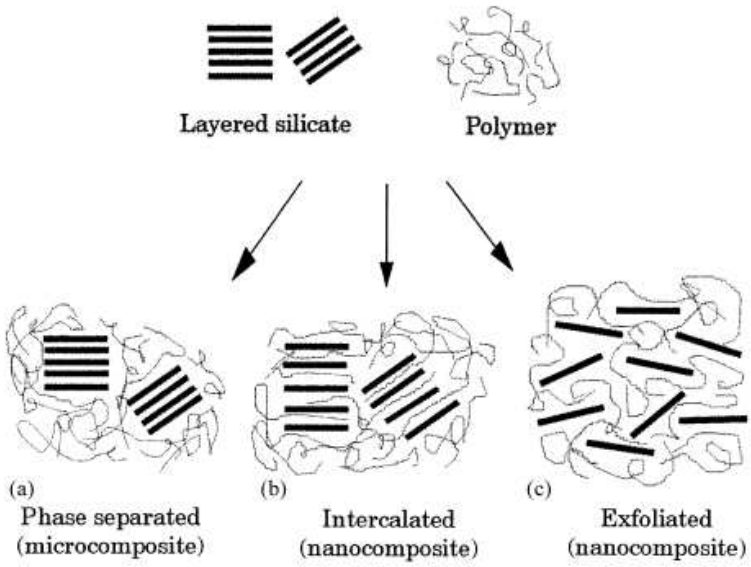

Figure 4.2: Formation of different types of composite arising from the interaction of polymer and layered silicate, mainly intercalated and exfoliated nanocomposites

For a system containing PEO as the polymeric matrix, the melt intercalation method is inappropriate given its degradation susceptibility at high temperatures. Given PEO's water soluble properties, the solution method is therefore the natural choice for sample preparation.

4.3 Materials and sample preparation

PEO was obtained from Sigma-Aldrich with the molar masses $1x10^5$, $4x10^5$ and $1x10^6$ g mol $^{-1}$. These molar masses were chosen because three varieties were desired that represented an even spread around those most commonly found in the literature. As the rheometer is only capable of holding ~ 20 ml samples, 20 g of water was chosen for the amount of solvent used with the PEO. It is popular to use amounts from 1-10% PEO when mixed with a solvent, for this reason 5% was chosen. This means that approximately 1 g of PEO was dissolved in 20 g of distilled water at room temperature. Mixing was carried out using a magnetic stirrer bar. The time for stirring was timed until the solution was homogenous in texture and colour; this was

approximately 3 h, over night, and 3 days for weights $1x10^5$, $4x10^5$ and $1x10^6$ g mol^{-1} respectively.

MMT (used as supplied) was obtained from Sigma-Aldrich. For samples containing the clay filler, 0.05 g of MMT was mixed in 5 ml of water to promote swelling of the clay galleries for improved intercalation[155]. This was then added to a separate solution containing 15 g of water and 1 g of PEO and was left to mix for approximately 30 min.

All rheology was performed by linearly increasing the imposed shear stress from 0 to 65 Pa (ramp up), whereupon it was held constant for 5 min (unless otherwise stated) before being linearly decreased back down to 0 Pa (ramp down). The experiments were carried out at room temperature. For ease of reading, the samples have been abbreviated by code names, see Table 4.1.

4.4 Experimental Procedure

I. Shearing Times and its Effect on Rheology

PEOM-1000k/5 and PEOM-1000k/0 were subjected to a linear shear ramp up to 30 Pa, where upon being held at a constant shear stress followed by a ramp down to 0 Pa. The duration where the shear stress is constant starts of at 30-60 s and is made progressively longer after each run until it is being held for approximately 100 min. The time PEOM-1000k/5 was left in the presence of shear was 157 min at 35 ºC.

II. Shear history and its Effect on Rheology

PEOM-400k/0 were subjected to rheological ramp ups to 14.5 Pa where upon they were held constant for 30 s before being ramped down to 0 Pa. The time interval between each successive run was varied from approximately 1 to 70 min at 25 ºC.

Table 4.1: Sample description and codes

Sample description	Sample code
100,000 M_w PEO and water	PEOM-100k/0
100,000 M_w PEO and water and MMT	PEOM-100k/5
400,000 M_w PEO and water	PEOM-400k/0
400,000 M_w PEO and water and MMT	PEOM-400k/5
1,000,000 M_w PEO and water	PEOM-1000k/0
1,000,000 M_w PEO and water and MMT	PEOM-1000k/5

III. Rheological analysis of viscosity as a function of sample volume

Rheology was conducted on 100,000 M_w PEO in water at 5%, 10% and 20% weight ratios. The sample volume at each concentration was varied from 5, 10, 15, 20, 22.5 and 25 ml.

IV. Rheological analysis of 1:1 PEO to MMT

Rheological analysis was performed on a sample containing 1 g PEO and MMT in water prepared in the standard manner.

V. Rheology and Dispersion

PEOM-1000k/5 was prepared in the standard manner except no magnetic stirring was carried out. This was prepared for the purpose of seeing the effect of shear on a

sample under the influence of minimum dispersion. The only stirring carried out was that from a glass stirring rod.

Samples from PEOM-100k/5 and PEOM-100k/0 were prepared in the standard manner and then dehydrated in a vacuum at 40 ºC for 2 -3 days. Dried aliquot were then melted and quenched at 25 ºC onto a microscope slide where polarising microscopy could be carried out.

4.5 Data Processing

Figures 4.3 and 4.4 show rheological data obtained from the 100k, 400k and 1000k samples respectively. From Figure 4.3 it is evident that the shear stress increases linearly with shear rate, indicating that the system belongs to a Newtonian fluid[1]. Increasing the molar mass introduces shear thinning to the rheology (Figure 4.4 (a) and 4.4 (b)).

The molar mass dependence of rheological data for hydrocarbon end capped PEO has been reported by Ma and Cooper[162] where the increase of shear thinning becomes stronger as one moves towards higher masses. Although they investigated shear thickening PEO with a $C_{18}H_{37}$ end group, from their plots, it can be seen that there is a noticeable increase in viscosity from 0.1 to 50 Pa s for the molar masses 10,000 and 35,000 $gmol^{-1}$ at 15 °C. The shift in shear thinning is also strongly evident as the onset starts at 300 s^{-1} for 10,000 $gmol^{-1}$ where as at 35,000 $gmol^{-1}$ it initiates at 45 s^{-1}. Unmodified 10,000 $gmol^{-1}$ PEO at 3% wt loading gave a viscosity of approximately 0.002 Pa s.

Khan[163] carried out viscometry measurements using a capillary viscometer in order to calculate the intrinsic viscosity of PEO and water systems. He used three M_w; 625,000, 896,000 and 1,038,000 $gmol^{-1}$. The specific (relative viscosity – 1) and reduced (specific viscosity/concentration) viscosities were used using Huggins plots to calculate the intrinsic viscosity. Intrinsic viscosity was seen to increase with molecular weight and decrease with temperature. Static light scattering experiments were carried out using Zimm Plots to investigate aggregation phenomena. This is carried out by

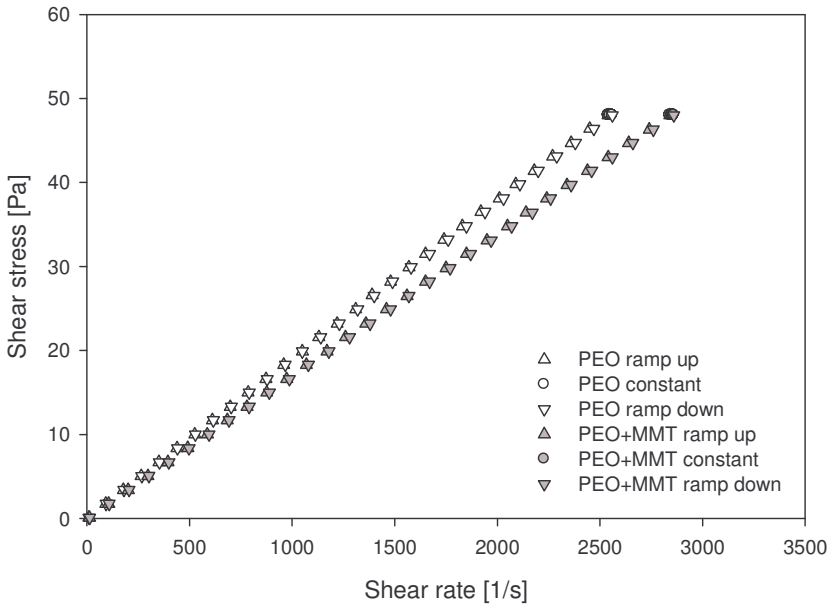

Figure 4.3: Shear stress as a function of rate for PEOM-1000k/5 and PEOM-1000k/0

measuring the angular dependence of the scattered light. It has been shown that low M_w PEO has a tendency to aggregate[127].

Ortiz, De Kee and Carreau[164] have conducted rheology on concentrated PEO solutions using both water and glycerine as a solvent (50% each) over the M_w 300k to 5000k kg/kmol. They used a variety of rheometers depending on the nature of the sample – from Weissenberb rheogoniometers, Ubbelhode capillary, parallel plate and concentric cylinder.

For their 1000k PEO and water systems at loadings of 2%, 3% and 5%, a zero shear viscosity of 0.5, 2.2 and 52.9 Pa s was measured respectively. Higher and lower M_w's yielded higher and lower zero shear viscosities respectively.

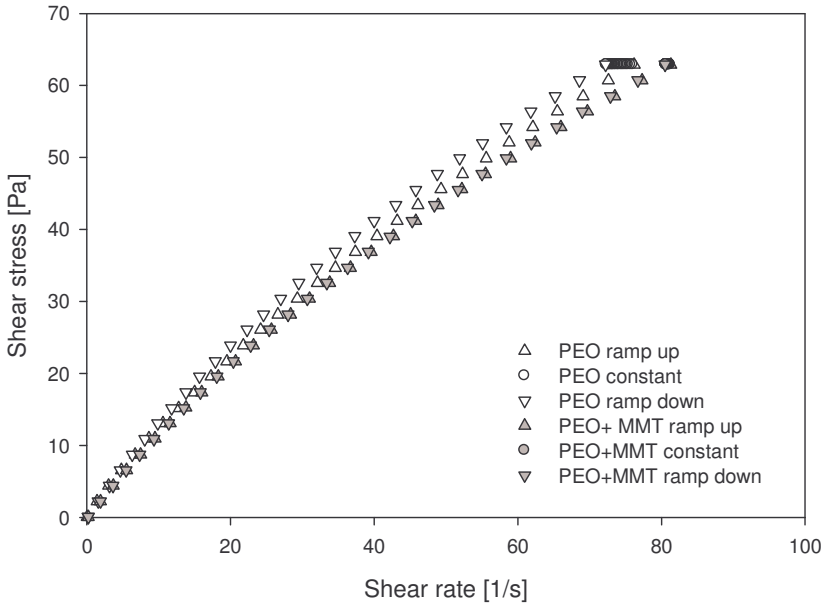

(a)

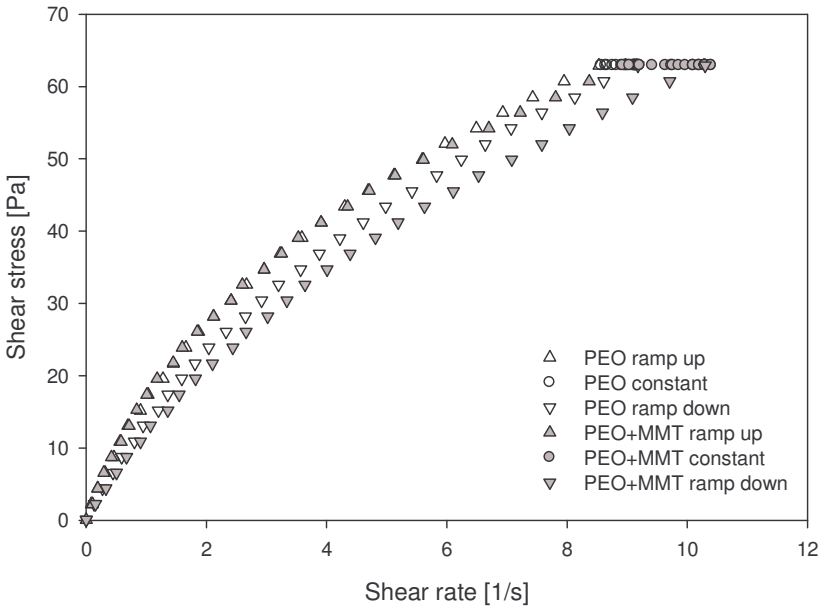

(b)

Figure 4.4: Shear stress as a function of rate for (a) PEOM-100k/5, PEOM-100k/0 and (b) PEOM-400k/5 and PEOM-400k/0

As stated at the start of this chapter, the objective for this work is to investigate the rheological properties of a filled hydropolymer to quantify dispersion. By doing this a secondary objective can be carried out in parallel, that being to develop a technique for analyzing data where the viscosity errors at low shear stresses can be negated. A method of dealing with this secondary problem can be found by fitting a function that conforms to experimental data and then, differentiating it.

Functions are often fitted to rheological data in order to gain insight into the physical processes occurring in the system. In many cases where shear thinning is evident, the shear stress can be said to depend on the shear rate in this shear rate region according to the Ostwald-de Waele equation[1] seen in Chapter 3.

$$\sigma = K\dot{\gamma}^n$$

Where σ is the shear stress, $\dot{\gamma}$ is the shear rate and *K* and *n* are constants.

This power law model has successfully been used to describe the shearing characteristics of many commercial food products such as German liquid honey[165], which was seen to exhibit shear thinning behaviour over 20-30 °C and 30-50 °C for crystalline honey. Carrot juice[166]; where the model described pasteurized juice from 200–1600 s^{-1}. Baby fruit purees[167], where the model successfully described the shear thinning behaviour of 2 out of 5 purees from 20 to 40 °C over the shear range 0 – 450 s^{-1}.

Composite materials such as modified trans-1,4-isoprene and wood flour have been studied[168] where the shear thinning behaviour was described by the Ostwald-de Waele model over 0-10 s^{-1}. The power law index was seen to decrease with the addition of increasing amounts of compatibilizer to the isoprene matrix.

Aqueous dispersions of carbon nanotubes have also successfully been described by the model at shear rates post 10 to 30 s^{-1}, depending on concentration[169]. Other models had to be employed to describe the behaviour below this level. A single model to describe the results were found as (a) the Herschel-Berkly for low concentrations – where a gradual transition from yield stress to power law behaviour could be modelled

and (b) the Bingham – superior fit at higher concentrations due to it being able to go suddenly from yield stress to Newtonian behaviour.

With respect to its versatility, this model is the simplest. Its single varying parameter can describe a shear thickening ($n > 1$) and shear thinning ($n < 1$) and a Newtonian ($n = 1$) solution.

This power law function was fitted to experimental data for PEOM-1000k/0 and can be seen in Figure 4.5. Sigma Plot 10.0 was used to models to the experimental data. As can be seen from Figure 4.5 the fit is poor; the residuals indicate that the form of data does not conform to this equation. Residual values are calculated values of shear stress subtracted from the ones returned by the rheometer software.

An ideal fitting function will display residuals that are small and randomly distributed. As the power law function has been proven to fail for this system a superior one needed to be found. To this end, numerous functions were considered, but the function that gave the best fit for all three systems was a 3 parameter hyperbolic function:

$$y = \frac{ax}{b + x} + cx \tag{4.1}$$

where y is the shear stress, x the shear rate and a, b, c are control parameters.

This can be seen for all molar masses in Figures 4.6-4.8.

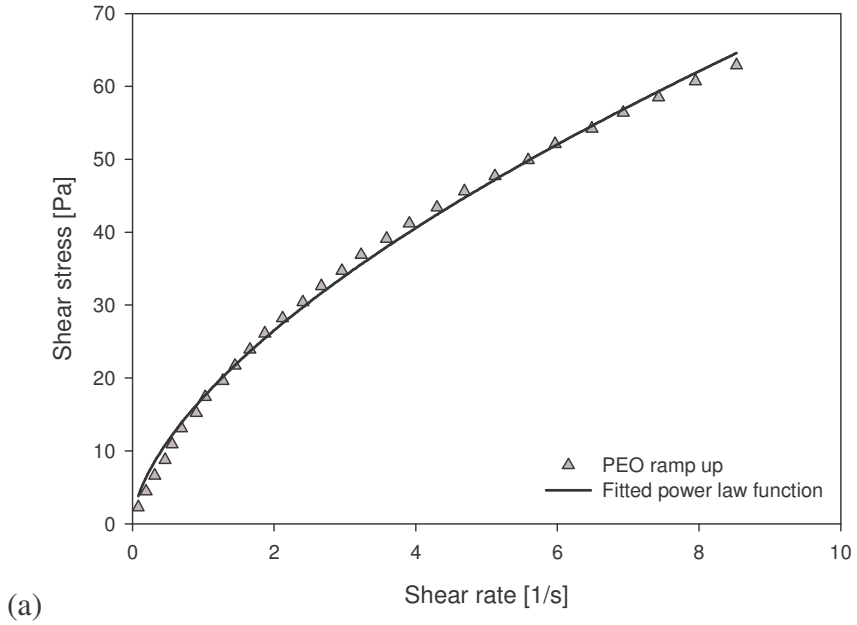

(a)

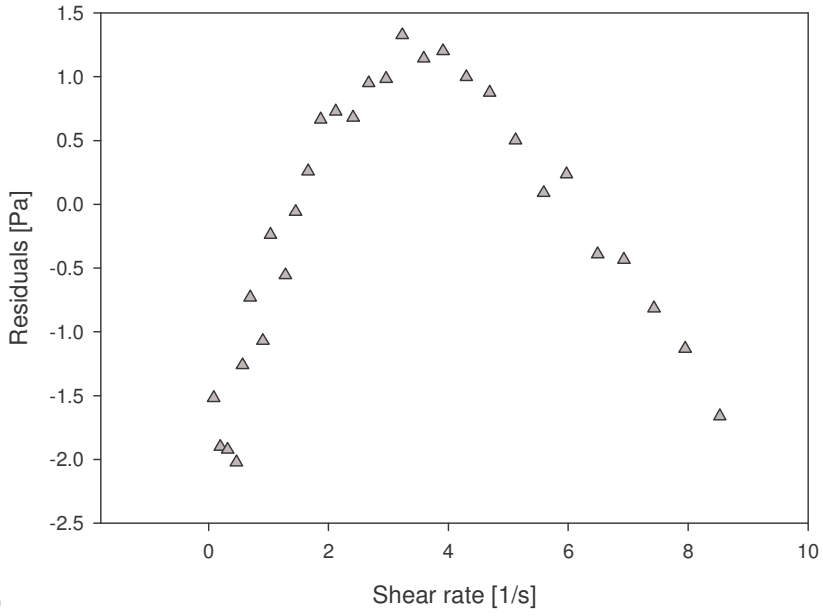

(b)

Figure 4.5: Shear stress as a function of shear rate for (a)PEOM-1000k/5 ramp up fitted with a power law function and (b) residuals obtained from experimental data and power law function.

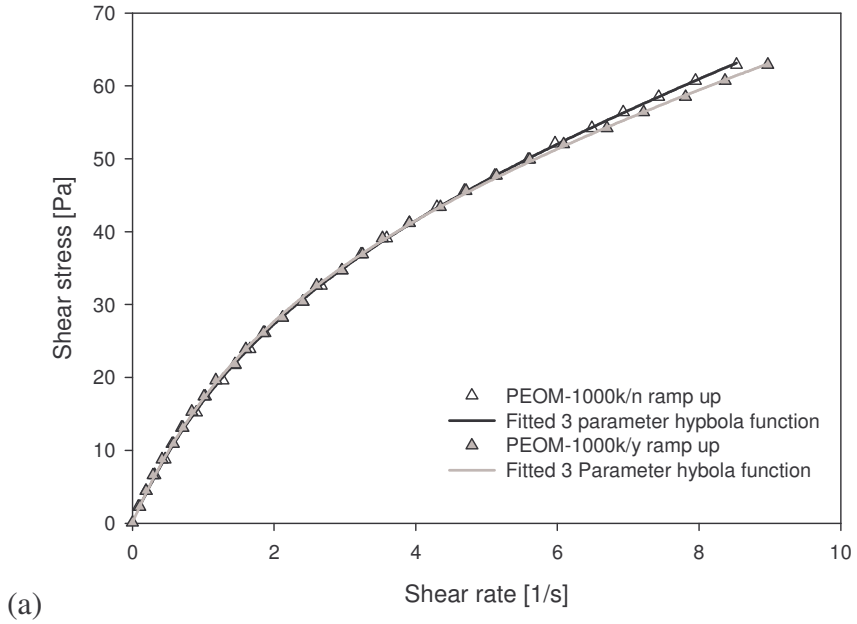

(a)

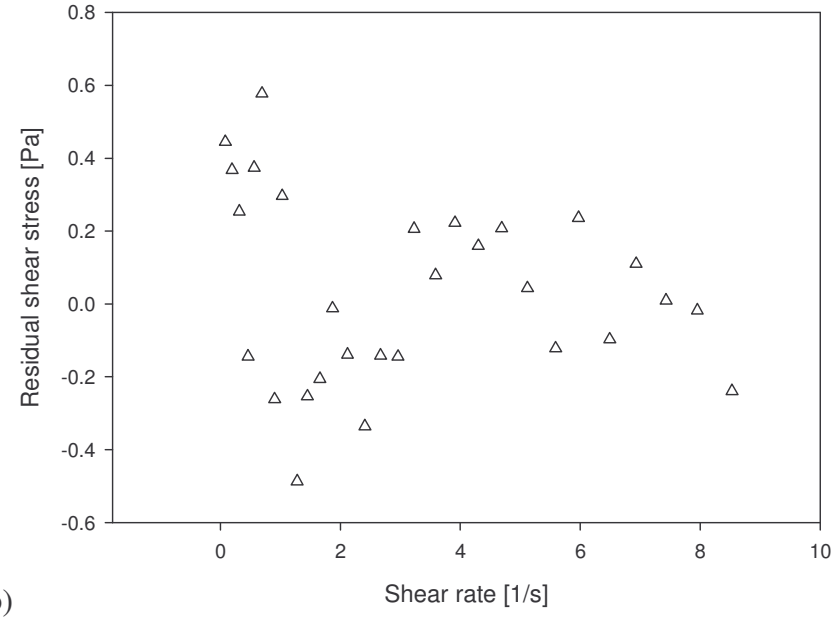

(b)

Figure 4.6: Shear stress as a function of shear rate for (a) Experimental results for PEOM-1000k/5 and PEOM-1000k/0 with a fitted 3 parameter hyperbolic function and(b) Residuals for the PEOM-1000k/0 system.

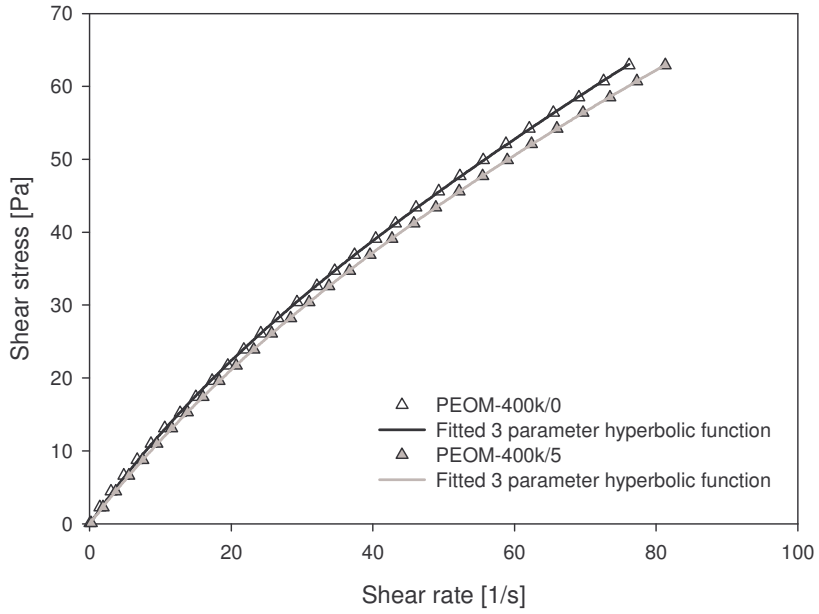

(a)

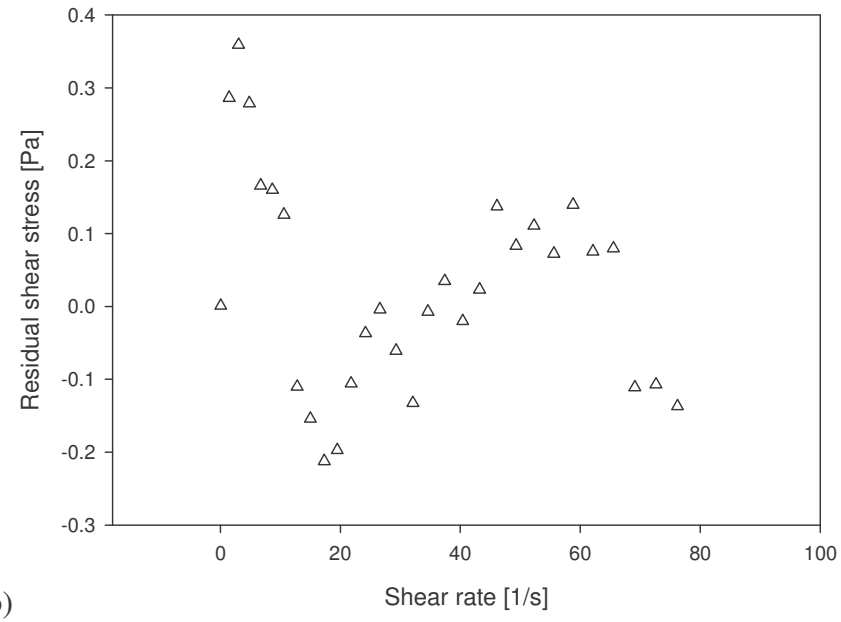

(b)

Figure 4.7: (a) Experimental results for PEOM-400k/5 and PEOM-400k/0 with a fitted 3 parameter hyperbolic function. (b) Residuals for the PEOM-400k/0 system

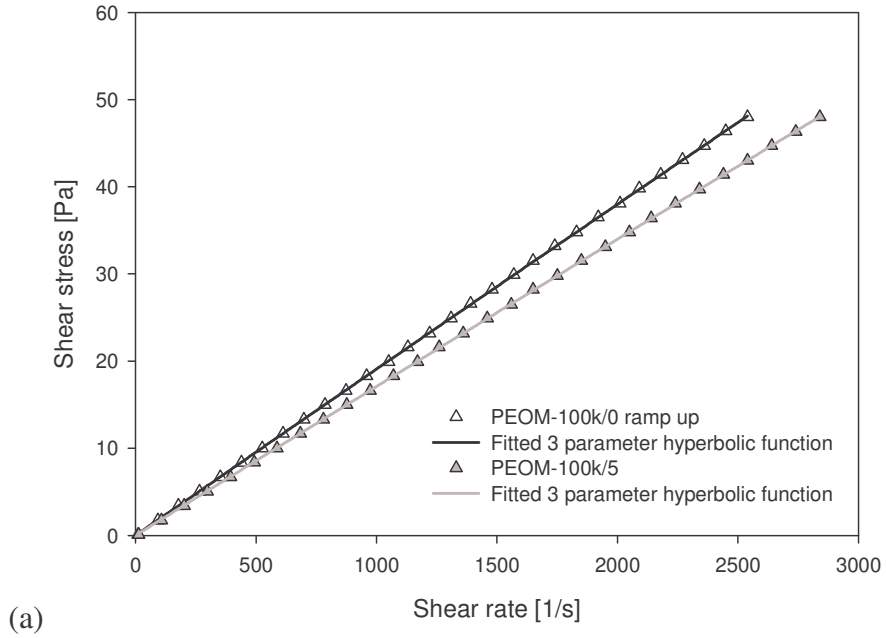

(a)

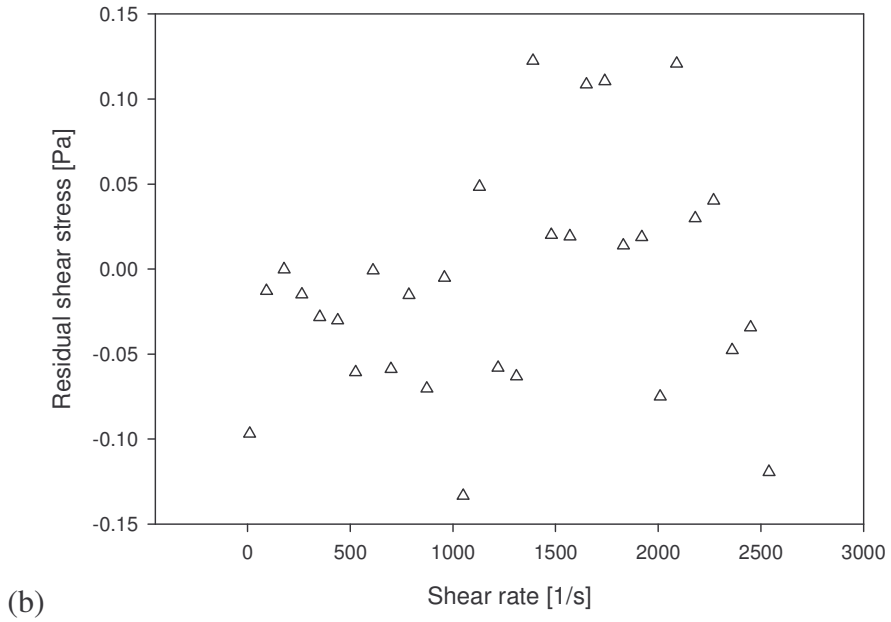

(b)

Figure 4.8: (a) Experimental results for PEOM-100k/5 and PEOM-100k/0 with a fitted 3 parameter hyperbolic function. (b) Residuals for the PEOM-100k/0 system

As can be seen from Figure 4.6(b), 4.7(b) and 4.8(b) the residuals that result from adopting this function are randomly distributed around the zero mark. This indicates that the hyperbolic function has a good fit to experimental results. The magnitude of the deviation from zero is also much smaller using the hyperbolic function; which peaks at 0.6 compared to 2.0 from the Ostwald de Waele power law function.

By differentiating equation (4.1) it is then possible to find the equivalent function for viscosity as a function of shear rate:

$$\frac{dy}{dx} = \frac{ab}{(b+x)^2} + c \tag{4.2}$$

The viscosity plot for PEOM-1000k/0 and PEOM-1000k/5 can be seen from Figure 4.9. Choi et al.[145] and Hyun[146] et al. who both worked with PEO-MMT composites applied the Carreau model for investigating the dependence of shear stress and rate for non-Newtonian viscosity curves for various polymeric systems. This model is unsuitable for the trends presented here so a different model was selected. This model is known as the De Kee model[170]:

$$\eta = \eta_1 e^{-t_1|\gamma|} + \eta_2 e^{-(0.1)t_1|\gamma|} + \eta_\infty \tag{4.3}$$

The parameters are η_1, η_2, η_∞ and t_1. The first three parameters have units of viscosity and the parameter t_1 has units of time. The model was derived by De Kee and Carreau in 1979[171] using Lodges molecular network theory[170]. The aim was to develop a simple to use model which can fit several material functions with parameters that can be easily determined and be physically meaningful. With respect to the network theory, De Kee made a significant contribution by proposing empirical relationships for the dependence of the probabilities of loss of segments on the rate of strain and the inverse dependence of the probabilities of loss on segments. The result is that the viscosity can be obtained by the summation of simple exponential functions as shown in Eq (4.3). In the same paper, the authors tested the model on a 4% (by weight) of polystyrene in Aroclor 1248 (chlorinated diphenyls), a 1% solution of polyacrylamide in a 50% mixture of water and glycerine and lastly a 6% solution of polyisobutylene in Primol (pharmaceutical grade white oil). A good fit to their data was found with a two exponential term model, especially at high shear rates. The failure to accurately

describe data in the low shear regime was attributed to shortcomings of the Weissenberg rheogonoimeter that they used. A three exponential term model improved the situation considerably. For all of the solutions De Kee and Carreau studied, they observed that the characteristic times followed the relationship $t_n = 10 \times t_{n+1}$ i.e. for all solutions studied the parameters t_n and t_{n+1} always differed by one order of magnitude and for cases where the constant a differs appreciably from 10, the η_n values could be adjusted to ensure acceptable predictions. This factor of 10 relationship between the characteristic times means that the number of parameters in the model can be reduced. Because of the exponential formulation, it is easier to treat the data in a semi-logarithmic fashion. This is so that the parameters η_n and t_n are easily estimated from the intercepts and slopes (at high shear rates) of the viscosity data. If the data follow a straight line on such a semi-log representation, they can be represented by a two-parameter version of Equation (4.3), given by the first term on the right side.

Viscosity/shear rate data were obtained for all samples and compared to the De Kee model.

4.6 Results

As can be seen from Figure 4.9 to Figure 4.11 the De Kee model offers a good fit to the viscosity data. From looking at the residual data for each sample, the distribution can be seen not to be randomly distributed. Instead it fluctuates about the zero mark. Although this trend resembles the one displayed by the power law function, the main difference is the dispersion of the data from the zero point, which at worst gives a deviation of about 3%.

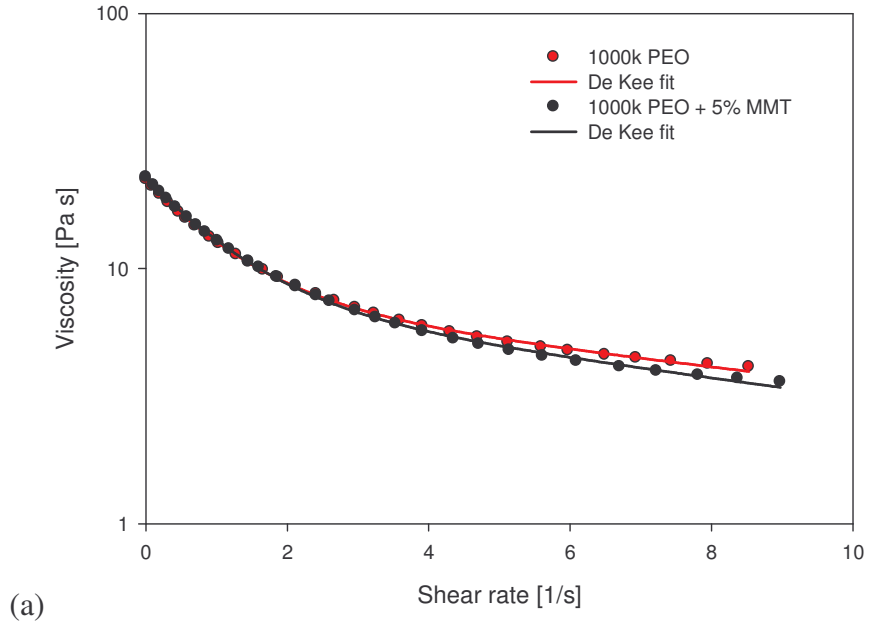

(a)

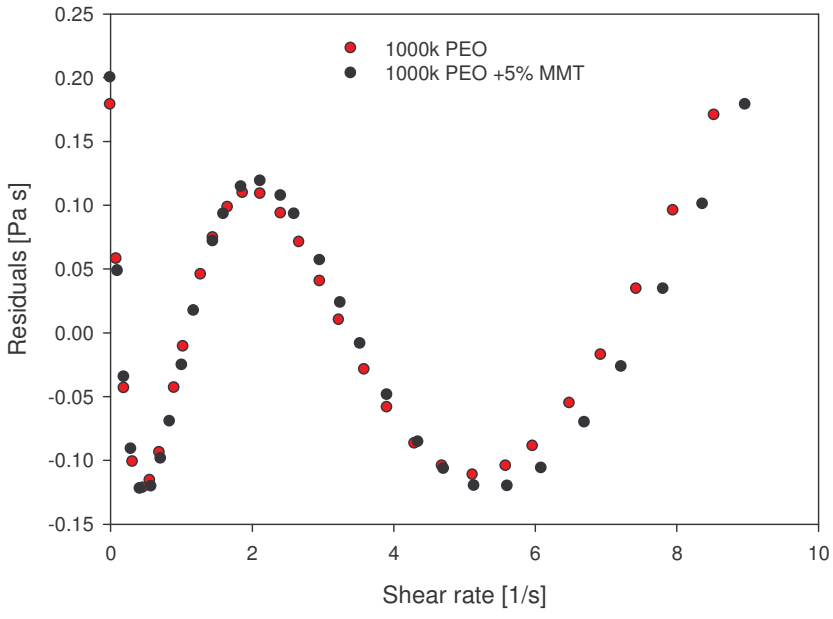

(b)

Figure 4.9: PEOM-1000k/5 and PEOM-1000k/0 (a) Viscosity as a function of shear rate with fitted De Kee models and (b) residuals.

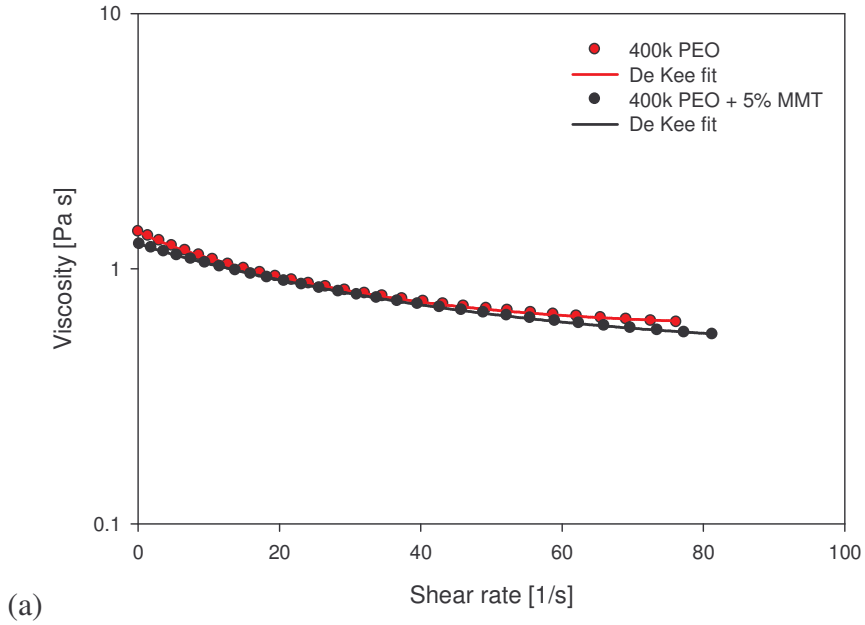

(a)

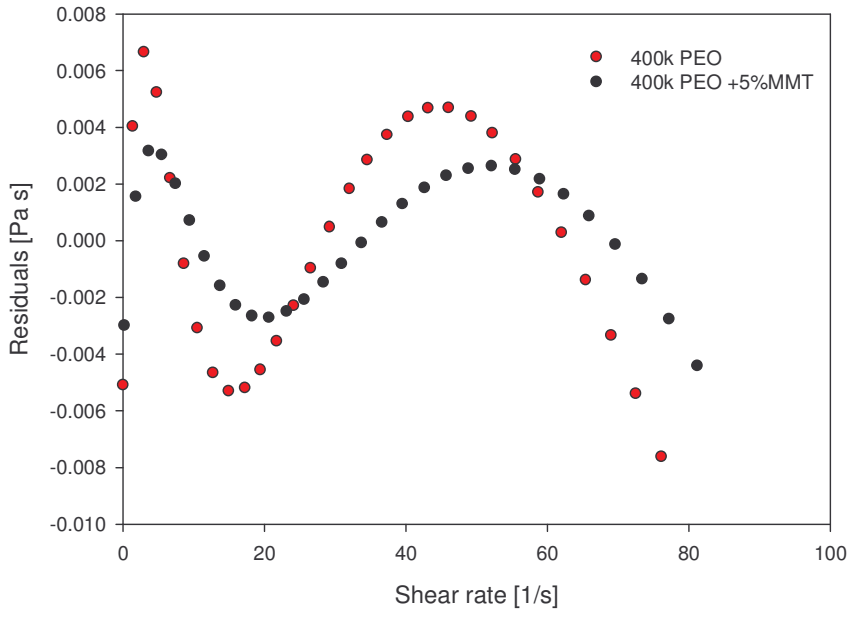

(b)

Figure 4.10: PEOM-400k/5 and PEOM-400k/0 (a) Viscosity as a function of shear rate with fitted Carreau models and (b) residuals.

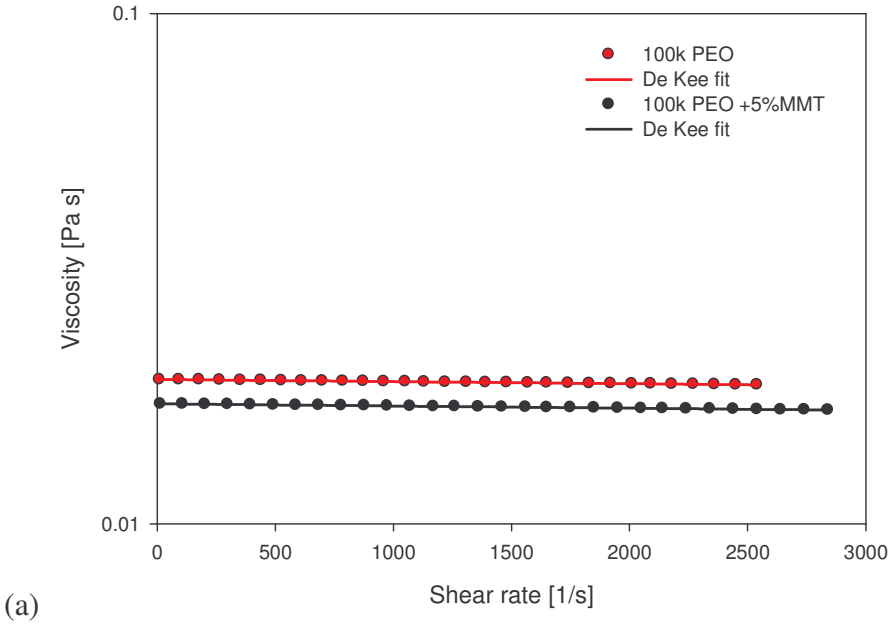

(a)

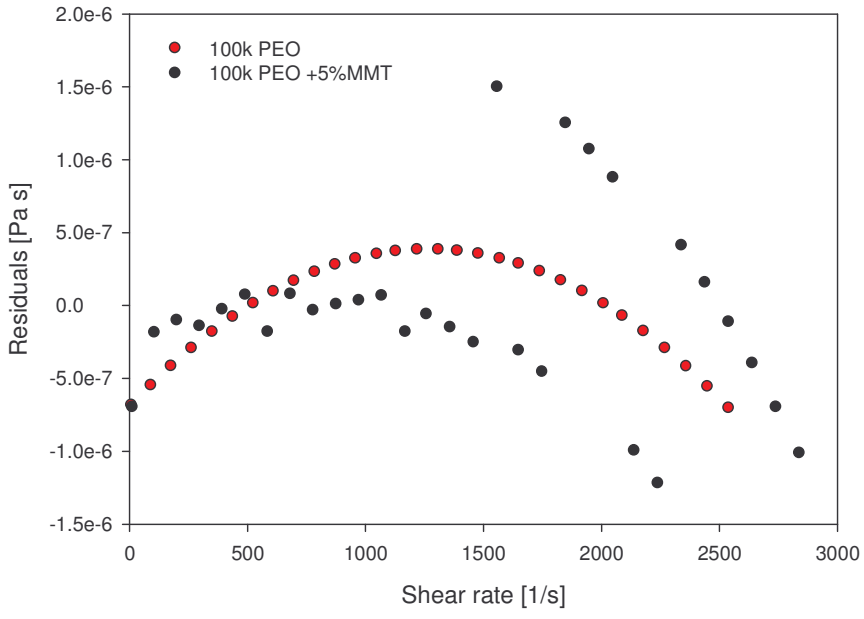

(b)

Figure 4.11: PEOM-100k/5 and PEOM-100k/0 (a) Viscosity as a function of shear rate with fitted Carreau models and (b) residuals.

The lower the molar mass, the smaller the residual scatter becomes. This is because the sample is approaching the Newtonian fluid regime where n → 1, therefore less influence is needed from the correction factors to make the function fit a shear thinning curve. This is most evident from Figure 4.11 where the sample shows Newtonian behaviour, where the residual deviation can be said to be zero.

The residual scatter plots also show that the systems containing MMT are more likely to behave like the pure PEO systems for higher molar masses. This can be seen most notably in Figure 4.9 (b) where for 1000k molecular weight the residuals are virtually identical compared to that of Figure 4.11 (b) where for 100k molecular weight there are definite 'kinks' in the scatter.

Another trend can be seen regarding the viscosity of samples containing pure PEO and those with MMT. The lower the molar mass of the matrix, the greater the difference in viscosity between the curves, where the samples containing MMT always having the lower viscosity. In order to disregard this difference from that of instrumental error, a series of repeated tests were carried out. These tests not only give a measure of reliability of the instrument with regards to repeatable results, but also test the dispersion characteristics with extended shear stress times.

The zero shear viscosity for PEOM-1000k/0 is approximately 23 Pa s. This is in excellent agreement with Ortiz De Kee and Carreau[164] who obtained 22 Pa s for their 5% 1000k PEO and water system. A possible reason why their value is slightly lower than the one presented here could be due to their measurements being carried out at 25 °C as opposed to room temperature ~22 °C.

I. Shear history and its Effect on Rheology

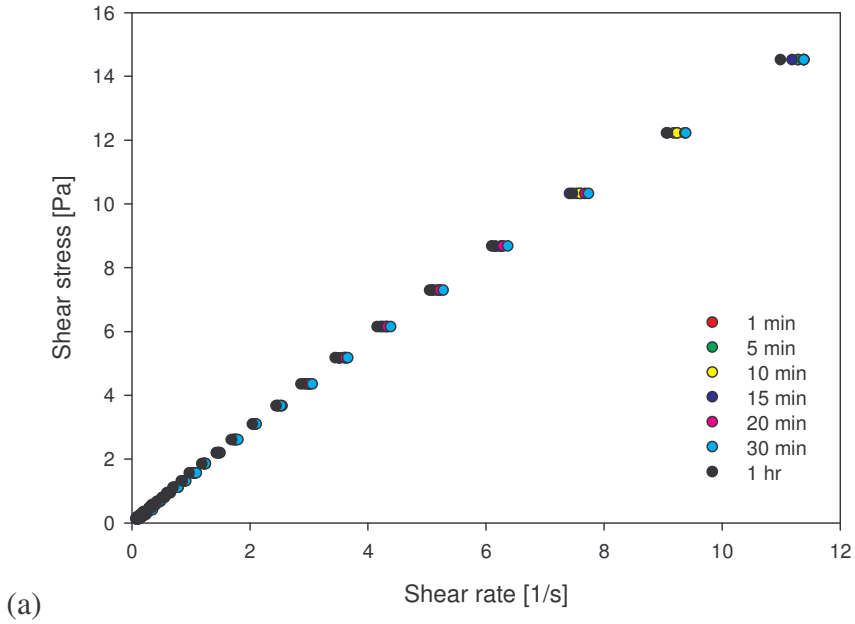

(a)

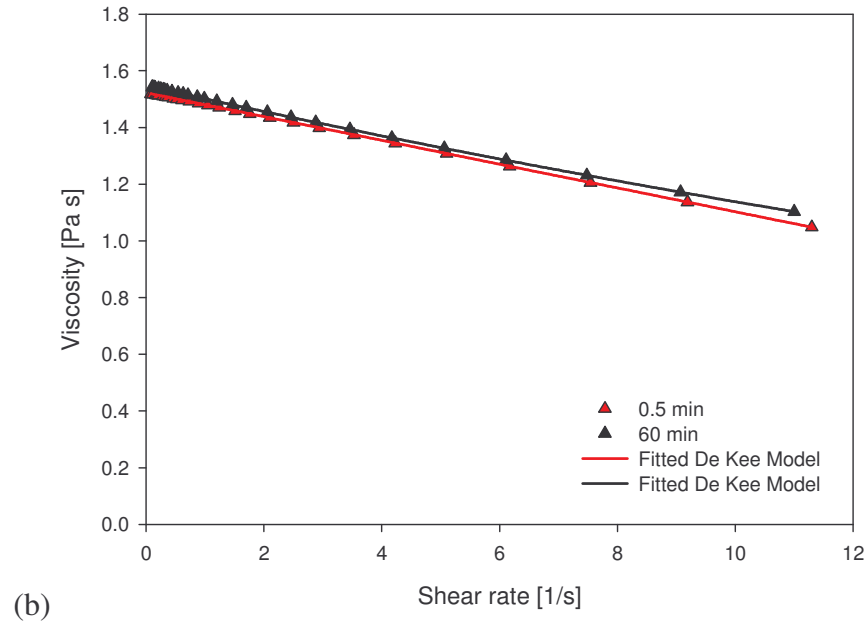

(b)

Figure 4.12: PEOM-400k/0 (a)Shear stress as a function of shear rate and (b) Viscosity as a function of shear rate with a fitted De Kee model.

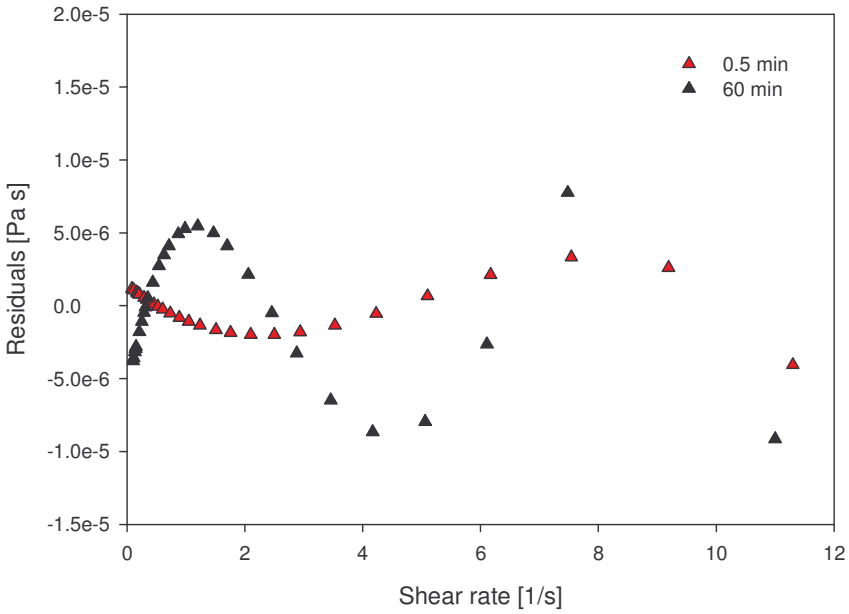

Figure 4.13: Residual plot between the De Kee model and calculated viscosity PEOM-400k/0

As can be seen in Figure 4.12 (b), the effect of history on the rheological characteristics seems to have no effect on the pure PEO system. There is a constant 2% difference between the two curves which is due to uncertainty within the experiment. This error in the equipment is confirmed in section 4.5.4 where repeated measurements have been taken with varying amounts of 100k PEO in the measuring cup.

II. Shearing Times and its Effect on Rheology

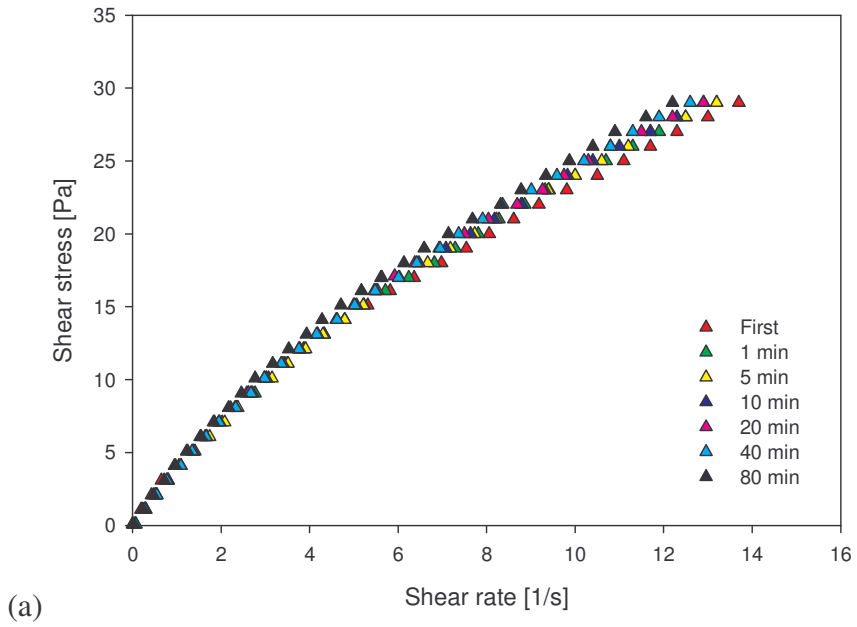

(a)

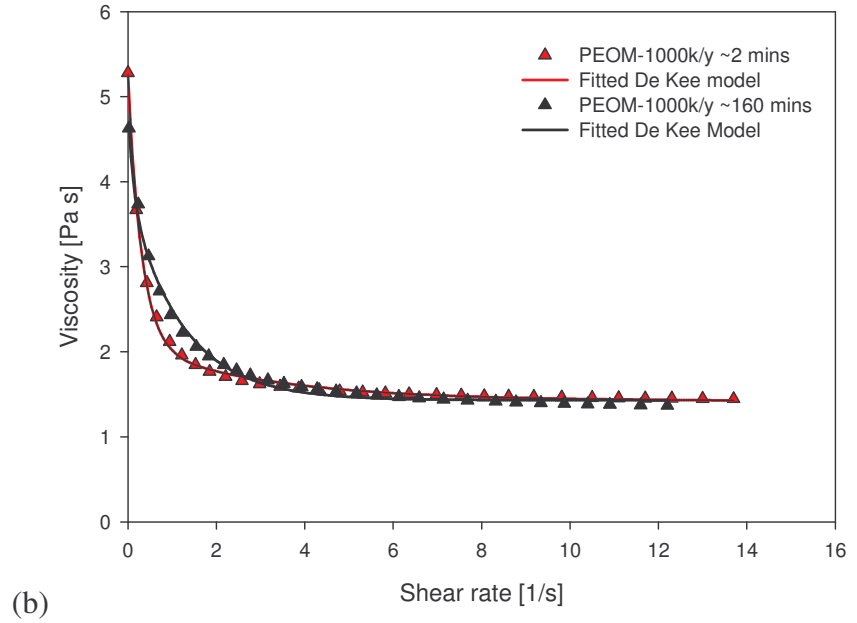

(b)

Figure 4.14: PEOM-1000k/5 (a) Shear stress as a function of rate for (b) viscosity as a function of shear rate with a fitted De Kee model

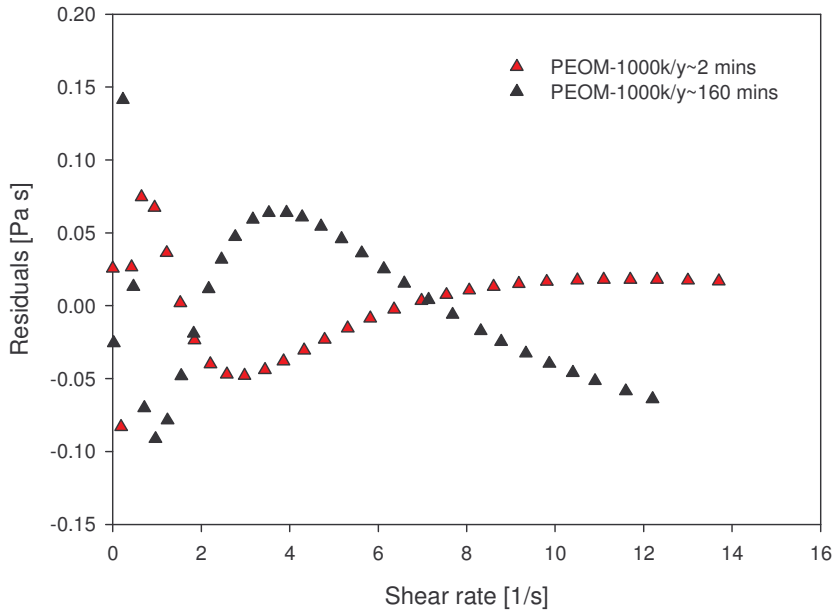

Figure 4.15: PEOM-1000k/5 residuals between the De Kee model and calculated viscosity.

From Figure 4.14 (a) and (b) there is a noticeable difference in what the data shows. In Figure 4.14(a) it would seem that the viscosity increases with time as the gradient of the curve increases. However, Figure 4.14(b), which is a far more accurate representation of viscosity, shows that there is minimal change of 0.08 between the last data points which is approximately 2%. This is seen from the very close correlation between the 1.5 min and the 160 min sample. From this it can be concluded that the MMT is thoroughly dispersed prior to rheology, and any extra dispersion taking place is too subtle to be shown in the rheology for the present volume fraction of MMT.

III. Rheological analysis of PEO as a function of sample volume

In order to observe the relationship between viscosity and sample volume during rheological measurements, 5%, 10% and 20% PEO concentrations were carried out at varying sample volumes in the measuring cup. This test was carried out to demonstrate the importance of the relationship of the variable *A* in Eq. (3.1) and (3.2) and the validity to which it extends for the measuring cup.

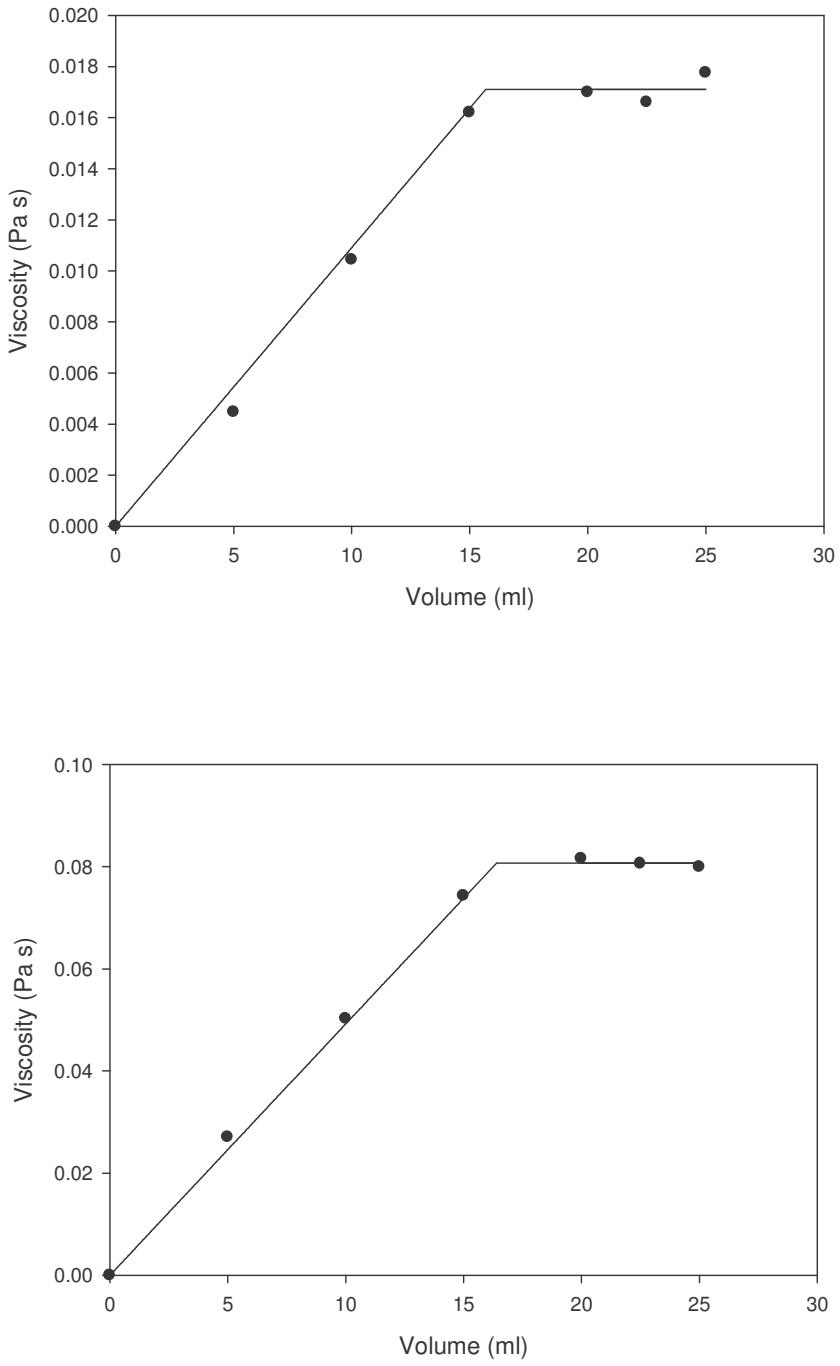

Figure 4.16: Viscosity as a function of volume for (a) 5% and (b) 10% PEO loadings

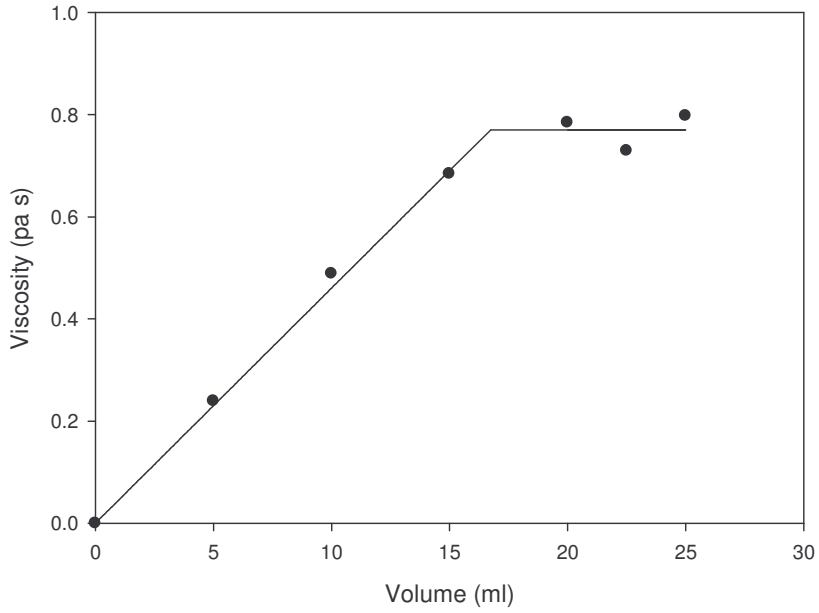

Figure 4.17: Viscosity as a function of volume for 20% PEO loading

As can be seen from Figures 4.16 and 4.17 there is a linear relationship between viscosity and sample volume. An equation of a straight line through the origin was used for the data 5 to 15 ml and a mean average value was taken for the horizontal line between 20 and 25 ml. The intersection of the two lines can be seen to be approximately 16 ml, which is expected as the total volume was calculated to be 16.6 ml in Chapter 3. Table 4.2 shows the gradient of the straight line over the volumes 0 to 15 ml and the statistics of the horizontal – 20 to 25 ml - for the concentrations 5%, 10% and 20%.

This result can be used to verify that the difference in viscosity for the data in Figure 4.11 between PEOM-100k/5 and PEOM-100k/0 is nothing more than uncertainty within the equipment, as the difference in the viscosities lies within 3 standard deviations of this result. This means that the equipment is not sensitive enough to detect subtle changes in the viscosity caused by the presence of MMT filler at its current volume fraction.

Table 4.2: Statistical values for 5%, 10% and 20% PEO loadings

	5%	**10%**	**20%**
Gradient	1.09e-3	4.92e-3	4.60e-2
Mean	1.71e-2	8.07e-2	7.70e-1
Standard Deviation	5.86e-4	8.27e-4	3.64e-2

IV. Rheological analysis of 1:1 PEO to MMT

As can be seen in Figure 4.18, there is an increase in viscosity with the addition of an equal mass of MMT to the PEO/water system. A quantitive way of analyzing these results would be to compare parameter values from those used in the De Kee model. Table 4.3 shows these values.

Sigma Plot 10.0 was used to output the coefficients t_1, η_1, η_2 and η_∞. The only condition applied during the least squares fitting procedure was that the outputs be greater than zero. No constraints were used for the control parameters outputted from the hyperbolic function (Eq. 4.1) while calculating the viscosities.

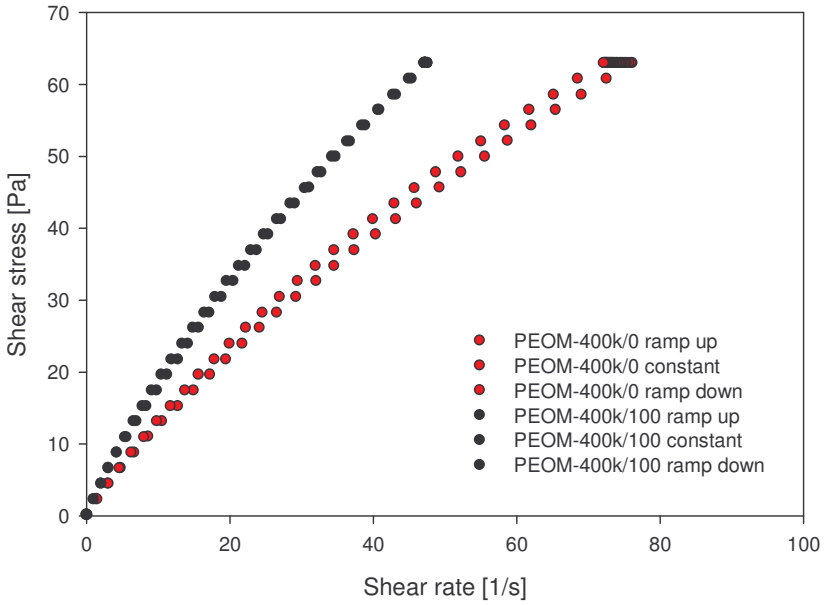

(a)

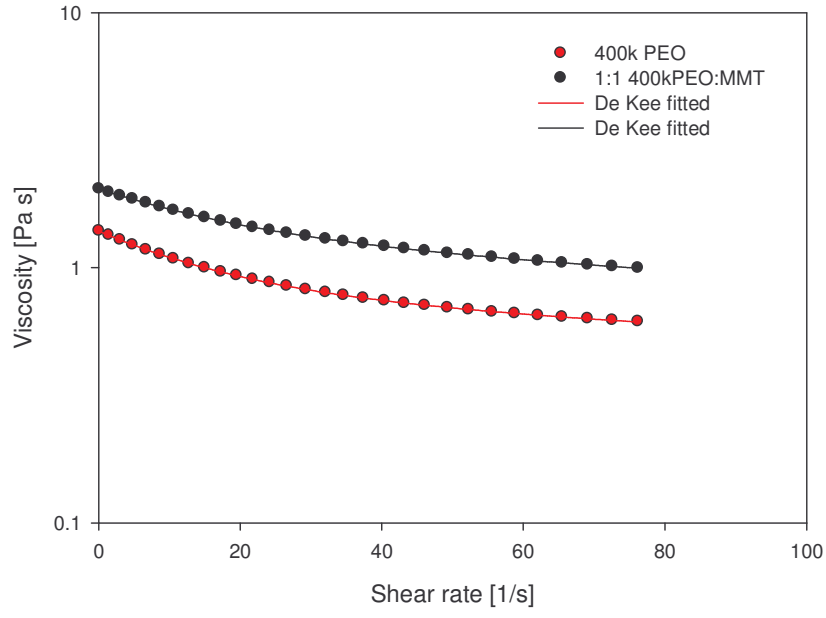

(b)

Figure 4.18: for parts PEO to MMT 1:1 for PEOM-400k/100 and PEOM-400k/0 (a) Shear stress as a function of rate and (b) Viscosity as a function of shear rate ramp up only

From Table 4.3 it can be seen that for PEOM-100k/0 and PEOM-100k/5 that all the parameters except η_2 are approximately zero. As 100k PEO was seen to be Newtonian (see Figure 4.11), only a single constant would be needed to describe its viscosity, while making the rest as small as possible. The software chose η_2 over η_1 as this constant because of the impact of 0.1 on t_1, bringing the indices of the second exponential closer to 0 by a factor of 10 compared to that of the first. However, this result is an artefact brought about by the software, as the obvious choice to represent the constant is η_∞, while making the exponential factors and their coefficients as close to zero as possible.

As the molar masses increases the function becomes more complicated due to the presence of shear thinning. The parameters t_1, η_1 and η_∞ increase with molar mass. The result showing PEOM-400k/100 shows similarities to PEOM-400k/0 in that η_1 is the

Table 4.3: Parameters with respect to the De Kee model

Sample	Parts PEO/g	Parts MMT/g	t_1/s	η_1	η_2	η_∞
PEOM-100k/0	1.00	0.00	9.55e-5	4.76e-13	0.019	3.66e-13
PEOM-100k/5	1.00	0.05	1.02e-4	2.9e-13	0.017	4.91e-4
PEOM-400k/0	1.00	0.00	0.402	0.05	0.765	0.588
PEOM-400k/5	1.00	0.05	0.282	0.031	0.746	0.480
PEOM-1000k/0	1.00	0.00	0.953	14.33	7.05	0.820
PEOM-1000k/5	1.00	0.05	0.918	15.13	7.33	0.201
PEOM-400k/100	1.00	1.00	0.499	0.048	1.101	0.902

same whereas t_1, η_2 and η_∞ have increased by 24%, 44% and 53% respectively.

V. Dispersion and Rheology

As stated at the start of this chapter, the primary objective to investigate the rheological properties of a hydropolymer/nano composite systems, and to quantify any dispersion phenomenon. In order to attain the levels of dispersion that rheology is capable of providing an experiment was carried out where the 5% mass MMT was placed directly into the PEO/water solution (which had only been stirred briefly by a glass stirring rod). As before, the experiment was prepared at room temperature under the same conditions mentioned earlier.

Figure 4.19 shows the results obtained during this experiment. As can be seen, the 'ramp up' values show slight abnormalities, most noticeably at approximately 50 Pa. This is presumably due to 'lumps' of filler/matrix present in the system which are soon broken down into small pieces when left under shear for the 5 min constant shear as

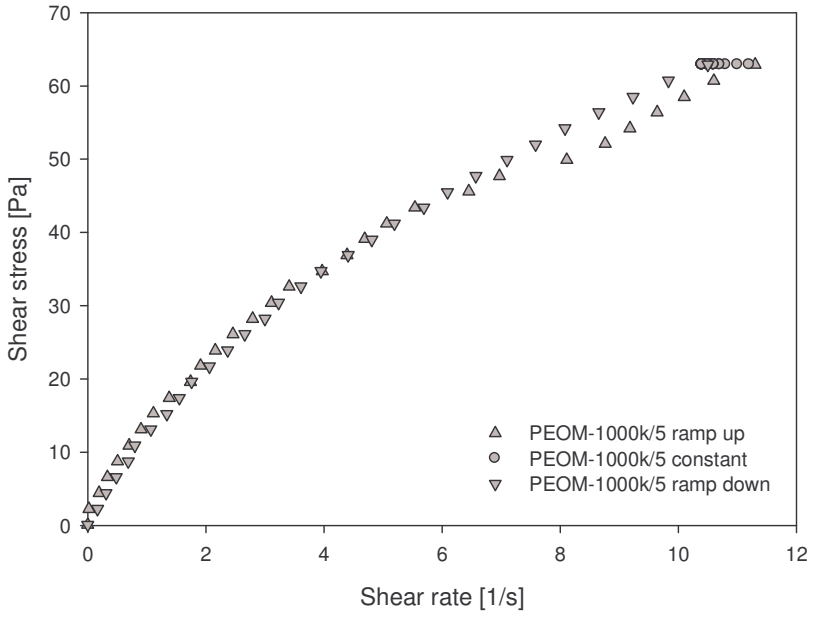

Figure 4.19: Shear stress as a function of rate for PEOM-1000k/5 using minimal dispersion sample preparation

(a)

(b)

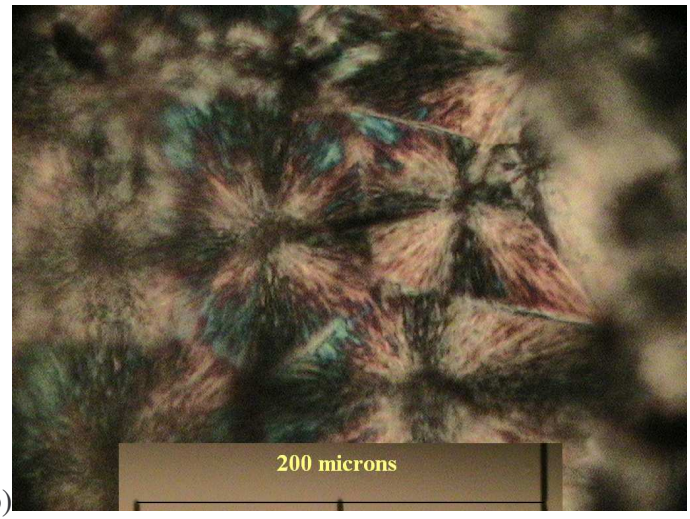

Figure 4.20: Optical microscopy pictures between crossed polarisers for samples (a) PEOM-100k/5 and (b) PEOM-100k/0

shown by the steady curve of the 'ramp down' values.

Optical microscopy between cross polarisers was carried out on PEOM-100k/5 and PEOM-100k/0 after dispersion from rheology. From Figure 4.20 the clay is seen to be well dispersed which has affected the crystallization of the PEO matrix which is shown by the lack of observable spherulites in Figure 4.20(a).

Vaughan et al.[172] reported that there was a dramatic enhancement of nucleation for well dispersed functionalized MMT. However, this served to disrupt the structural evolution, which can be clearly seen in Figure 4.20(a). Other researchers[173,174,175,176]

have discovered an increase in nucleation density in the presence of layered silicates. P. Maiti[173] et al. investigated the crystallization behaviour of MMT on polypropylene nanocomposites at 2, 4 and 7.5% wt loadings. They reported that the clay particles acted as a nucleating agent where increased clay loadings resulted in smaller and smaller spherulite sizes. Despite this, the overall rate of crystallization was unaffected by high loadings of clay. However, it has been reported that increased nucleation density be due to shear effects and not the action of the MMT itself[177]. It has also been suggested that clay platelets can reduce the mobility of polymer chains[142] and thus, give less ordered structures upon nucleation. Regardless, the work of Vaughan demonstrated that the insulation properties of the material were not affected when samples where quenched, unlike isothermally crystallised samples, which showed a decrease in breakdown strength.

4.7 Conclusion

The aim of this chapter was to perform a rheological study of a hydropolymer/inorganic composite dispersion. To this end, the three different molar masses of PEO used were, 1×10^5, 4×10^5, and 1×10^6 g.mol^{-1}. MMT was used as the inorganic filler due it being the subject of a vast of research in the literature.

A function fitting technique was adopted that was used to give accurate viscosity plots. The De Kee model was fitted to the data points using Sigma Plot. Although a good fit was found from the model, only one trend was seen, that is with increasing molar mass caused an increase in model parameters. Not enough measurements were made from varying samples to observe any trends that may appear that could be used later to characterise materials of this nature.

Rheologically, the addition of 5% MMT gave lower (within 2%) viscosity readings than that of the pure PEO/water matrix. This was surprising as previous literature showed increases in viscosity in the presence of functionalized MMT. Viscosity as a function of volume experiments showed that instrumental errors existed in the order of

3%. Therefore it was concluded that the equipment was not sensitive enough to measure the viscosity change caused by the presence of 5% filler loadings.

When rheological data were taken for a system containing MMT and PEO on a 1:1 ratio, a 50% increase in zero shear viscosity was found. The shear thinning behaviour for both was approximately the same.

Although dispersion could not be dynamically observed during rheological experimental runs, dispersion was achieved. This was shown using optical microscopy for the 100k molar mass PEO systems. After rheology, 100k PEO processed in the presence of MMT showed an absence of spherulitic development. This implies that the MMT was well dispersed after 10 min shearing and, that its presence in the matrix affected crystallisation.

CHAPTER 5: Epoxy Composite Systems

5.1 Introduction

In the previous chapter, a semicrystalline polymer was used as a matrix. A semicrystalline polymer has two phases; crystalline and amorphous. Shear thinning is seen in systems where long molecular structures can form. This was seen in the last chapter where the long molecular chain structures in high molecular weight PEO became large enough for shear thinning to be detected by the rheometer.

The equipment was seen to not be sensitive enough to record any dispersion effects that could be taking place in the PEO matrix at 5% loadings. Due to the liquid phase of polymeric matrices during rheology, it is hypothesised that at increased temperatures, dispersion effects might be made visible, as the rheology becomes less and less dominated by that of the matrix. For this reason, a temperature stable polymeric matrix was chosen in the form of an epoxy resin. Epoxy resin adds an additional advantage in that due to its amorphous nature, no shear thinning effects will be present that could otherwise be misinterpreted as dispersion phenomena.

Epoxy resin is one of the most important thermosetting polymers used in electrical insulation today. Its use as an insulator extends to the encapsulation of integrated circuits and for the fabrication of printed circuit boards. Epoxy resin also has good mechanical properties allowing it to also find application in environments such as dry type transformers, coil insulators within rotating machines and as spacers within gas insulating switchgear (GIS).

In the last chapter a single inorganic filler was introduced into a polymeric matrix. In this chapter, a filler will be used that is available with two variations of surface chemistry i.e. inorganic and organic. The nature of these two different interfaces on the rheological properties of an epoxy resin will be investigated.

5.2 Chemistry of Epoxies

Epoxy resins were originally developed by Pierre Castan in the late 1930s. It is a polymer based on the three-membered system either as the epoxy or oxirane ring[178] (Figure 5.1):

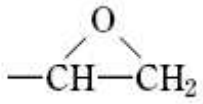

Figure 5.1: Epoxy ring chemical structure

The major portion of epoxy resins are derived from bisphenol –acetone and epichlorohydrin. It is characterised by the highly reactive oxirane ring above which can be reacted with curing agents or catalytically homopolymerized to form a cross linked polymeric structure. These resins are manufactured by reacting epichlorohydrin and bisphenol A in the presence of aqueous caustic soda. The reaction is always carried out with an excess of eichlorohdrin so that terminal epoxy groups exist. Resins of low, medium or high molecular weights can be produced by varying the manufacturing conditions and the excess of epichlorohydrin. The simplest possible epoxy resin derived from the reaction of bisphenol A and epichlorohydrin is the diglycidyl ether of bisphenol A (DGEBA)[179], see Figure 5.2:

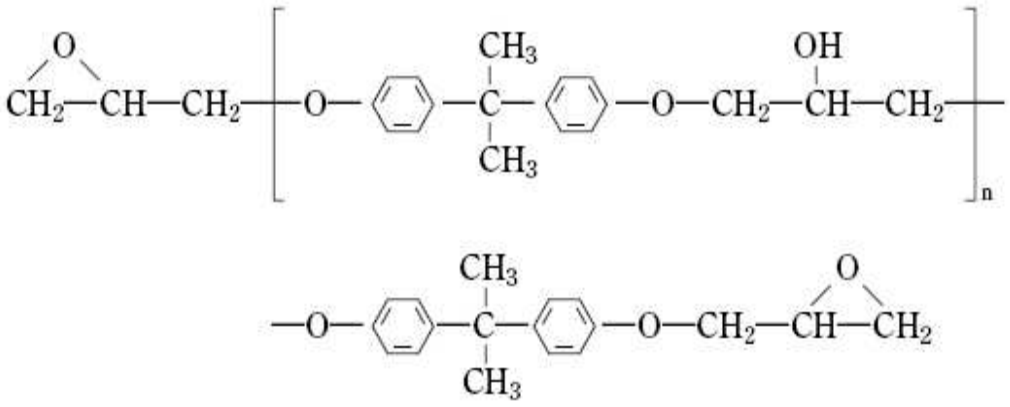

Figure 5.2: Bisphenol A based epoxy resin chemical structure

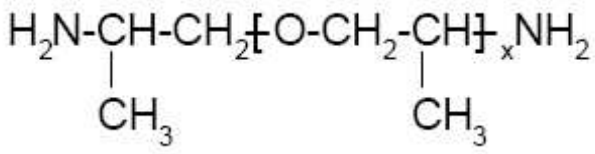

Figure 5.3: Molecular structure of Jeffamine D-230, x ~ 2.6.

It should be noted that as the molecular weight increases, the epoxide content is decreased and the hydroxyl (OH groups) content is increased[179]. This group can react at higher temperatures with anhydrides, organic acids, amino resins, and phenolic resins, or with epoxide groups (when catalyzed) to give additional cross-linking.

In this research the epoxy resin used is a commercial DGEBA known as D.E.R 331 (Dow Chemical Company). The value of 'n', which is the number of repeating units commonly referred to as the degree of polymerisation is typically about 0.15.

Epoxy resins can be cured or crosslinked through the oxirane ring by a large variety of chemical compounds. In this case the aliphatic curing agent used in this research is polyamine known as Jeffamine D-230 polyoxypropylenediamine (see Figure 5.3). As the name indicates, it is a di-functional primary amine with an average molecular weight of approximately 230. Its amine groups are located on secondary carbon atoms at the ends of an aliphatic polyether chain.

Figure 5.4 shows the reaction of a di-primary amine as it reacts with epoxide groups to form a cross linked structure. Each of the four active amine hydrogens react with one epoxide group.

In theory, the hydroxyls formed should be capable of reacting with epoxy groups to form an ether linkage, see Figure 5.4f

(a)

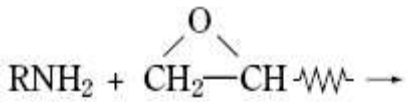

(b)

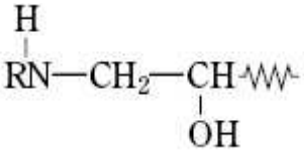

(c)

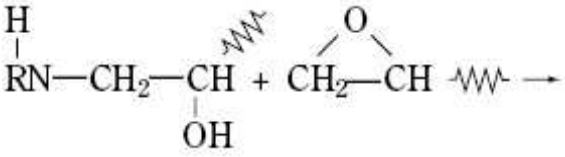

(d)

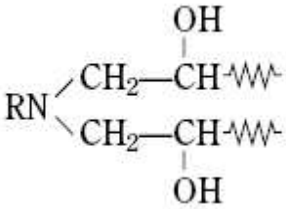

(e)

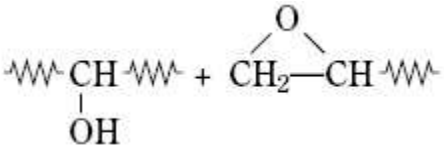

(f)

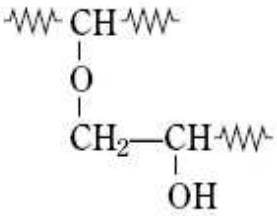

Figure 5.4: Reaction of (a) primary amine with an epoxide group to form (b) a secondary amine. Secondary amine with an epoxide group to form (c) a tertiary amine. Hydroxyl groups reacting with epoxide ring to form (f) an ether linkage.

5.3 Experiental Procedure

5.3.1 Pure epoxy systems

The stoichiometric ratio of epoxy to hardener for all samples that required curing was 1000:315. Samples were cast from the mold using a Kapton spacer of ~ 50 μm. The initial cure was 90 °C for 2.5 h and a post cure of 110 °C for another 2.5 h.

I. Rheology: Viscosity as a function of temperature and volume

Rheology was carried out on pure epoxy over the temperature range 30 °C, 40 °C and 50 °C over the sample volumes 5 ml, 10 ml, 15 ml and 20 ml. Sample volumes were weighed out given that the density of the epoxy at 25 °C is 1.164 g ml^{-1}.

Temperatures were controlled using an attached circulating water bath, which was calibrated using a digital Hanna thermometer.

II. Gel-time

In order to formulate a materials processing methodology, the behaviour of the material under processing conditions must be known. In the case of an epoxy resin composite, various questions arise, such as, should the filler be added with subsequent mixing after the inclusion of the curing agent or before? How much time do we have to cast after the curing agent has been added? These are all questions concerned with the kinetics of a curing epoxy resin. A standard procedure to answer these questions would be to conduct a series of experiments using a differential scanning calorimeter (DSC) taking several isothermal scans at different temperatures[180,181,182]. However this procedure is not without risk, as it is possible that should the selected temperatures cause the curing reaction to become volatile, damage to the equipment is possible. A safer way forward is to monitor the viscosity as a function of time at varying temperatures. This can be achieved by constructing a rolling sphere viscometer. A rolling sphere viscometer was constructed by suspending a test tube (2.5 cm in diameter) in a temperature controlled glass water bath. The time it took for a steel ball

bearing (1 mm in diameter) to fall a distance of 7 cm was recorded on a digital stop watch. Stokes law (see Eq (5.1)) was applied to calculate viscosities at varying times throughout the cure.

The validity of stokes law relies on the following assumptions:

1) The ball bearing has reached terminal velocity before it reaches the first marker.
2) The diameter of the ball bearing is much smaller than the diameter of the test tube (Reynolds number << 1)

The epoxy and hardener were mixed together with a 1000:315 stoichimetric ratio with a magnetic stirring bar for ~ 5 min before being degassed in a vacuum oven for a further 5 min. Steel ball bearings 1 mm in diameter were dropped from a height of approximately 4 cm into the resin/hardener mixture where the time it took to fall 7 cm was measured using a digital stopwatch. It was made sure that the 7 cm fall distance was a further 4 cm under the surface of the epoxy resin to ensure that terminal velocity was attained before timing took place. Eq. (5.1) was used to calculate approximate values of viscosity[85]:

$$\eta = \frac{2r^2\left(\rho_s - \rho_f\right)gt}{9AB} \tag{5.1}$$

Where ρ_f is the density of the epoxy/hardener mixture, ρ_s the density of the steel ball bearing, g the acceleration due to gravity, r the radius of the ball bearing and AB the distance the ball bearing travels during the timed measurement.

The values given on the data sheets were used for the densities of both the epoxy, hardener and steel ball bearing. These are shown in Table 5.1. The 1000:315 mix represents the density of the combined mixture of epoxy and hardener when mixed with the stoicimetric ratio of 100:31.5. This was calculated using the density values given in Table 5.1.

Table 5.1: Density values

	D.E.R 331	**Jeffamine D-230**	**1000:315 mix**	**Steel**
Density [g/cm]	1.164	0.948	1.1	7.83

III. Electrical characteristics

The low electrical breakdown strength of composite systems has been attributed to poor dispersion of the filler and aggregation. For this reason, electrical breakdown tests were carried out as a secondary means of studying the effect of dispersion on a polymeric matrix. Samples were cast using a mold that consisted of a top plate with two reservoirs and a bottom plate. Sample thickness was controlled by placing a Kapton spacer between the two plates, see Figure 5.5. The mold was lubricated with Dow Corning 200/20cs silicone oil prior to use and epoxy samples were pumped through the space provided by the Kapton spacer using a positive pressure of nitrogen gas. 80 μm thick Kapton spacers were used for all samples. The samples were cured using the aforementioned schedule. Upon being removed from the mold, the cured sample (100 x 50 mm) was cut into strips (100 x 10 mm).

Electrical breakdown tests were then carried out according to the principles laid out in ASTM D187-89. All of the samples were uncoated and varied in thickness from 90 μm to 120 μm. Each sample was immersed in Dow Corning 200/20cs silicone oil between opposing 6.33 mm steel ball bearings. Approximately 6 breakdown sites were carried out per strip. The lower electrode was connected to earth while the upper electrode was connected to an AC 50 Hz voltage. The sample was put under electrical stress at a ramp rate of 50 V s^{-1} until the sample failed. This was done 30 times per sample. The results were analysed using Weibull statistics with 90% confidence bounds.

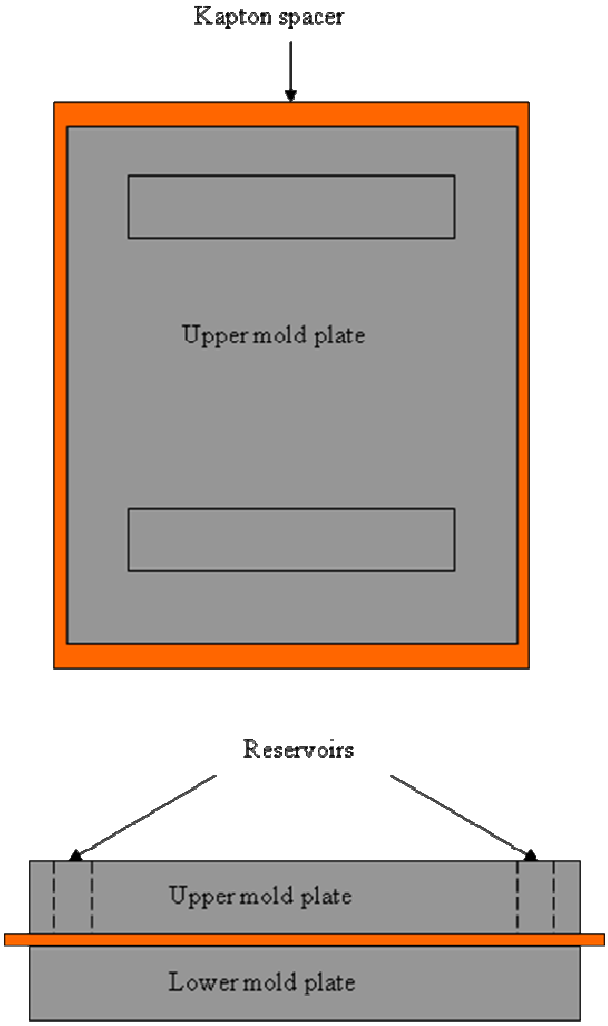

Figure 5.5: Mold geometry

5.3.2 Functional characterisation of boehmite

The functionality of both functionalised boehmite was not known at the start of this study. It was identified with the use of Raman spectroscopy. Functionalised boehmite and un-functionalised boehmite (supplied by CimTec labs, Trieste) and Disperal; pure boehmite (supplied by SASOL) which will be referred to as reference boehmite. These inorganic fillers were pressed into 13 mm diameter discs using a Specac press prior to testing. Each sample was tested at 100% laser power over a 9 h total integration time. The data was recorded using Grams software.

5.3.3 Epoxy composite systems

Throughout this chapter, three types of filler have been used. Montmorillonite (MMT), boehmite (AlOOH) and surface modified boehmite. The size distribution of the fillers is unknown.

Boehmite is one of the polymorphs of aluminium oxide hydroxide, AlOOH. This compound occurs in nature in the European bauxites, and it can be easily prepared by hydrothermal treatment of aluminium hydroxides. The crystallininity of boehmite is known to be related to preparation conditions[183].

When boehmite is annealed, it undergoes a series of polymorphic phase transformations: from boehmite into γ-alumina and then into δ- and θ- alumina which are known as transitional aluminas, and eventually into α-alumina, the thermodynamically most stable alumina phase[184]. Transformation temperatures strongly depend on boehmite crystallinity – boehmite with low crystallinity traditionally has been named as pseudoboehmite, which has been assumed to have water molecules in its crystalline structure[185,186]. It has been demonstrated that boehmite and pseudoboehmite are the same crystalline phases but with different crystallite sizes[187,188], and that pseudoboehmite does not have intercalated water in its structure as has been claimed by many authors[185,186,189].

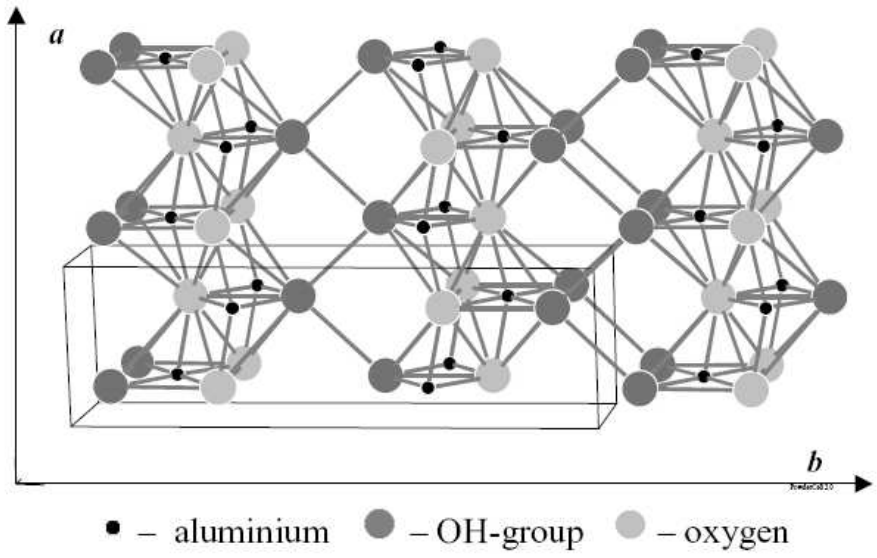

Figure 5.6: Structure of boehmite

Each aluminium atom is surrounded by a distorted octahedron of oxygen atoms, and these octahedrons are joined by sharing edges in such a way that they form zig-zagged layers parallel to the 010 plane. These layers are linked together by hydrogen bonds between hydroxyl groups in neighbouring layers[190] (see Figure 5.6)[191].

I. Sample preparation

5% filler loadings by weight were applied to epoxy resin and mixed with a stirrer bar at approximately 50 °C until the mixture took on a homogenous colour (~10 min). The sample was then poured into the rheometer measuring cup and then left until the measuring cup reached room temperature. Rheology was conducted at room temperature ~21 °C, 30 °C, 40 °C and 50 °C following the standard procedure of ramp up to 65 Pa, hold for 5 min followed by a ramp down to 0 Pa.

Post rheology, the samples were de-gassed overnight in a vacuum. The curing agent was applied and a magnetic stirring bar was mechanically used to mix the mixture for 10 min before being de-gassed again for a further 15 min. Casting was carried out in a mold with a Kapton spacer of ~50 μm. The initial cure was 90 °C for 2.5 h with a post cure of 110 °C for a further 2.5 h. See Figure 5.7 for a summary of the curing procedure.

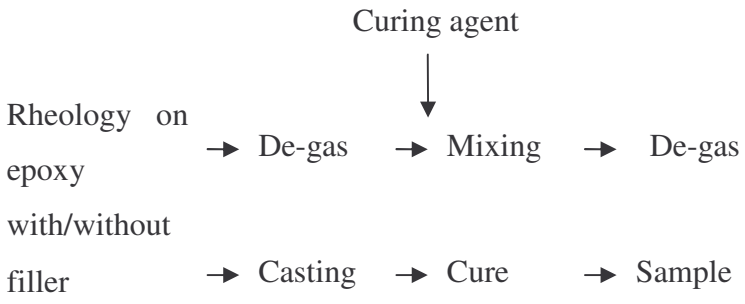

Figure 5.7: Preparation schematic for epoxy composite samples

II. Preparation for Scanning Electron Microscopy (SEM)

A SEM was used to observe and record the structure of the fillers used in this research in their un-dispersed form.

The filler particulates were sprinkled onto SEM stubs that had been smeared with araldite adhesive. The samples were allowed to set for approximately 30 min before being gold coated with a sputter coater. This procedure was carried out for functionalised boehmite, unfunctionalised boehmite and MMT.

III. Electrical characteristics

The introduction of a second phase into a polymer matrix has been known to affect the insulating properties of a dielectric. The insulating properties of a nanocomposite can therefore be said to give a crude measure of dispersion; poor dispersion with large aggregates can lead to lower breakdown field values which are often accompanied by two distinct phases (matrix and matrix/filler breakdown phases) in its Weibull distribution. Good dispersion usually leads to improved breakdown field values and a single phase (matrix/filler breakdown phase) in its Weibull distribution. For this reason, electrical breakdown tests were carried out on the composite samples. They were carried out in exactly the same manner as those for the pure epoxy section.

5.4 Problems From Model Fitting to Newtonian Systems

5.4.1 Statistical analysis of raw rheological data

The main purpose of rheology throughout this research is to monitor dispersion and gain insight into the mechanical characteristics that distinguishes between functionalised and unfunctionalised filled composites. Throughout the course of a rheological measurement various peaks can be seen in the raw data when looking at the gradient changes between two consecutive points. To investigate whether these

points can be used as a quantitative means for obtaining a measure of dispersion, statistical analysis was carried out to see if they were anything other than instrumental errors.

Figures 5.8 to 5.10 show the change in shear stress ($\Delta\tau$) as a function of the change in shear rate ($\Delta\gamma$) (ramp up only). It is different to the method outlined in Chapter 2 in that no differentiation is taking place i.e. the limit on the small changes between successive data points – see Eq(5.2) is not tending to 0.

$$\frac{\Delta\tau}{\Delta\gamma} = \frac{y_n - y_{n-1}}{x_n - x_{n-1}} \tag{5.2}$$

This is a crude measure of the system's viscosity however it is a good measure of the spread in data collected by the rheometer. Figure 5.8 shows this method of looking at the raw rheological data for pure epoxy at room temperature and 60 °C. As can be seen there are 3 prominent spikes in the data at both temperatures. These spikes can be seen to occur in the filled systems in a random manner, see Figure 5.9 to Figure 5.10.

In order to see if these spikes are related in any way to the presence of the fillers, plots of ln(variance/mean) against temperature were created. A plot of ln(variance/mean) is often applied when analysing large amounts of data as it gives a indication of noise within the data. This makes it possible to observe whether there is any significant difference between filled and unfilled samples in regions where the noise has the lowest impact by seeing if there is any deviation from that of the pure epoxy. See Figure 5.11. As can be seen, the noise decreases with temperature for all systems.

As can be seen from Figure 5.8, the higher the temperature that rheological measurements take place, the smaller the noise present in the recorded data becomes. This is again verified in Figure 5.11 where the values are at their lowest for low temperature (T). It can also be seen that there is no significant deviation from the trend shown by the pure epoxy giving the conclusion that spikes in the data sets are just instrumental fluctuations.

For the purpose of this investigation, two particulate geometries were used; plates (boehmite) and spheres (SiO_2).

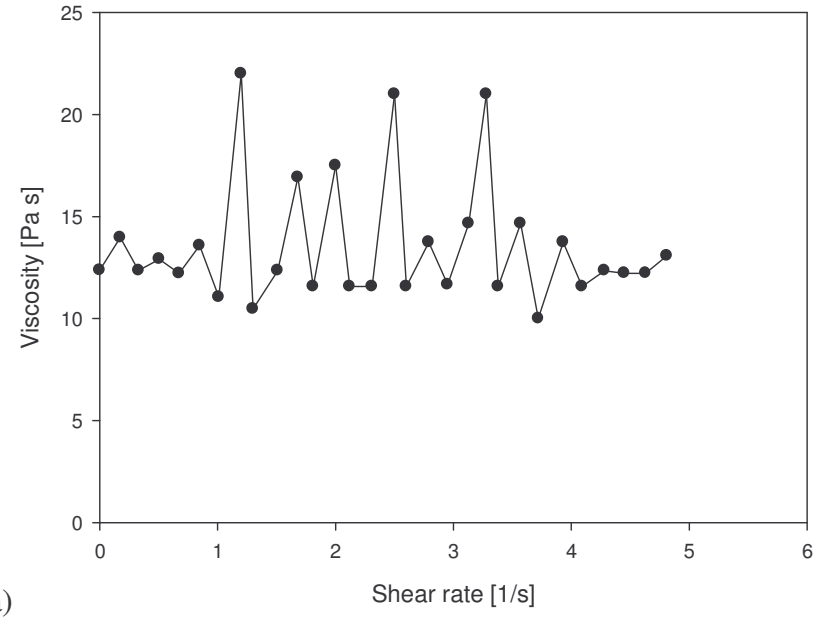

(a)

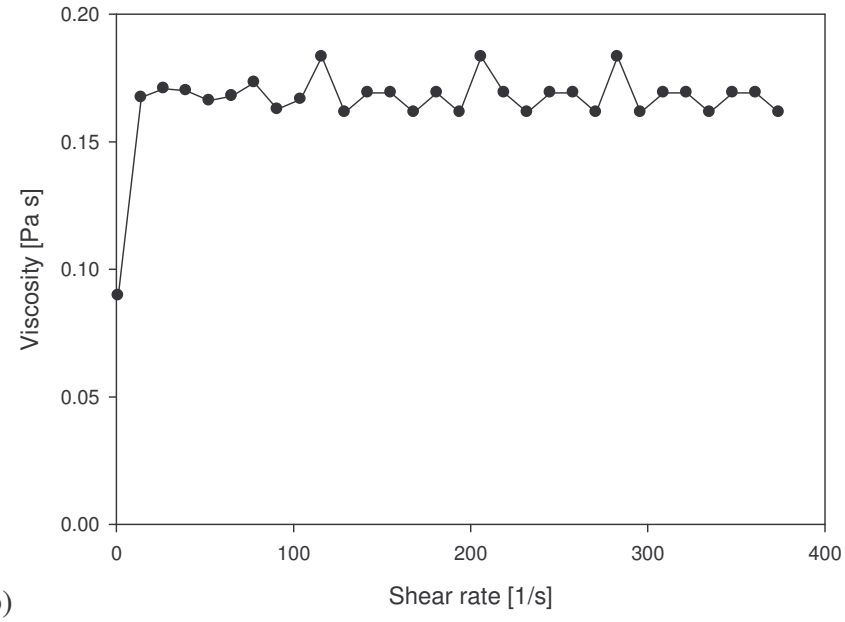

(b)

Figure 5.8: Change in shear stress with respect to shear rate for epoxy at (a) 21 °C and (b) 60 °C

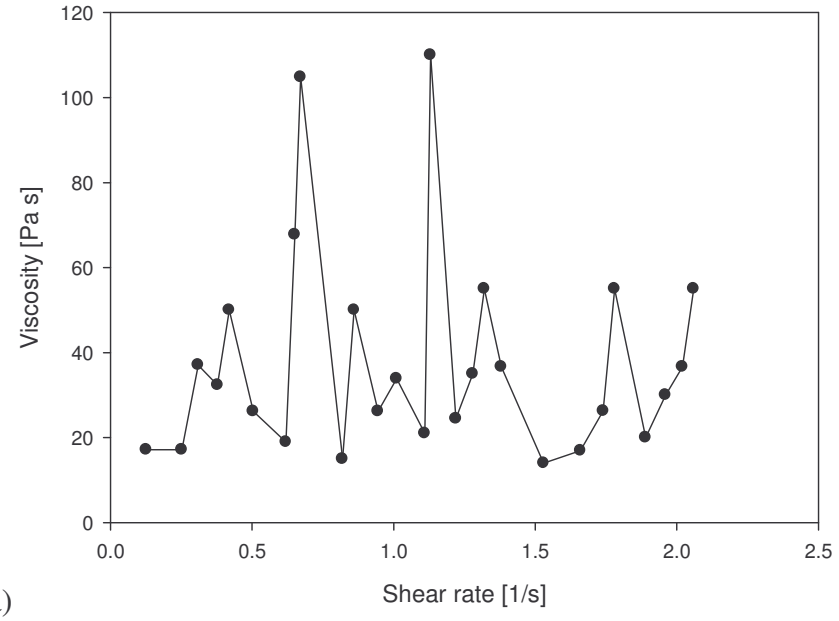

(a)

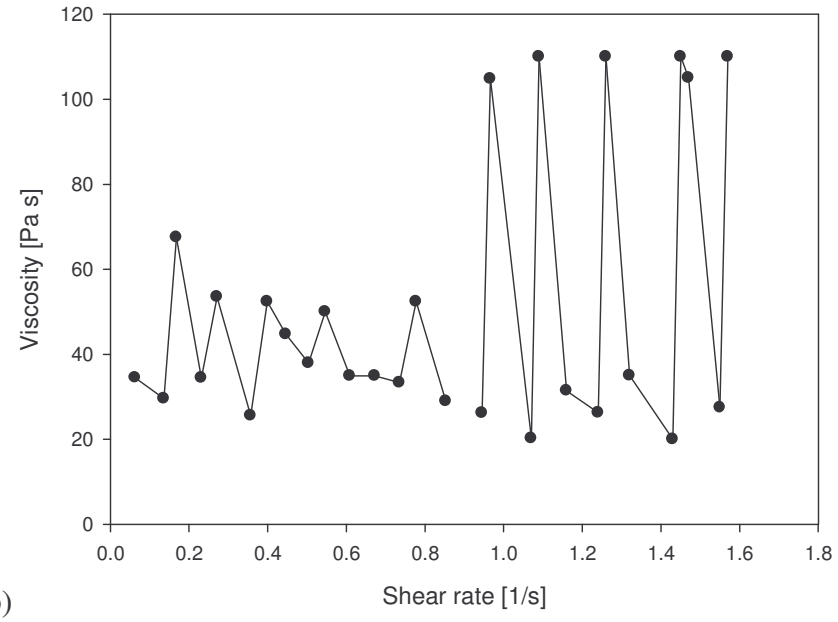

(b)

Figure 5.9: Change in shear stress with respect to change in shear rate for (a) functionalised boehmite and (b) unfunctionalised boehmite at ~21 °C

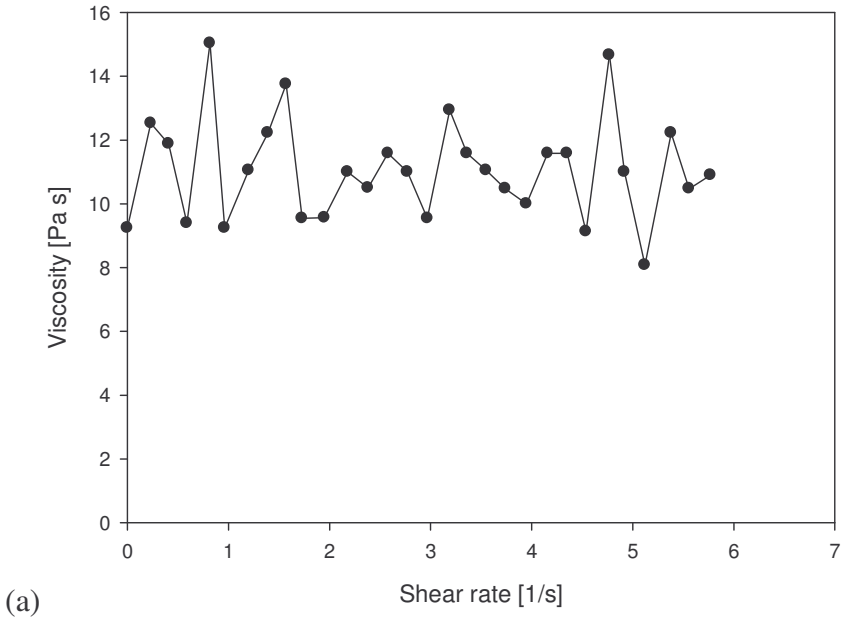

(a)

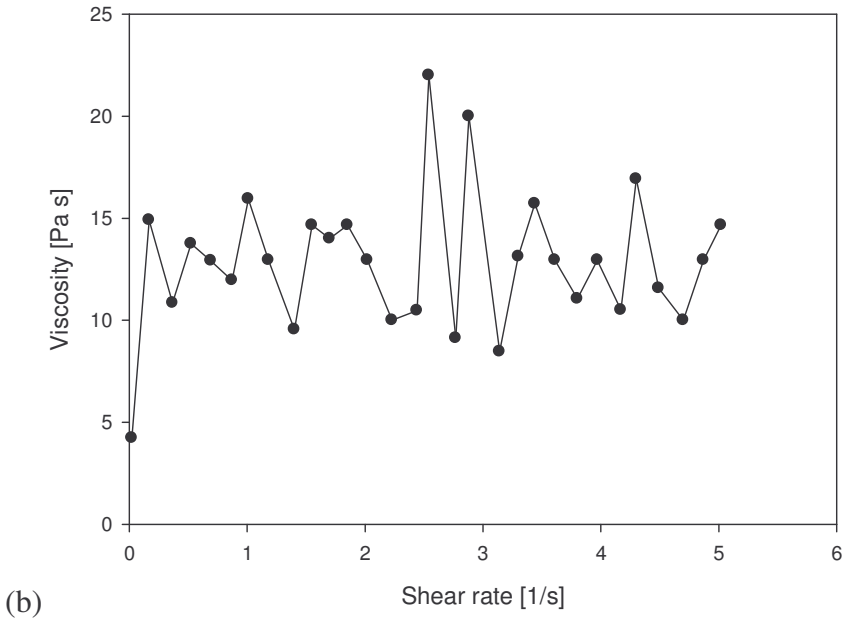

(b)

Figure 5.10: Change in shear stress with respect to change in shear rate for (a) micro SiO_2 and (b) nano SiO_2 at ~21 °C

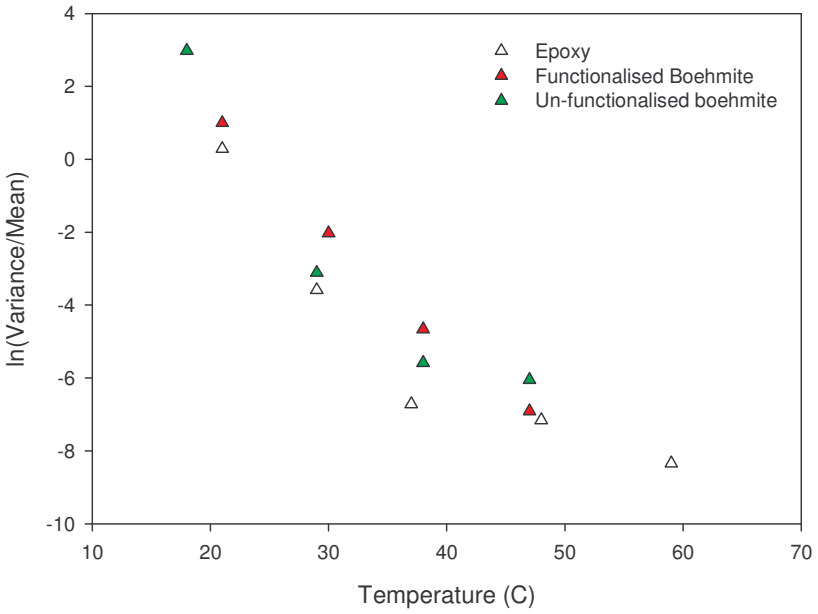

(a)

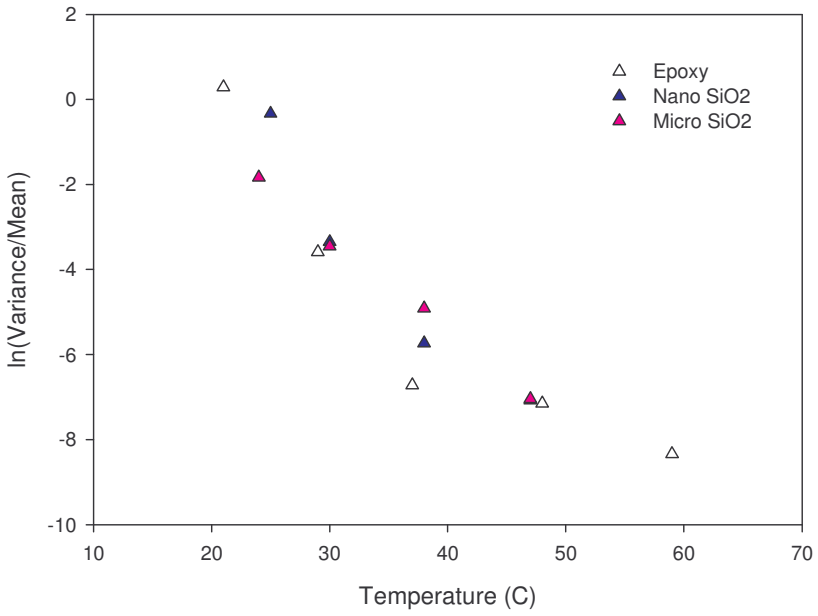

(b)

Figure 5.11: Measure of the noise of the systems as a function of temperature for (a) unfunctionalised and functionalised boehmite and (b) micro/nano SiO_2.

This result however is not meaningless. If these spikes occur at the beginning of a measurement, it can have a significant impact on how the hyperbolic and therefore the De Kee model gets fitted to the data. This is best demonstrated by Figure 5.12.

Figure 5.12 (a) shows rheological results at 50 °C for 5% functionalised boehmite. The sample has had no previous shear history which leads to the sample showing a yield stress on the ramp up of the measurement. On the ramp down the sample appears to be Newtonian. Figure 5.12 (b) shows the outcome of the model fitting procedure for the ramp down portion of Figure 5.12 (a) using the crude viscosity plot similar to those of Figures 5.8 – 5.10. Notice how the potential spikes in the data at the low shear stress regime has caused the hyperbolic/De Kee model to tend towards higher values of viscosity where it is seen to overshoot by ~50%.

It must be stressed that this is not dispersion phenomena being seen. Firstly, it is on the low shear stress regime of the ramp down cycle – dispersion would likely take place at high shear rates. Secondly, if it was dispersion phenomena similar behaviour would likely be seen in other systems. Other data sets do not show the same trend – meaning that it is not repeatable, implying instrumental error.

Even if the plot showed the same trend for ramp up data, it would still be held in question as there would be only 2 data points over the apparent 'shear thinning' regime. For further investigations to take place, a logarithmic ramp up would be required so that many more data points could be collected at low shear stresses.

From this result, it must be concluded that for a matrix that is Newtonian where there has been the addition of particulates, that the changes in shear rate with respect to the changes in shear stress must be taken into consideration before proceeding with the data analysis procedure outlined in Chapter 4. By observing the spread in viscosity values using Eq (5.2), one can then say whether any shear thinning/thickening taking place in a particulate filled Newtonian matrix, is due to (a) dispersion effects or (b) model fitting trying to accommodate instrumental errors.

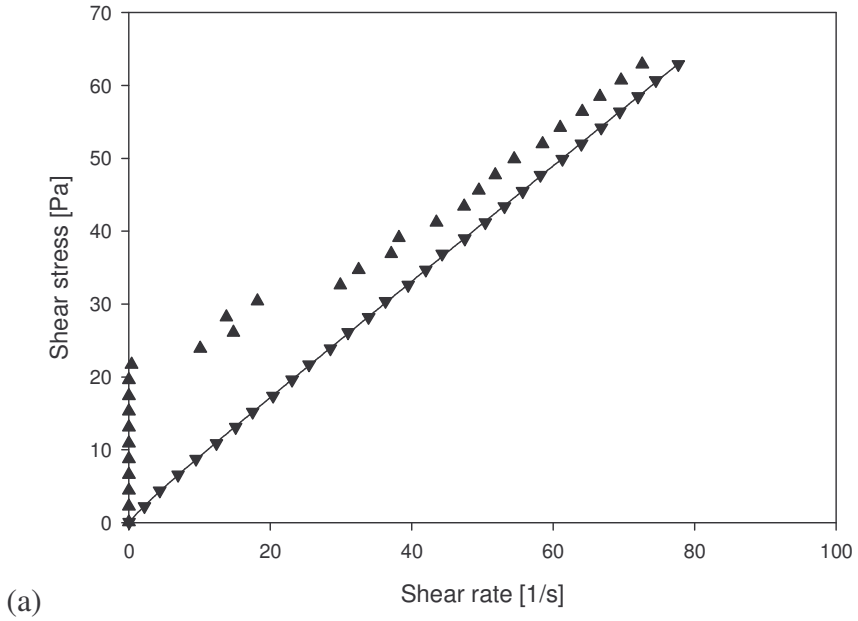

(a)

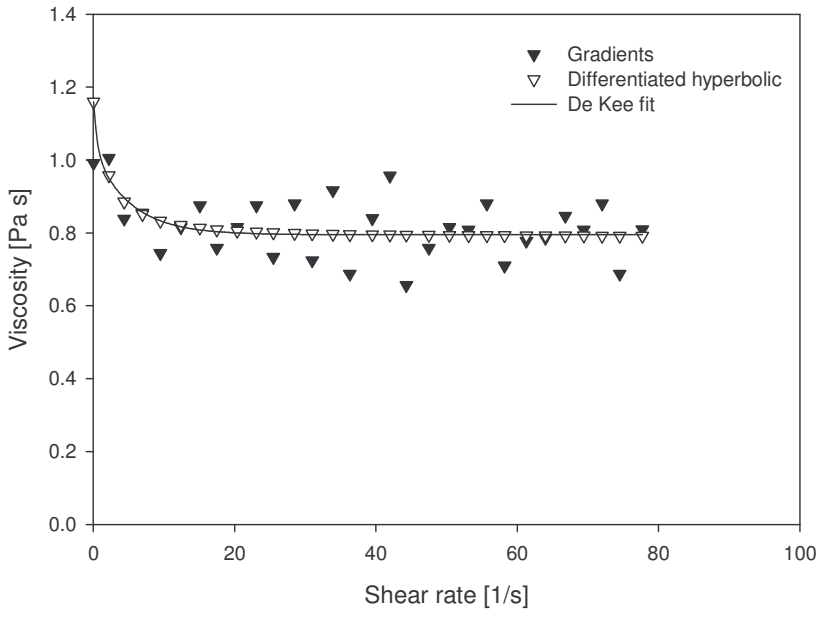

(b)

Figure 5.12: (a) Shear stress as a function of shear rate for functionalised boehmite and (b) Viscosity as a function of shear rate using the De Kee model fitting procedure and the spread in raw data (50 °C). ▲ represents ramp up, and ▼ represents the ramp down.

5.5 Results

5.5.1 Pure epoxy systems

Figure 5.13 shows that it takes approximately 30 min for the measuring cup to stabilise in temperature when containing 20 ml epoxy. It also shows the temperature gradient that exists between water bath and rheometer cup. As can be seen from the red points, the higher the temperature of the bath, the greater the difference in temperature between the bath and cup i.e. the temperature gradient increases as a function of bath temperature.

I. Rheology: Viscosity as a function of temperature and volume

As can be seen from Figure 5.14 there is an exponential relationship between the measured viscosity and the temperature of epoxy within the measuring cup for all four volumes.

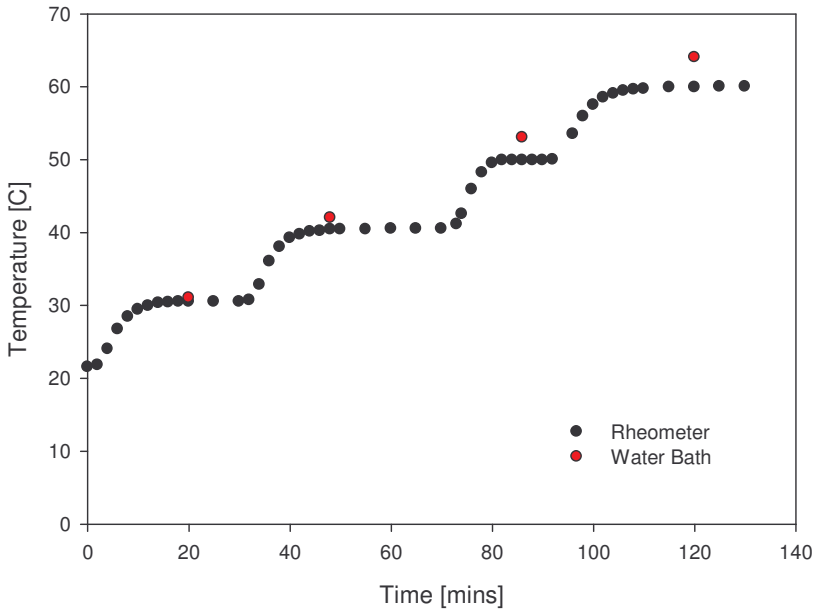

Figure 5.13: Calibration plots for epoxy in the measuring cup

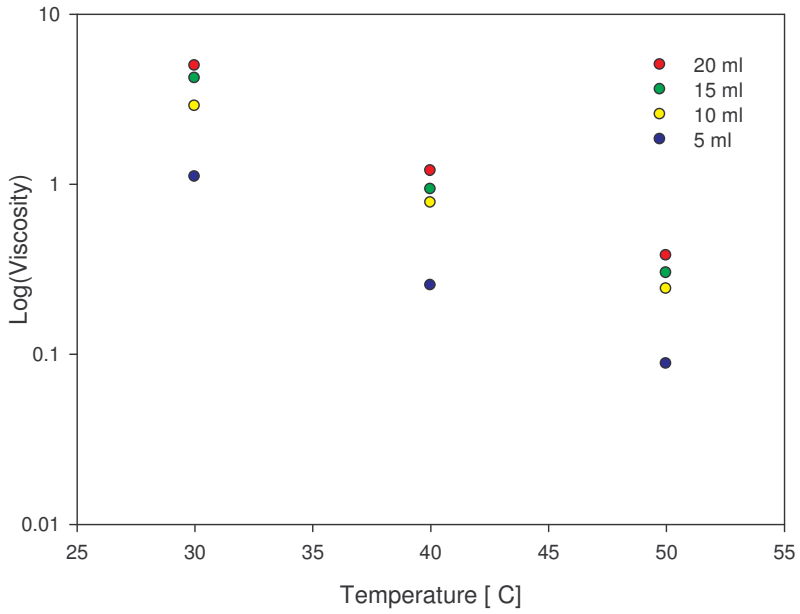

Figure 5.14: Relationship between viscosity and temperature for 5, 10, 15 and 20 ml of pure D.E.R 331 epoxy

It is well documented[1,170] that the viscosity of polymer solutions usually varies with temperature, according to an exponential Arrhenius type relation, i.e.

$$\eta = Ae^{-\frac{B}{T}}$$

Where A is a pre-exponential factor with units of viscosity, and B ($=E/R$) is associated with the activation energy E for viscous flow and with the gas constant R. In general, A and B depend on the solvent, on the concentration, and on the molecular weight distribution of the polymer[170].

II. Gel-time

Figure 5.15 shows how the viscosity of the curing D. E. R 331 resin changes with respect to time. From this graph, two pieces of information can be seen. Firstly it can be seen that the higher the curing temperature, the faster the system is seen to cross-

link, as evident by the shorter time periods recorded before the onset of increasing viscosity begins.

Secondly, that at 30 °C there is approximately 30 min before the resin begins to gel which is where it becomes increasingly viscous. This is problematic as prior to mixing the viscosity of the epoxy needs to be lowered by heating so the system can be mixed using a magnetic stirrer bar. This means that the system would likely to be at 30 °C or higher upon mixing with the resin. This does not leave enough time for rheological analysis and casting within the mould.

The last point of contention is for future experiments where dispersion of a filler is promoted with the use of a sonicator. During sonication the sonotrode imparts mechanical energy to the sample causing it to increase in temperature. Largely this temperature increase can be controlled using a water bath to act as a heat sink. However, during sonication a temperature gradient will always exist between the middle of the sample and the outer wall of the sample container. It is possible that over a sonication period of 30 min the temperature might well exceed that of 30 °C making it impossible to cast later on. With these issues in mind one must conclude

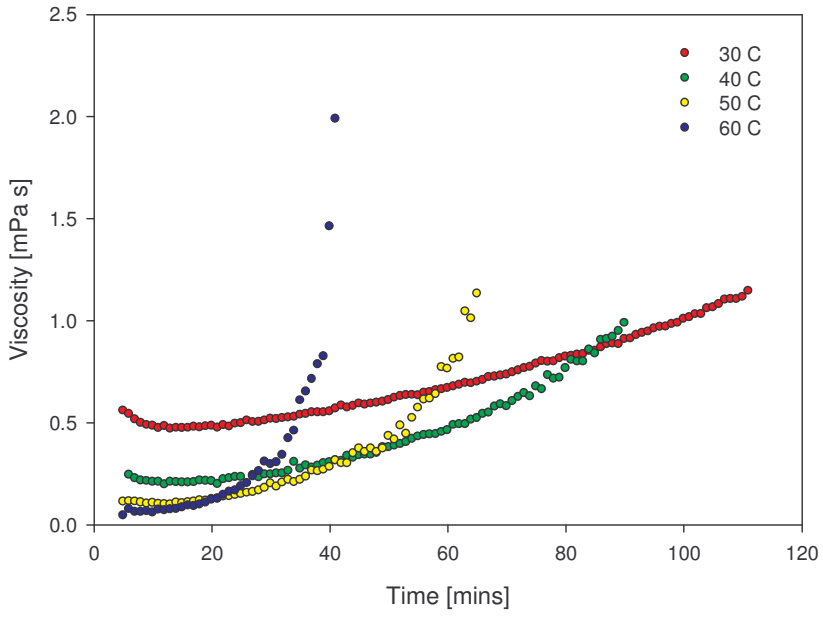

Figure 5.15: Viscosity as a function of time for curing epoxy at 30, 40, 50 and 60 °C

that when it comes to dispersing a filler in epoxy it must take place in the absence of the curing agent.

As a rolling sphere viscometer, the results of viscosity are lower than expected (Figure 5.14). The viscosity of water at 30 °C, is 0.8 Pa s^{90}. The viscosity of both curing agent and epoxy is greater than that of water, so when mixed – even though the reaction is endothermic- it would still be believed that the viscosity be higher instead of 38% lower. Certain assumptions in the experiment could lead to these errors. Firstly, it is assumed the density remains constant throughout – which is not the case; it would increase as the resin cures. Secondly laminar flow is assumed – this might not be the true at the start of the experiment where the viscosity if very low. Thirdly it is assumed that terminal velocity is reached – again this might not be true for low viscosity samples. Lastly, human reaction errors are a factor, especially at low viscosities when reaction times make up a large percentage of error compared to that at high viscosities.

III. Electrical characteristics

Figure 5.16 shows the electrical breakdown data obtained for post cured D.E.R 331 epoxy resin. The α and β parameters are 141±5 $kVmm^{-1}$ and 9 respectively and were calculated by the Weibull ++ sotware.

E. Tuncer et al.[192] who studied the electrical characteristics of epoxy based nanocomposites worked with a DGEBA Araldite resin. Their average electrical breakdown strength was approximately 100 $kVmm^{-1}$, whereas the results presented here are 141 kV mm^{-1}. Tuncer's sample preparation and breakdown test geometry differed from the one presented here. For electrical tests their 25.4 mm electrodes were embedded in their samples within their epoxy samples during their cure schedule and subjected to AC tests using a 150 kV power supply.

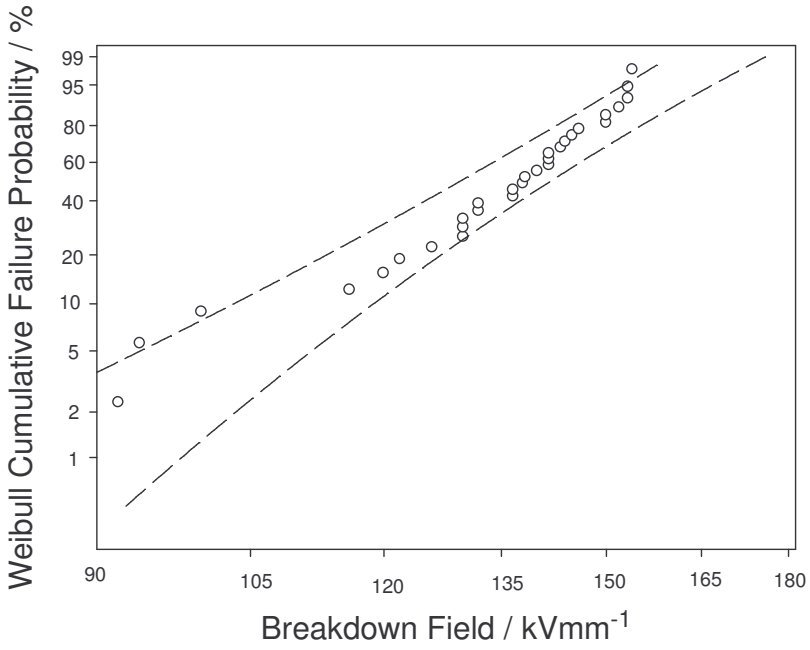

Figure 5.16: Electrical breakdown data presented using a Weibull distribution

5.5.2 Functional characterisation of boehmite

Figure 5.17 shows that both functionalised and unfunctionalised boehmite can be characterized using Raman spectroscopy. As can be seen from Figure 5.17(a), unfunctionalised boehmite has identical spectra to that of the pure boehmite. Ruan et al.[193] characterized boehmite using Raman spectroscopy from 200-3700 cm^{-1}. It is from their work that the peaks shown in Figure 5.17(a) are assigned.

The most visible peaks can be seen to be in the region 400-800 cm^{-1}. A vibrational mode exists at the strongest observable peak at 360 cm^{-1} that occurs within the Al-O bond within the mineral. Other vibrational modes of this molecule exist at 451 cm^{-1} and 495 cm^{-1}, both of which can be seen in Figure 5.17 (a). The two peaks at 632 cm^{-1} and 734 cm^{-1} can be seen and these are due to hydroxyl deformation modes. Finally the broad band at 1600 cm^{-1} has been assigned to the bending and stretching modes of absorbed water.

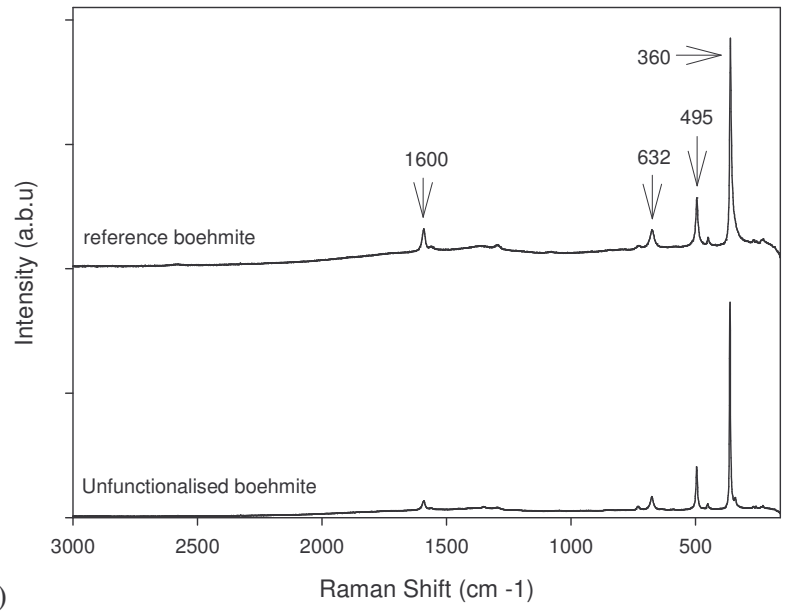

(a)

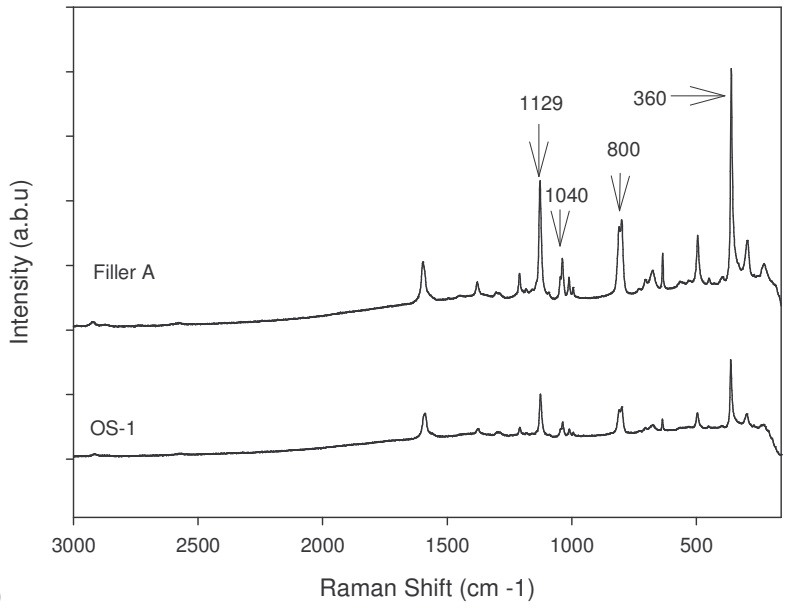

(b)

Figure 5.17: Raman spectrogram characterising (a) unfunctionalised and (b) functionalised boehmite

Figure 5.17 (b) shows the Raman spectra for functionalised boehmite. As can be seen it possesses additional Raman bands to that of the pure boehmite systems and can therefore be said to be organically modified. This is more clearly shown by subtracting the pure boehmite spectra from functionalised boehmite which leaves behind the Raman data associated with the functional groups of the chemicals used to modify the filler. Bocchini et al. have studied the organically modified boehmite filler DISPERAL OS-1 (SASOL) and demonstrated that DISPERAL OS series are organically modified by grafting of *p*-toluenesulfonic acid[194].

By comparing the spectra of the functionalization groups of functionalised boehmite to that of 4-octybenzene sulfonic salt, a clear similarity can be seen between the two cases, see Figure 5.18.

This reinforces the fact that functionalised boehmite has likely been treated in much the same way as SASOL's DISPERAL OS-1 filler. Their band classification correlates well with the spectra shown in Figure 5.17(b). The second largest band seen in Figure 5.17(b) at 1129 cm^{-1} are from the stretching of the sulfur oxygen double bond of the sulfonate salt and the band to the left of it at 1040 cm^{-1} is attributed to symmetric

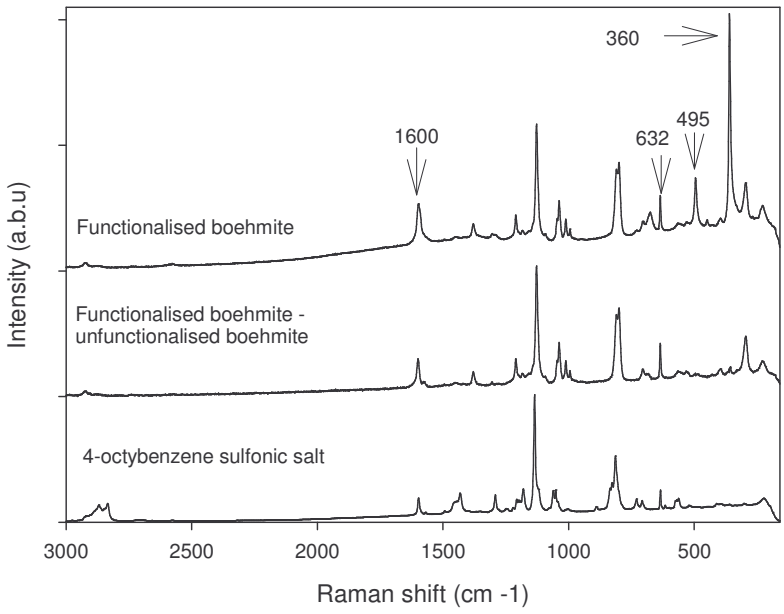

Figure 5.18: Raman spectrogram characterising functionalised boehmite

SO_3^- stretching[195]. The doublet at 800 and 814 cm^{-1} is due to the anion ν(CS) mode.

5.5.3 Epoxy Composite Systems

Figure 5.19 shows the nature of the fillers in their dry powdered form prior to mechanical mixing in the epoxy matrix. As can be seen, the functionalised boehmite (a-b) is covered in a coating that has caused it to aggregate into globular lumps. The

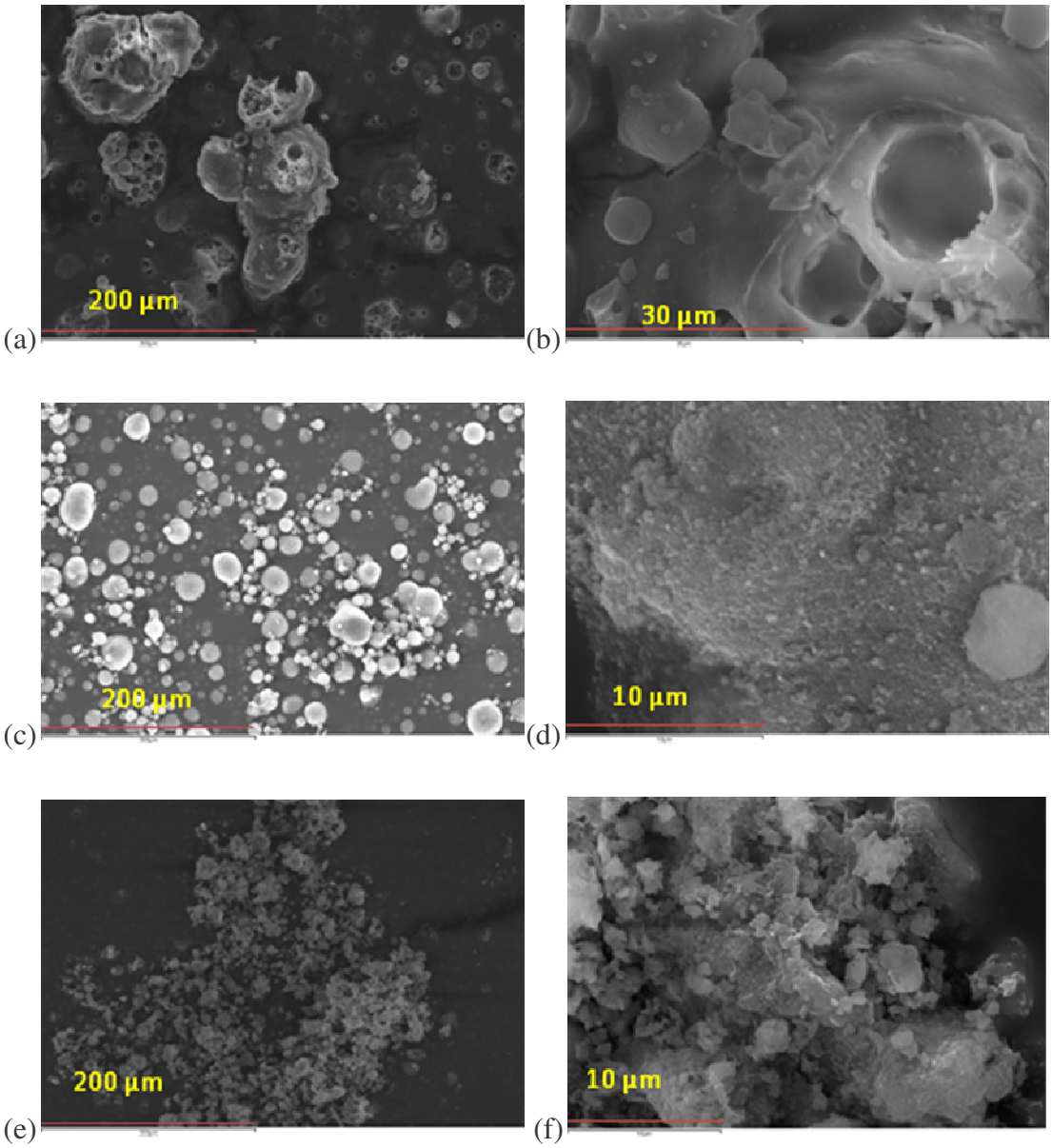

Figure 5.19: SEM images of (a-b) functionalised boehmite (c-d) unfunctionalised boehmite (e-f) MMT in dry powder form

unfunctionalised filler (c-d) lacks this coating and has thus remained as individual spherical aggregates. MMT (e-f) appears as smaller clusters with a less defining aggregate shape or form.

I. Rheology of epoxy composite systems

Figure 5.20 shows the temperature dependence of the fillers on the epoxy matrix. As can be seen, the filled systems follow the same exponential trend as that of pure epoxy when plotted as a function of temperature. It can also be seen that as the temperature of the systems increase, the filled systems have a greater % viscosity from that of the pure resin. This can be seen from differing gradients between the epoxy and the filled systems points on the plot. This is a valuable way of monitoring the affect the fillers have on the rheological properties on the system, i.e. by observing their viscosity values at increased temperatures. By doing so one can see that from Figure 5.20 that functionalised boehmite yields a higher viscosity than that of its unfunctionalised counterpart. Table 5.2 shows the values quantitively

The results are similar to those obtained by Mohan et al.[58] who used 10% organo MMT in a epoxy resin matrix at temperatures in the range of 120 °C. They reported a

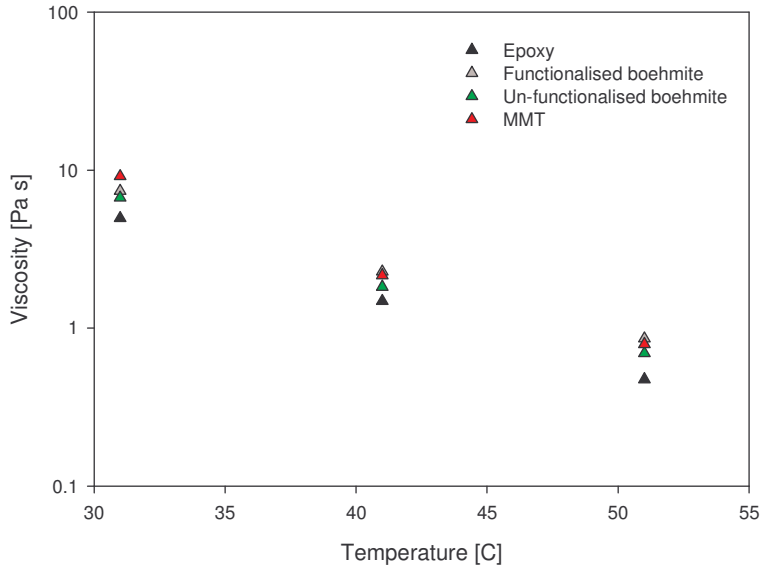

Figure 5.20: Viscosity as a function of temperature for pure epoxy, MMT, (un)-functionalised boehmite

Table 5.2: Viscosity data [Pa s]

	30 °C	**40 °C**	**50 °C**
Epoxy	5	1.5	0.4
MMT	9.1	2.2	0.8
Filler A	7.4	2.3	0.9
Filler B	6.7	1.8	0.7

93% increase in viscosity compared to that of the base resin whereas unmodified clay gave a 91% increase. At 120 °C the viscosity of the base resin fell by 94% relative to the viscosity at room temperature. The presence of 10% organo modified clay again gave a 93% increase in viscosity whereas the unmodified clay gave only 84%. The increase in viscosity due to the organo clay was claimed to be due to the homopolymerization of epoxy within the clay galleries. This swelling causes an increase in clay size due to increased separation of clay layers. Swelling is claimed to be critical for nanocomposite structure[196].

Intercalation of guest molecules into boehmite galleries has been reported to be incredibly difficult due to the nature of the strong hydrogen bonds between the layers[197]. This is a likely reason why the unfunctionalised boehmite has the lowest viscosity readings throughout rheological analysis.

MMT consists of Van der Waals forces between consecutive layers[142]. Van der Waals bonds are much weaker then hydrogen bonds therefore making it easier to promote intercalation/exfoliation. This could partially explain why the viscosity of unfunctionalised MMT is consistently higher than that of the unfunctionalised boehmite.

II. Electrical characterisation

Figure 5.21 shows the electrical breakdown properties of 5% MMT filled epoxy composite compared to that of the pure resin. Although it appears that the MMT filled

composite is superior because of the shift to the higher voltages, the fact that the confidence intervals overlap mean that the data sets are indistinguishable.

Figure 5.22 shows the electrical breakdown properties of both functionalised and unfunctionalised boehmite compared to that of pure epoxy. The functionalised boehmite, like the MMT, is indistinguishable from that of the pure epoxy. However, the unfunctionalised boehmite has substantially lowered the field to breakdown. Similar results have previous been reported by Vaughan et al.[198] with poorly dispersed functionalized MMT in polyethylene and by J. K. Nelson et al.[199] with micro sized titanium dioxide in epoxy. These authors work showed that the inclusion of their fillers gave a weaker breakdown to that of the base matrix due to large aggregates and poor dispersion. R. Sarathi et al.[65] has attributed the increase of breakdown voltage in the presence of nano-dispersed functionalized MMT/epoxy composite system to an increase in the surface area of nano-particle and a scattering mechanism.

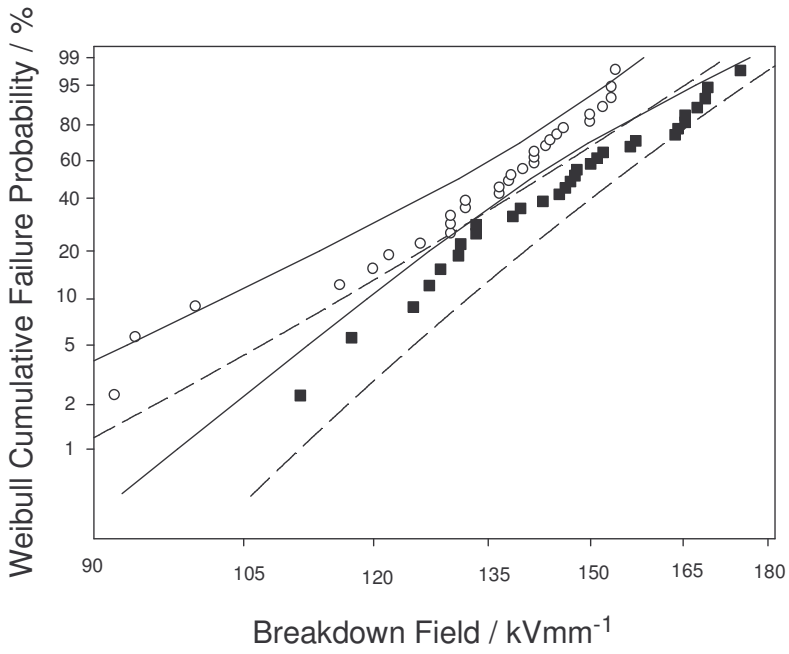

Figure 5.21: Weibull distribution plots MMT filled epoxy composite ■ compared to that of pure epoxy ○.

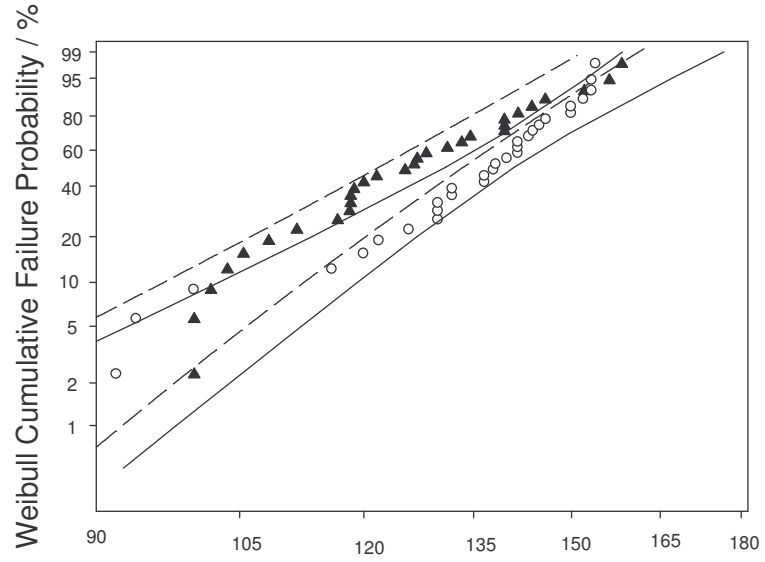

(a)

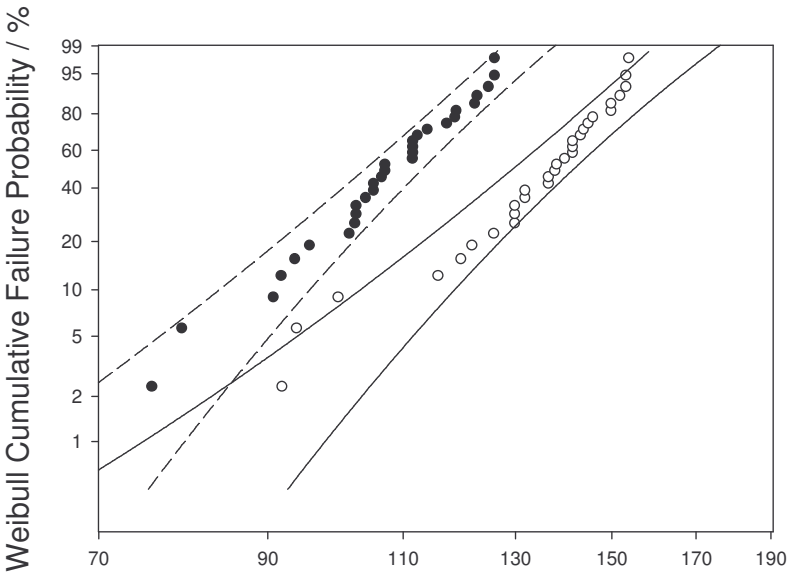

(b)

Figure 5.22: Weibull distribution plots for (a) Functionalised boehmite ▲epoxy composite and (b) unfunctionalised boehmite ● epoxy composite. Pure epoxy ○ is included as a control.

Table 5.3: Weibull parameters

	α ± δα	**β ± δβ**
Epoxy	141 ± 5	9 ± 2
MMT	154 ± 5	11 ±2
Filler A	133 ± 5	10 ±2
Filler B	113 ± 5	9 ±2

Both of these factors improve with well dispersed nano-particles.

Tanaka insists that nano fillers are too small to act as scattering sites[82]. He discusses a method where breakdown voltage can be increased on the basis of the multi-core model[73]. He believes that the Electric Double layers around nano particles can act as sources for Coulombic attraction or repulsion for moving electrons, depending on the polarity of the filler. Electrons are supplied from the negative electrode and/or the Gouy-Chapman diffuse layer, and experience acceleration due to the applied field. When electrons move within the Debye shielding length, they with either be scattered or attracted by the Coulombic force to lose the energy they have gained from the field. When electrons are outside the Debye shielding length, they are accelerated in a polymer matrix and collide with the third layer or enter inside the Debye shield. In any case, electrons are decelerated to increase breakdown voltage.

The correlation between rheology and breakdown results cannot go unnoticed. The filler that gives the lowest viscosity also gives the lowest breakdown value. The fact that the filler is the unfunctioalised boehmite is a positive result, especially where it has been reported that well dispersed organo modified fillers yield superior electrical properties then that of the un-modified variety.

Table 5.3 shows the alpha and beta values outputted from the Weibull++ software used for the Weibull analysis.

5.6 Conclusion

Throughout this chapter, a methodology was developed whereby epoxy composites could be processed and cured to give 100 μm thick samples. To this end, a series of experiments were carried out on pure epoxy to determine gel-times at various temperatures using a simple falling sphere viscometer. It was found that due to the curing kinetics of the epoxy/hardener dispersion should take place in the absence of the curing agent.

Raman spectroscopy was used to characterize the surface chemistry of two varieties of aluminium oxide hydroxide (boehmite). Reference bohemite (un-treated) and sulfonic salt crystals were used to this end. It was seen that the functionalised boehmite had been modified with sulfonic acid.

Montmorillonite (MMT) and boehmite were dispersed in an epoxy matrix using rheology. Although the effects of dispersion could not be quantified at 5% filler loadings using the techniques described in Chapter 4, various flaws were discovered in the model fitting procedure brought about by instrumental fluctuations for Newtonian systems at low shear stresses. This was discovered by calculating how the gradient changes in increment steps between successive data points recorded by the rheometer software.

All systems were seen to remain Newtonian at 5% filler loadings with functionalized boehmite and unfunctionalised MMT consistently giving higher viscosity values than unfunctionalised boehmite across a temperature range 20-50 °C. Unfunctionalised MMT was believed to yield higher viscosities due to the Van der Waals forces between the galleries allowing for easier dispersion as opposed to the hydrogen bonds in the case of unfunctionalised boehmite.

Samples were cast and electrically tested using a standard AC electrical breakdown technique. Unfunctionalised MMT and functionalized boehmite did not seem to affect the insulating properties of the epoxy matrix whereas unfunctionalised boehmite weakened it considerably. This weakening was believed to be due to poor dispersion and interfacial bonding.

CHAPTER 6: Surface Modifications and Silicon Dioxide

6.1 Introduction

This chapter focuses on developing a methodology for surface modifying an inorganic filler to improve interfacial bonding in an epoxy resin matrix.

In the last chapter Raman spectroscopy was seen as a valuble tool in identifying chemical compounds used in modifying inorganic particles. Using various Raman bands, a batch of functionalised boehmite was characterised as having been modified with sulfonic acid. This tried and tested method is applied here, where the addition of a silane coupling agent is monitored quantitively using the Raman technique.

A silane coupling agent bonds very strongly to glassy substances. For this reason, Silicon Dioxide (SiO_2) was used as the inorganic particles in this study. Batches of SiO_2 exist in spherical geometries which also make calculations for amounts of coupling agent to be used a easier task then that of platelets.

Rheological and electrical characterisation are conducted on the organo modifed SiO_2 to observe how the variation of interfacial chemistry has affected the epoxy matrix.

6.2 Raman Spectroscopy; a brief introduction

Raman spectroscopy hinges on the principle of Raman light scattering which was discovered by the Indian professor C. V. Raman in 1921[200]. The simplest picture of the mechanism of the Raman effect can be found by imagining the interaction between a quantum if light (*hv*) and a molecule, as a collision satisfying the law of the conservation of energy. If the incident quantum suffers a loss of energy as a result of the encounter, it appears in the spectrum as a radiation of increased wavelength, i.e. as

a Stokes line, while the molecule which takes up the energy is excited to a higher level of rotation or vibration. It is also possible to conceive of collisions in which the molecule, already in an excited state, gives up its energy to the light quantum and comes down to a lower energy level. The scattered radiation will then appear in the spectrum as a line diminished in wavelength or of increased frequency, i.e. as an anti stokes line. The spectral shifts of the modified radiations from the incident quanta give a measure of the rotational or vibrational frequencies of the molecule.

The important parameters obtained from Raman spectroscopy are the frequency shifts, the state of polarization, and the intensity of the Raman lines. The frequency shifts are expressed in wave numbers (cm^{-1}) and are obtained as the differences of the wave numbers of the incident exciting line and the corresponding Raman lines. If these are multiplied by *c*, the velocity of light, then one gets the actual frequencies of the different modes of vibration. The observed range of frequencies in any Raman spectrum extends from a few cm^{-1} to about 3800 cm^{-1}[1201]. The state of polarization if often expressed as the ratio of the intensities of the horizontal component to the vertical component of the Raman line. If the value is less than 0.1, the line is considered polarized, if it is greater than 0.5, it is considered depolarized.

While infrared absorption involves only one transition – the direct transition between two states - the Raman effect is the result of a double transition involving three stationary levels. The Raman line corresponding to a transition from an initial level to a final level of the system can only occur when there is an intermediate level – the virtual state that can combine with the initial and final state in absorption or emission. The probability of a transition between two states in infrared absorption has no effect on the intensity of Raman scattering. The selection rules which determine the appearance of a Raman line have been worked out by Placezk who has shown that the vibrations of a molecule which produce changes in the induced electric moment (i.e., polarizability) of the molecule are active in the Raman Effect. The symmetrical oscillations of the molecule which are usually missed in the infrared come out more prominently in the Raman scattering, while the antisymmetic vibrations generally show the opposite behaviour. Raman and infrared absorption spectre are complementary in character, the frequency shift, the intensity which depends upon the

change in the polarizability of the molecule during the vibration, the state of polarization of the Raman line which depends on the symmetry character of a particular vibration and the appearance or absence in infrared absorption are the four features that are necessary for the identification of the mode of vibration responsible for any particular Raman line.

6.3 Experimental Procedure

I. Raman Spectrometer

A Renishaw RM1000 Raman spectrometer was used in this research. The laser outputs a 25 mW 785 nm beam.

II. Epoxy and silane z-6040 systems

Three samples were tested in this section. Each one was tested at 100% laser power over a 9 h integration time. The samples are as follows; pure uncured D.E.R 331 epoxy resin, post cured epoxy and silane z-6040.

III. Functionalising silicon dioxide

Nano SiO_2 (7.5 nm) was ordered from Sigma Aldritch. Six samples each consisting of 0.1 g of nano SiO_2, 1 g of methanol and 0, 4.55, 15, 25, 35 and 40 mg of silane z-6040 were added to a beaker. The samples were gently stirred and left overnight. The samples were then washed off using methanol by adding methanol, stirring, and pouring of the excess from the top. This was done three times for each sample. The samples were then heated in a fan oven at ~100 °C for 15 min. The samples were then pressed into 13 mm diameter discs using a Specac press. The samples were tested at 100% laser power over ~30 minute integration period.

Further modifications were made to a 7^{th} sample of SiO_2 with the addition of 15 mg of both silane z-6040 and Jeffamine d-230 hardener. This was done to test whether the

epoxy rings on the silane molecule could be reacted with the amines of the curing agent.

IV. Rheological properties of untreated nano and micro SiO_2

5% weight micro and nano SiO_2 were added to epoxy resin and rheologically tested using the procedure; ramp up to 65 Pa, constant 5 mins, ramp down to 0 Pa. This was carried out at room temperature, 30 °C, 40 °C and 50 °C.

V. Dispersion of silane treated nano SiO_2 with the use of a sonicator.

In order to aid dispersion further, a sonicator was used prior to rheology. The fillers were dispersed by diluting with 10% methanol and sonicating for 30 min. A water bath was used as a heat sink to stabilise the temperature. A solvent was to dilute the epoxy for the following two reasons

(1) To lower the viscosity of the sample such that dispersion could be promoted further.
(2) To keep the viscosity as constant as possible during sample preparation.

Previous experiments demonstrated that the filler dominates the rheological characteristics at high temperatures. For this reason rheology on the dispersions were conducted at 50 °C. 10%wt methanol was used as the dilution amount as in order to reduce the viscosity of the room temperature dispersion to that of epoxy at 50 °C. This can be seen in Figure 6.1(a) where the data point for pure epoxy at 50 °C has the same viscosity for 10% methanol at room temperature.

Functionalised nano SiO_2 was sonicated using a Hielsher UP200S sonicator fitted with a S2 sonotrode (2 mm tip diameter). The frequency of the acoustic wave generated was a constant 24 kHz. Sonication took place at 45 % amplitude power for 30 min.

Post sonication the methanol was removed by placing the material within a vacuum for approximately 1 h. This time was determined empirically by weighing the sample periodically every 5 min. See Figure 6.1(b).

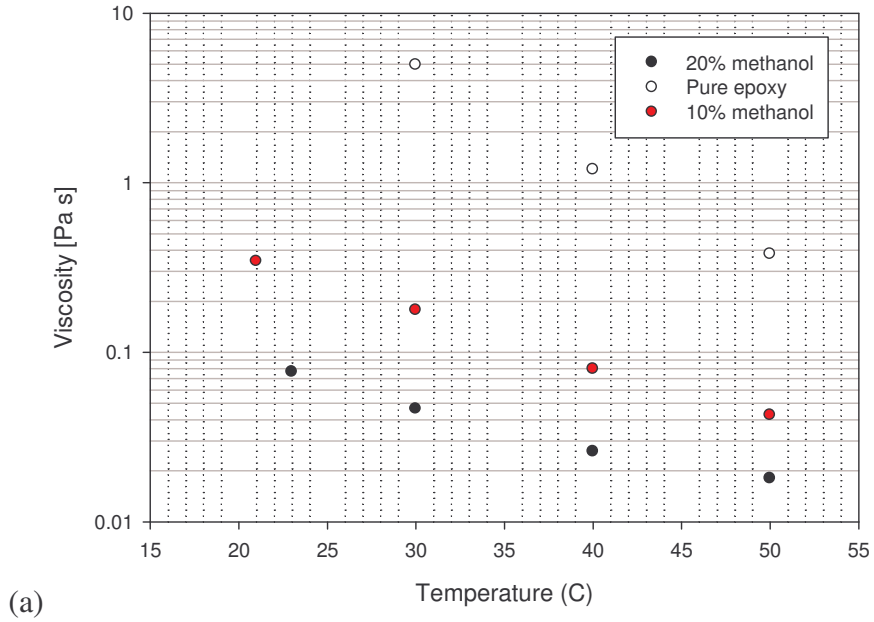

(a)

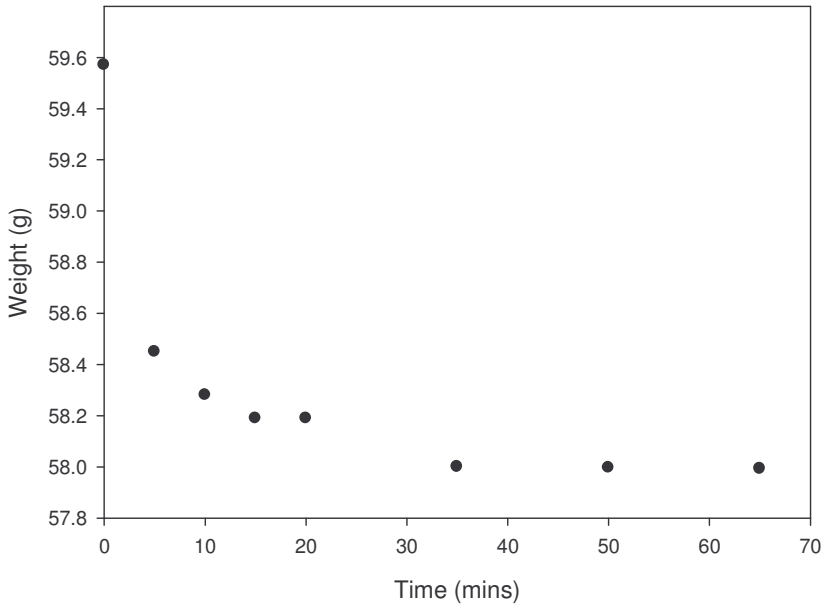

(b)

Figure 6.1: (a) Viscosity as a function of temperature for various epoxy dilutions and (b) methanol evaporation curve in a vacuum.

1%, 5% and 10% silane treated nano SiO_2 was dispersed within 20 ml of epoxy resin described in this way. Rheology was conducted at 50 °C using the procedure; ramp up to 65 Pa, constant 5 mins, ramp down to 0 Pa.

The samples were then cast in the same manner as that described in Chapter 5.

VI. Electrical characterisation of silane treated nano SiO_2

Samples for electrical breakdown were prepared in the same procedure outlined in Chapter 5. All samples were uncoated and varied in thickness from 90 μm to 120 μm.

Electrical breakdown tests were then carried out according to the principles laid out in ASTM D187-89. Each sample was immersed in Dow Corning 200/20cs silicone oil between opposing 6.33 mm steel ball bearings. The lower electrode was connected to earth while the upper electrode was connected to an AC 50 Hz voltage. The sample was put under electrical stress at a ramp rate of 50 V s^{-1} until the sample failed. This was done 20 times per sample. The results were analysed using Weibull statistics with 90% confidence bounds.

6.4 Results

I. Epoxy and silane z-6040 systems

Figure 6.2 shows the Raman spectrogram taken for pure epoxy, post cured epoxy and the coupling agent silane z-6040. The major peak at 1112 cm^{-1} remains relatively constant during the cure process. The energy and intensity of this peak are consistent with an asymmetric breathing vibration of the aromatic rings in the DGEBA resin. Other peaks also remain relatively constant during the cure, including a peak at 1180 cm^{-1}.

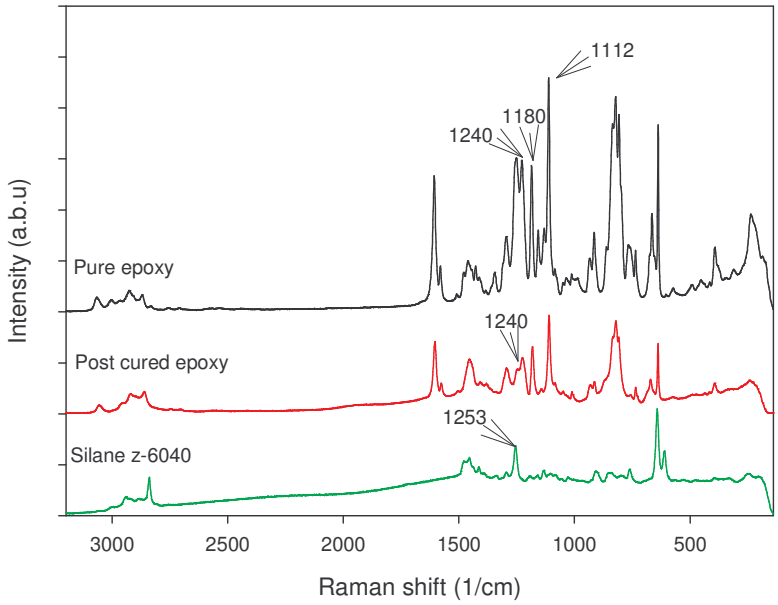

Figure 6.2: Raman spectrogram of Silane z-6040, post cured epoxy and pure uncured epoxy

Several peaks disappear or shift during the curing process, while several new peaks appear. The most obvious change is in the peak located near 1240 cm^{-1}. This peak loses much of its intensity during the cure, and can be assigned to a stretching vibration of the epoxide ring.

Myrick et al.[202] studied the process of a curing epoxy with Raman spectroscopy. The resin and hardener in their study was Dow D. E. R 332 (equivalent weight 176) and T-403 Jeffamine hardener (polyether triamine). They found that all of their peaks appear to change in absolute intensity, which they believed was in response to the changing density of the epoxy as it cures. Both their 1240/1112 cm^{-1} and 1240/1180 cm^{-1} peak intensity ratios were seen to decrease smoothly during the cure process, with the former exhibiting greater sensitivity to the degree of cure. This is also seen for the data presented in Figure 6.2 and is shown in Table 6.1.

Table 6.1: Peak ratios for cured and uncured D.E.R 331 resin

Ratio	**1240/1112 cm^{-1}**	**1240/1180 cm^{-1}**
Uncured epoxy	0.82	1.02
Post cured epoxy	0.73	0.86

The molecular structure of the silane coupling agent used in this research is shown in Figure 6.3. It is designated 3-glycidoxypropyltrimethoxysilane. As can be seen from Figure 6.3, an epoxy ring is present. This is also confirmed from the Raman scan in Figure 6.2 where the assigned stretching of the epoxide ring for the un-cured epoxy resin at near 1240 cm^{-1} is also present for the silane z-6040 scan. The epoxy group on the silane z-6040 molecule has a reactivity similar to that of organic epoxides in that it will undergo ring opening reactions with acids, amines, alcohols, thiols and other epoxides.

The trimethoxysilyl portion of the compound undergoes typical chemistry of alkoxysilanes. The methoxysilyl group is subject to hydrolysis in water or water/alcohol solutions.

(i)

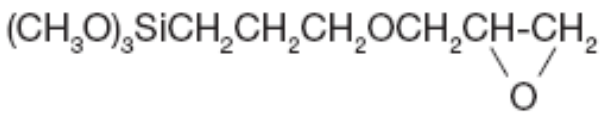

(ii)

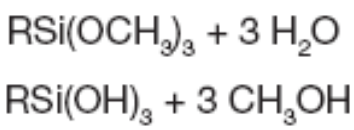

Figure 6.3: (i) Silane z-6040 molecule and production of a (ii) silanetriol from hydrolysis

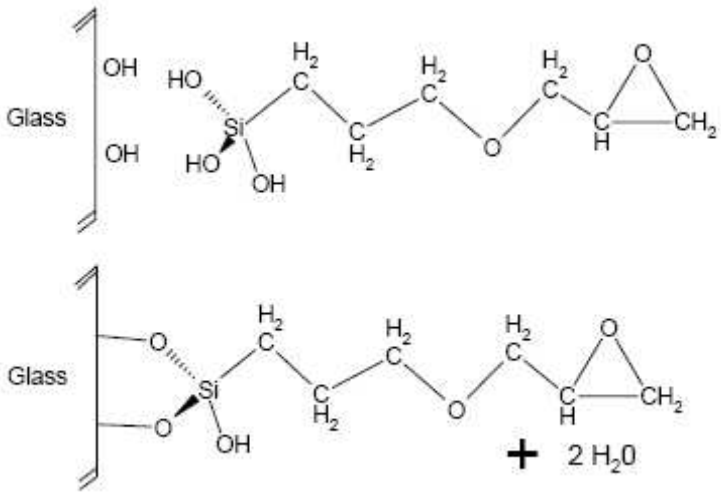

Figure 6.4: Bonding process of silane z-6040 molecule to a siliceous surface

The initial product of hydrolysis is a silanetriol. Silanetriols are moderately stable at dilute concentrations in polar solvents such as water and alcohols. Dispersions of z-6040 are more stable and tend to have favourable orientation on siliceous surfaces if they are applied from a slightly acidic solution.

Silanol groups are capable of condensing with hydroxyl groups at the surface of glass and siliceous minerals (i.e. silicon dioxide) as shown in Figure 6.4. After condensing with the mineral surface, the remaining silanol groups are capable of hydrogen bonding or condensing with adjacent silanol groups. By this combination of covalent and hydrogen bonding, the coupling agent is bonded to the inorganic surface and modifies it so that it is organoreactive.

II. Silicon Dioxide

Figure 6.5 shows a Raman spectrogram of nanosized SiO_2 at 10% and 100% laser power. The scan range was from 200-1700 cm^{-1}. The entire scan range wasn't needed as the epoxide ring is seen at ~1240 cm^{-1}. Minimum and maximum laser powers were used to verify that the laser power at 100% did not ablate the SiO_2 during a 30 min integration time. As can be seen there is no significant difference between the two scans, other than more noise being present in the 10% power setting. This is expected because at 10% power less photons are being emitted, scattered in-elastically and

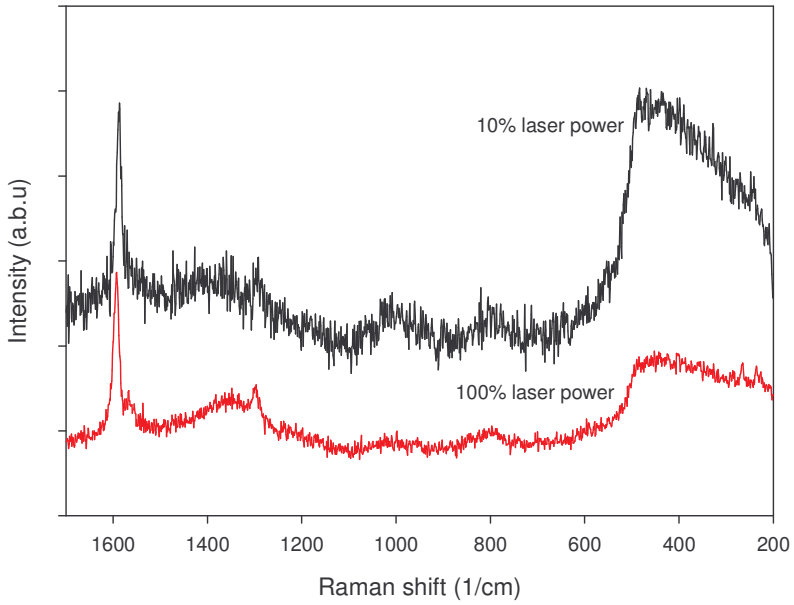

Figure 6.5: Raman spectrogram for SiO_2 at 10% and 100% laser power

therefore detected by the spectrometer. As noise is always being detected by the spectrometer, the less photons from the sample detected means that noise is a higher portion of the signal than for that of 100% laser power.

III. Functionalisation of Silicon Dioxide

Silicon dioxide has an extremely weak Raman spectrum. It is best studied using Fourier transform infrared (FT-IR) if one wants to characterise its spectra. However, for the purposes of this research, detailed analysis of its spectra is not required, only so far as to characterise the chemical treatment applied to its surface. It has already been shown that Raman is suited for the identification of epoxide ring, and that the surfactant to be used has one per molecule. It should then be satisfactory to determine if the technique outlined here is suitable to surface treat the silicon dioxide.

Theoretical calculations were made on the approximate amount of z-6040 that would be needed to coat a nano sized SiO_2 particulate. By considering the surface area of a sphere of a size akin to that of the nano SiO_2, and extending it by the thickness

produced if a silane z-6040 molecule was attached to its surface, one can calculate the mass required to give such a thickness provided the densities are known.

Given a particulate radius r, a surfactant coating thickness t, and the densities of both the particulate ρ_s and the surfactant ρ_z, the relation between their masses can be expressed as

$$\frac{3t\rho_z}{r\rho_s} = \frac{m_z}{m_s}$$

Where m_z and m_s are the masses of the surfactant and particulate respectively. The thickness of a silane z-6040 can be approximated to a couple of nanometres and taking standard data sheet values of density for SiO_2 to be 2200 kgm^{-3} and silane z-6040 to be 1070 kgm^{-3}, a mass of ~40 mg is needed to treat a 0.1 g mass of SiO_2 on the assumption that the particles are all of radii 7.5 nm. This is approximately 40% weight z-6040 to that of the amount of nano SiO_2 to be modified.

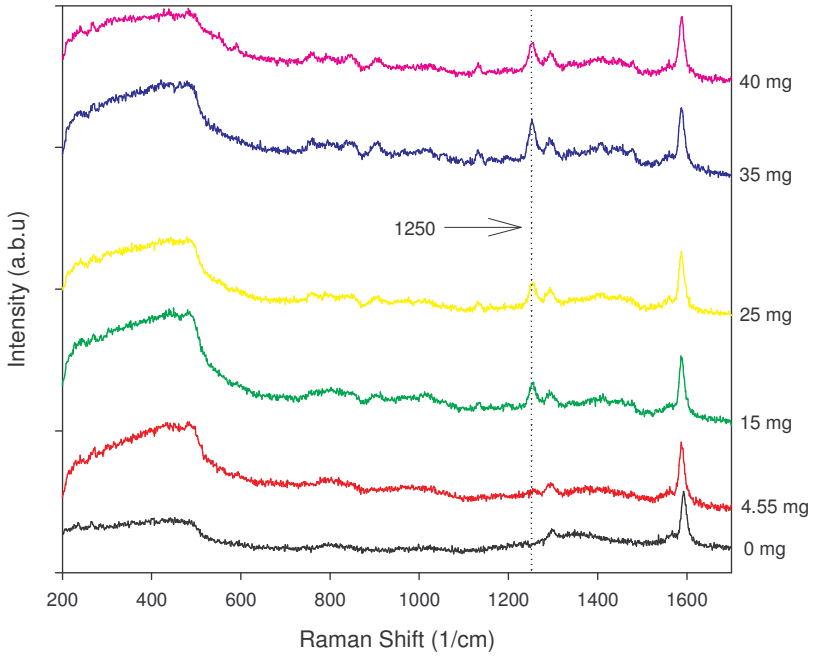

Figure 6.6: Raman spectrogram showing SiO_2 with the addition of varying amounts of silane z-6040 compound

This calculation was the basis for the range of z-6040 masses to be used when attempts of surface treatment were carried out. Figure 6.6 shows the Raman spectrogram taken from samples that had been treated. As can be seen, untreated SiO_2 (0 mg) has no peak around 1250 cm^{-1}. However, with the addition of the silane compound an epoxide peak can be seen to appear at ~ 1250 cm^{-1} that peaks at 15 mg. This is confirmed to be due to the silane z-6040 from Figure 6.2, where an epoxide peak can be seen at ~ 1250 cm^{-1}. This means that it takes 15% z-6040 to modify a known mass of nano SiO_2.

15 mg is lower than the calculated mass needed to coat a SiO_2 particulate, which is due to the fact that not all the particulates will be 7.5 nm in radius and, that many will be existing as large aggregates, meaning there is a smaller surface area to be coated.

Figure 6.7 shows the Raman peaks at ~1250 cm^{-1} normalised (to the 1600 cm^{-1} peak) to that of the untreated SiO_2. This figure is a much clearer representation of Figure 6.6 in the context of a growing peak at ~1250 cm^{-1}. As can be seen, 4.55 mg causes the smallest of increases from the best fit line of the pure SiO_2 whereas amounts of 15 mg + there is a sudden increases in peak height that does not change with additional amounts of silane. This demonstrates that the silane z-6040 compound has actually bonded to the surface of the SiO_2, and that the washing stages of the sample

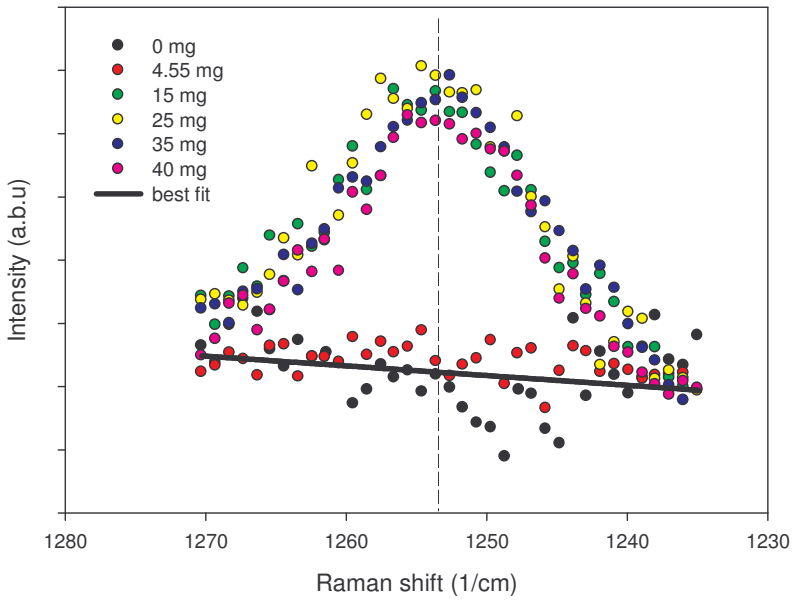

Figure 6.7: Normalised Raman peak at ~1253 cm^{-1} for the silane treated nano

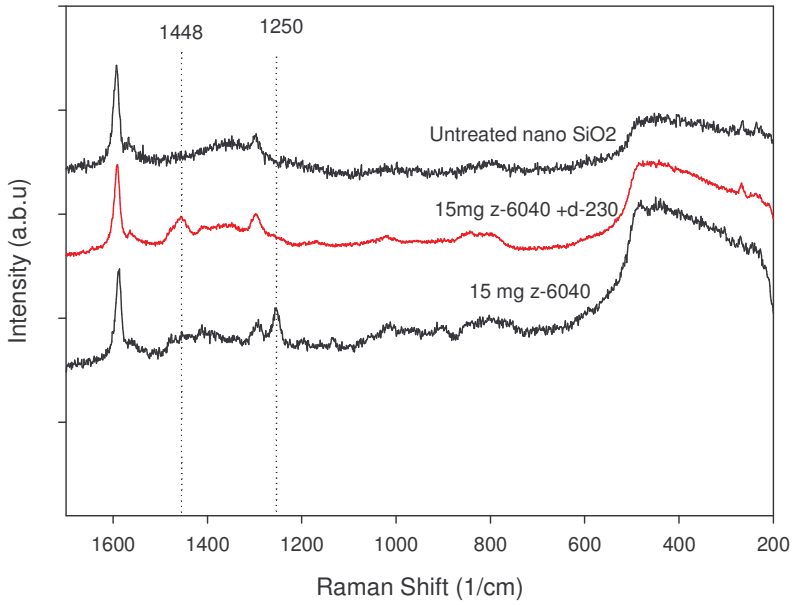

Figure 6.8: Raman spectrogram showing the impact of curing agent Jeffamine d-230 has on SiO_2 treated with silane z-6040

preparation - which removes the residue silane - fails to remove the quantity bonded onto the particulates surface.

Figure 6.8 shows the silane epoxide ring undergo ring opening when the di-amine curing agent is applied during surface modification. This can be seen by the obvious absence of the peak at 1250 cm^{-1} that is so prominent for silane treated SiO_2. The addition of the diamine curing agent has also caused another peak to appear at 1448 cm^{-1}. Unfortunately, no Raman spectra was taken for the curing agent to further verify that the 1448 cm^{-1} peak is due to the presence of the amine groups.

Anastassopoulou et al.[203] who did a thorough study of diamine-copper complexes also found many Raman peaks one of which was at ~ 1448 cm^{-1}. This they claimed characteristic of the bending vibration of the CH_2 group which is a probable explanation as CH_2 molecules exist in the primary, secondary and even tertiary amines that can occur when epoxies cure.

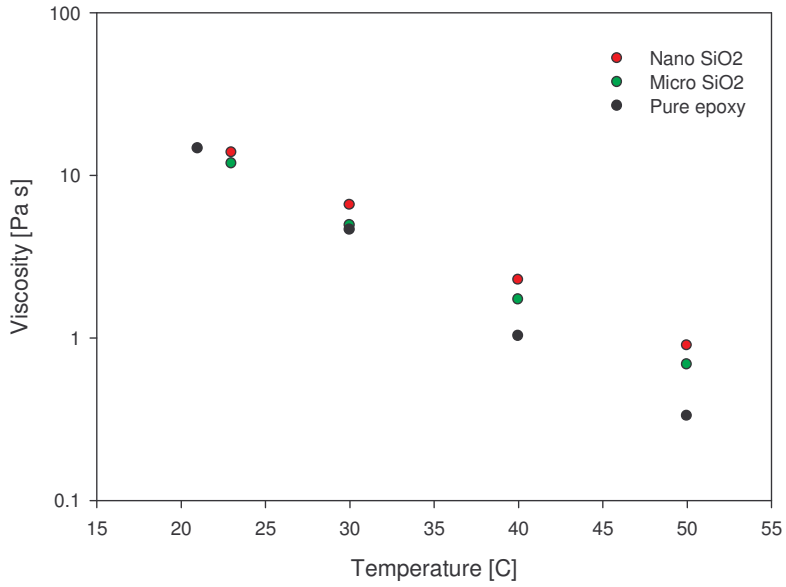

Figure 6.9: Viscosity as a function of temperature for untreated nano and micro SiO_2

IV. Rheological properties of untreated nano and micro SiO_2

Figure 6.9 shows the relationship between untreated nano and micro sized SiO_2 as a function of temperature. Nano SiO_2 has a greater viscosity compared to micro SiO_2 and both consistently give a greater viscosity than the pure epoxy resin throughout the temperature ranges covered here. The fact that the nano silica has a higher viscosity is most likely a consequence of a greater amount of interfacial interactions between filler and matrix. As the temperature increases it can be seen that the silicon systems seem to pull away in terms of viscosity from the pure epoxy resin, in a similar manner to that of the boehmite systems in Chapter 5. Again this is unsurprising as temperature changes in this range would only affect a material already past its glass transition temperature in the context of its viscosity, i.e. only the epoxy is being affected. And as can be seen, the epoxies temperature falls rapidly with temperature, meaning that the impact of any filler present will be revealed at increasingly alleviated temperatures. The absolute values of viscosity and their respective percentage increases over pure epoxy are shown in Table 6.2.

The increases in viscosity over the base resin for micro, nano SiO_2 and the boehmite systems at 30 °C, 40 °C and 50 °C are also shown in Table 6.2 for comparative

Table 6.2: Viscosity values [Pa s] and their % increases over pure epoxy

5% filler loading	**30 °C**	**40 °C**	**50 °C**
Functionalised boehmite	7.4 48%	1.5 53%	0.4 125%
Unfunctionalised boehmite	6.7 34%	1.8 20%	0.7 75%
Micro SiO	4.9 7%	1.7 70%	0.7 133%
Nano SiO_2	6.5 41%	2.3 130%	0.9 200%
Epoxy	4.6	1	0.3

purposes. As can be seen from Table 6.2, the untreated SiO_2 gives a higher increase in viscosity then either of the functionalised or un-functionalised boehmite at 50 °C. The micro SiO_2 gives the smallest increase at 30 °C but rapidly increases at 40 °C and 50 °C. This could be a sign of the filler dispersing within the matrix during rheology, which is a reasonable hypothesis as the nano sized SiO_2 gives continually the highest increase in viscosity except at 30 °C where the functionalised boehmite is greater by 7%.

The unfunctionalised boehmite gives the lowest increases in viscosity post 30 °C. This has been attributed to poor intercalation and dispersion due to the nature of the strong hydrogen bonds that exist between consecutive aluminium layers.

V. Rheological properties of silane treated nano SiO_2

As can be seen from Figure 6.10, the addition of treated SiO_2 at 1% and 5% loading has decreased the viscosity of the resin by ~18%. At 10% an increase of 21% in the composites viscosity was recorded. At 50 °C, an untreated nano SiO2 nanocomposite was reported to have a viscosity of 0.9 Pa s at 5% wt loading (see Table 6.2). However, 10% silane treated nano SiO_2 nanocomposites appears to have half the viscosity ~0.46 Pa s (see, Figure 6.10).

These results are very surprising; however, silanes from Dow Corning have been known to produce these effects when it is used to dilute epoxy. This suggests that excess silane existed in the dispersion despite the washing procedure.

It has often been observed that silane-treated fillers provide lower viscosities in filled resins than do untreated fillers[204,205,206].

Silane coupling agents have been known to reduce the viscosity of aluminium nitride (AlN) particle dispersions within an Araldite epoxy resin[204]. The study looked at the rheological effects of silane with three different head groups. 2% wt. *p*-Tolytrichlorosilane and *p*-Tolytrimethosilane were seen to increase the viscosity of

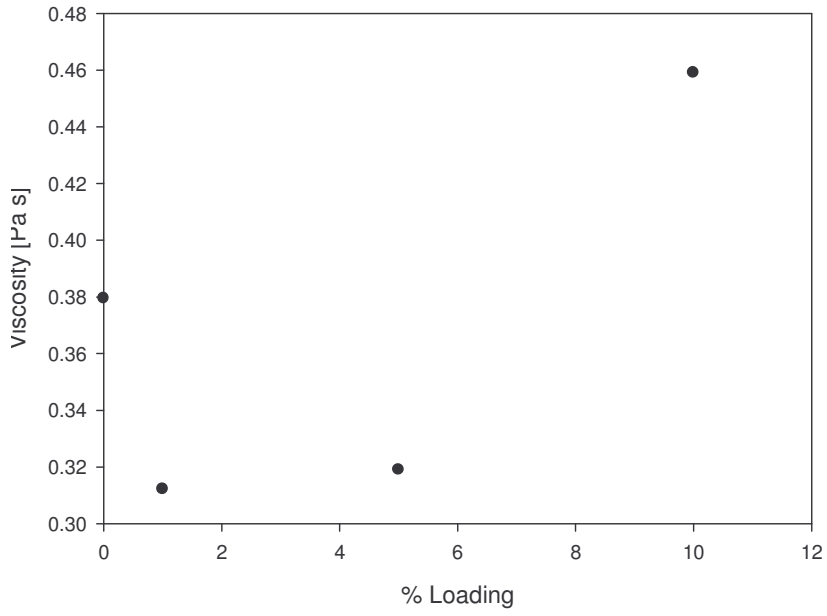

Figure 6.10: Viscosity as a function of silane treated nano SiO_2 loading

treated AlN at 31% vol. solid loading in the epoxy solution at 25 °C. *p*-Tolytrymethylsilane was seen to decrease the viscosity. The degree of viscosity reduction was not linear, at shear rates of 0.2 s^{-1} the reduction was approximately 6% and at 5 s^{-1} it was approximately 66%. The authors proposed that the acidic silanol groups (formed from chloro- and methoxysilanes) may interact far more strongly with the epoxy monomers- causing them to not bond properly to the AlN surfaces - initiate cross linking of epoxy monomers and therefore increase the viscosity, while methylsilanes are thought to be strongly attracted to the AlN surfaces and less so to the epoxy and therefore act as a shield to protect the AlN in epoxy environments. Further research was required by the authors to confirm their hypothesis.

The study progressed by focusing on methylsilane but with 6 different functional groups. The sulfonate functional groups were seen to increase the viscosity considerably – this they reasoned to be due to the polar nature of the functional groups causing the AlN particles to aggregate. The other 5 methylsilanes (acetate, propionic acid, and butyneol) were seen to decrease the viscosity.

Ismail et al.[205] have also reported reductions in viscosity when they used a silane coupling agent (bis(triethoxysilane propyl) tetra sulphide) to compatabilise their bamboo fibres for dispersion within natural rubber.

Marmo and Mostafa[207] showed that matrix filler interactions could be predicted from acid-base considerations and could be modified by selecting the appropriate solvent. The relative acidity of a filler may be designated as the isoelectric point of its surface in water. Polymers may be characterised as acids and bases from Drago's[208] correlation of enthalpies of interaction of organic compounds in neutral solvents. Silanol groups of prehydrolyzed silanes are strongly acidic, neutral alkoxysilanes are neutral to slightly basic, while aminofunctional silanes are basic.

It has been found that the effect of organofunctional additives on viscosity filled resins is strongly influenced by acid-base reactions in filler-additive resin systems. It is possible to predict which silane will have optimum effect on viscosity as well as on strength due to coupling during resin cure[206].

1. Neutral polymers require surface-active additives with all fillers for good dispersion. Almost any polar additive will lower viscosity markedly, but acid-functional additives are most effective with basic fillers, and basic additives are recommended with acid fillers.
2. Acid fillers in basic polymers or basic fillers in acid polymers give fairly good dispersions without additives. Lewis acids (titanates and aluminium alkoxides) may be beneficial on acid fillers in basic polymers, but should not be used with basic fillers in acid polymers.
3. Additives may be very helpful in dispersing acid fillers in acid polymers or basic fillers in basic polymers. Cationic silanes or Lewis acids are of most benefit on acid fillers in acid polymers.
4. Neutral silanes (of which z-6040 is one) modified with catalytic amounts of an amine or a titanate are generally more effective as additives than pure silane in modifying viscosity. Performance as a coupling agent also is improved by such modification.

During treatment, washing silane of small quantities (<1 g) of nano SiO_2 is arduous. Future treatments should be altered by either (a) modifying large quantities of filler, so any loss of SiO_2 during washing won't alter the filler content of the composite or (b) if separate batches for each sample are prepared, the inclusion of centrifuging will be necessary to ensure as much silane is removed prior to mixing with the epoxy.

Figure 6.11 shows SEM images of micro and nano SiO_2 as they exist in their batches.

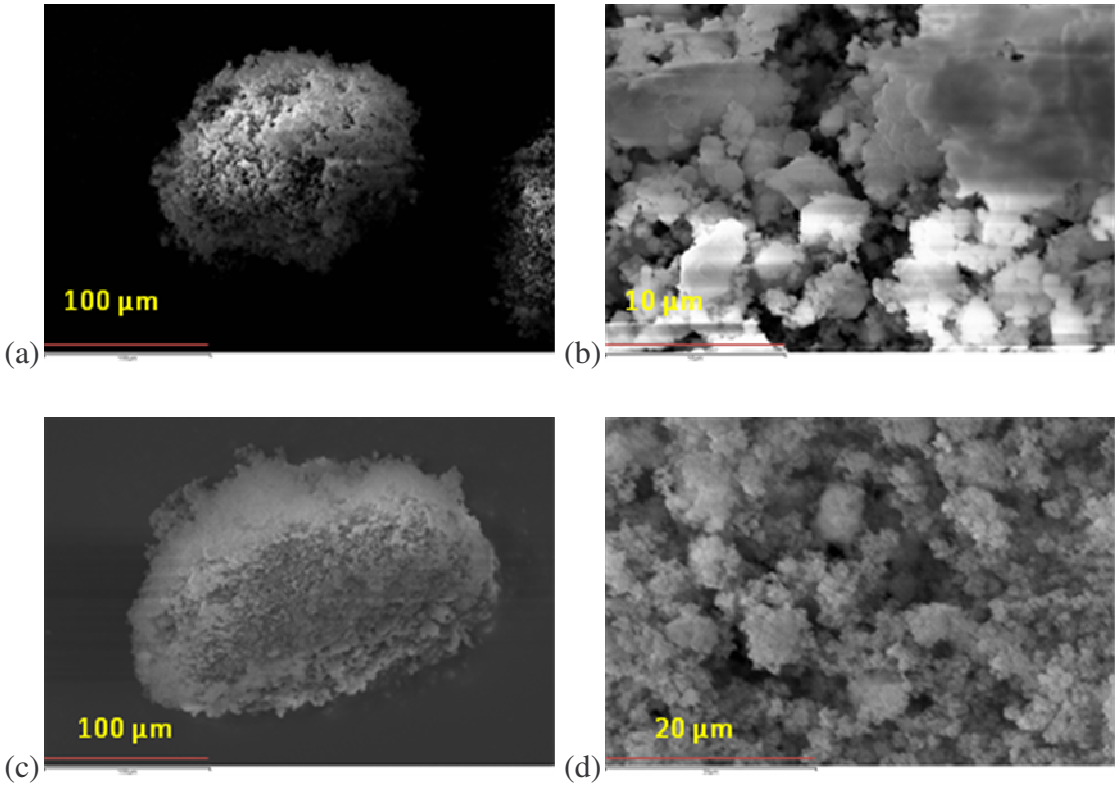

Figure 6.11: SEM images of micro (a-b) and nano (c-d) SiO_2 in powdered form

VI. Electrical characterisation of silane treated nano SiO_2

Figures 6.12 and 6.13 show the electrical breakdown characteristics of silane treated nano SiO_2 using Weibull statistics. Two obvious trends can be seen between the three nanocomposites. Firstly, that silane treated nano SiO_2 has had a positive impact on the electrical breakdown strength for the three filler loadings; 1%, 5% and 10%. The second trend is the greater the filler loading, the lower the spread in breakdown voltages. Simply put, the greater the filler loadings up to 10%, the greater the shape parameter β and, the lower the α values.

Similar results have been reported by Kozako et al.[81] who showed that boehmite samples with 5% and 10% loadings of OS-1 increased the strength of the base resin by 265% at 5% loadings however, there was large scatter in the data that could be interpreted as two Weibull phases. This can be thought of as a matrix and filler phase, which suggests poor dispersion. Their sample at 10% loading showed a much lower spread in data points (lower α value than 5% loaded samples), but again not as low as

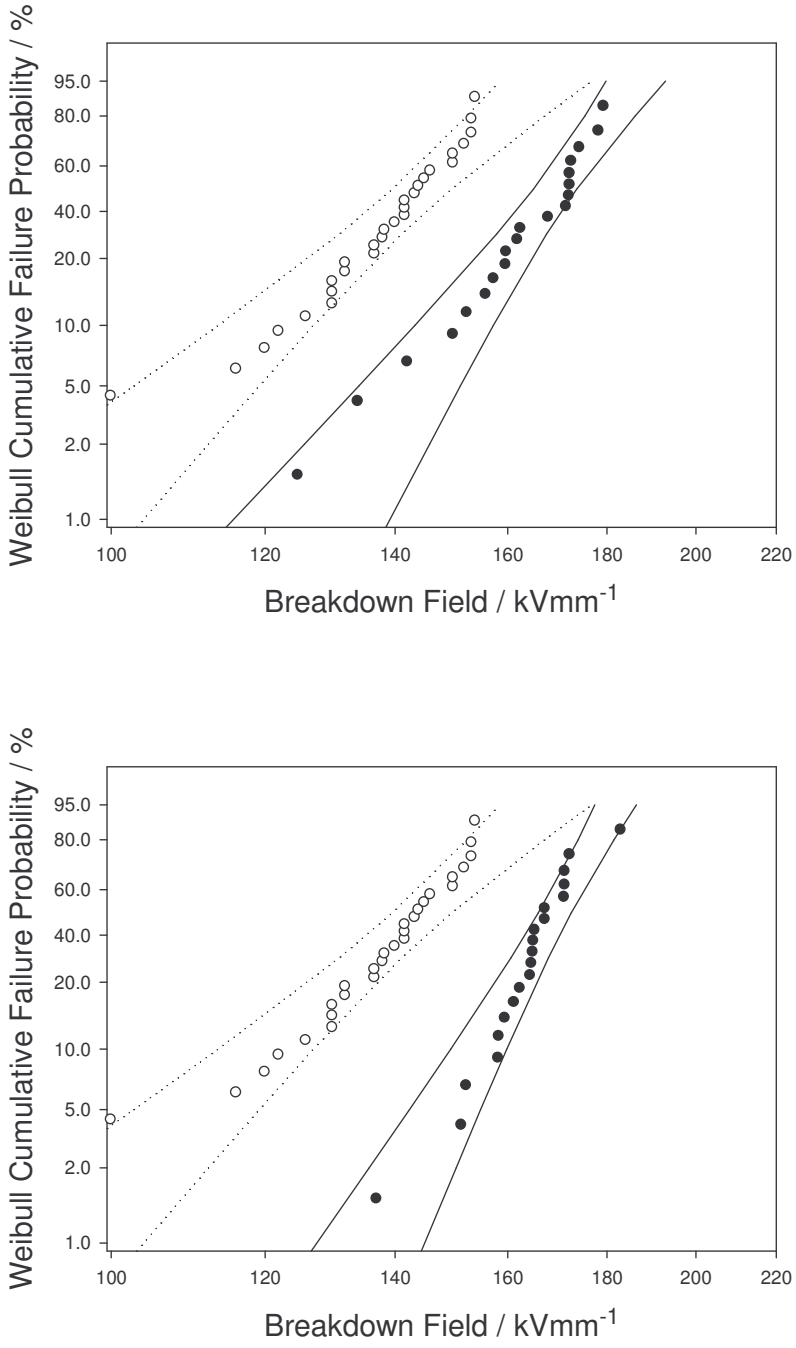

Figure 6.12: Electrical breakdown data for (a) 1% and (b) 5% functionalised nano SiO_2. Where, ○ represents pure epoxy sample and ● the composite sample.

the pure epoxy. The authors claimed the sample was well dispersed using SEM fracture surfaces which provided the improved breakdown results.

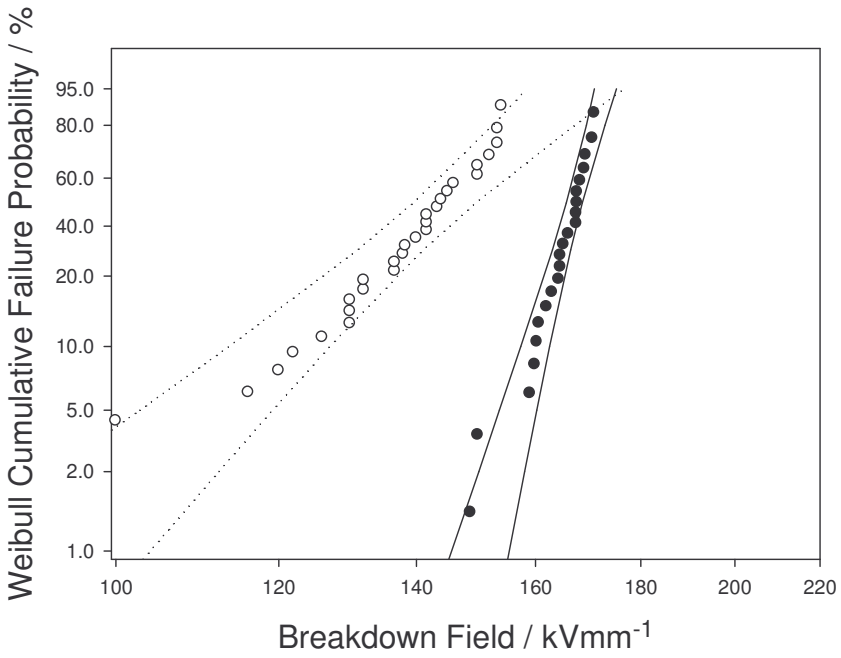

Figure 6.13: Electrical breakdown data for 10% functionalised Nano SiO_2. Where, ○ represents pure epoxy sample and ● the composite sample.

The interfacial bonding between filler and matrix was claimed to be poor for their samples, which they based of their Tg results which remained un-changed throughout increasing filler loadings.

This trend in breakdown behaviour has also been reported for polyethylene/MMT nanocomposites[209]. By going from 5 to 20 parts master batch (master batch - 40% functionalised MMT in a polyethylene pellet) Green et al. reports an increase in β from 8 to 24 which was accompanied by an increase in α of 159 to 171 $kVmm^{-1}$. This result means that not only does the spread in dielectric breakdown readings decrease with filler loading, but the electric field value for a 63% chance to breakdown increases significantly.

Table 6.3 shows the α and β parameters outputted from the Weibull++ statistics software. As can be seen, the α parameter does not change significantly with filler loading. This means that by increasing the amount of silane treated nano SiO_2 from 1% to 10% does not change value of the electric field needed for a 63% chance to breakdown the dielectric. The β parameter, which is related to the spread in recorded

Table 6.3: Weibull parameters for silane treated nano SiO_2

Wt %	**α /kV mm^{-1}**	**β**
0%	141 ± 5	9 ± 2
1%	167 ± 5	15 ± 5
5%	168 ± 3	10 ± 5
10%	166 ± 2	41 ± 12

data points gets significantly larger with increased filler loadings. This means that for increasing organo SiO_2 loadings, the more electrically stable the nanodielectric is as an electrical insulator.

These results are very positive. It shows a good indication of dispersion and interfacial bonding between filler and matrix.

6.5 Conclusion

The aim of this chapter was to develop a methodology to chemically surface treat an inorganic filler using Raman spectroscopy. This method was carried out using by tracking the epoxide vibration mode at 1250 cm^{-1} present on the silane z-6040 coupling agent. This peak was seen to reach a maximum intensity after 15% wt silane had been applied to the nano SiO_2.

The surface chemistry was altered further by the addition of a di-amine curing agent to the silane treated nano SiO_2. The epoxide peak was absent for samples further modified by the curing agent and the addition of a CH_2 peak was seen at 1448 cm^{-1}. CH_2 groups exist in primary, secondary and tertiary amines, so the conclusion that epoxy ring opening and cross linking had taken place. Unfortunately no Raman data of the curing agent was recorded for complete verification.

With the use of a sonicator in addition to the concentric cylinder rheometer, silane treated nano SiO_2 nanocomposite samples were prepared and electrically tested using a standard breakdown procedure. Rheologically, the samples gave the lowest viscosity readings when compared to their untreated counterparts, which was surprising given the results of Chapter 5. This was believed to be due to excess silane being present. 1%, 5% and 10% samples had a very positive impact on the insulation properties of the epoxy matrix. This was seen by the 18% increase in breakdown strength. At increasing loadings the samples demonstrated smaller and smaller spreads in breakdown values; the samples became increasingly more stable when acting as insulators. This was attributed to good dispersion and interfacial bonding between matrix and filler.

Further work using transmission electron microscopy would be needed to allow for further discussions on the dispersive/interfacial qualities of these nanocomposites.

CHAPTER 7: Conclusions and Contributions

The aim of this study was to investigate the rheological properties of a variety of systems in an attempt to quantify dispersion. Although dispersion could not be measured dynamically - and hence be quantified - variation of interfacial chemistry that existed between a variety of fillers was seen to give interesting results in light of their insulation properties when subject to AC breakdown tests.

The rheometer used was of the concentric cylinder geometry. Initial studies with aqueous surfactant systems showed that the equipment gave inaccurate readings below a shear stress of 0.6 Pa. High shear rates ($>1200s^{-1}$) for systems with viscosities lower than 0.001 Pa s were seen to lead to the formation of Taylor vortices that are often associated with the onset of turbulence.

Using poly(ethylene oxide) (PEO) and montmorillonite (MMT), a methodology for data analysis was formulated that could accurately present the data provided by the inaccurate software that collected the data from the rheometer. The De Kee equation was used to model various PEO/MMT compositions, where typical shear thinning phenomena agreement was recorded as the polymeric matrix shifted to high molecular weights. During the course of this work, it was discovered that the rheometer was not sensitive enough to detect variations in viscosity between 0% and 5% filled systems over the three molecular weights tested. As a consequence of this, for the compositions of the systems studied, dispersion could not be measured dynamically or quantified. Optical microscopy techniques showed that the rheometer was adequate as a means of mixing which was demonstrated by the lack of spherulites present in a dried sample.

Dispersions of unfunctionalized MMT, unfunctionalised boehmite and functionalized boehmite in an epoxy matrix were investigated. At increasing temperatures, the fillers were seen to dominate the rheology of the systems. Unfunctionalised boehmite was seen to give the lowest viscosity values, which was thought to be because of the poor interfacial bonding and poor dispersion – due to the nature of the hydrogen bonds

between alumina sheets. The unfunctiomalised boehmite was seen to correlate well with standard AC electrical breakdown tests, in that unfunctionalised boehmite composites gave a significantly lower breakdown than that of the functionalized boehmite and MMT samples; a characteristic of nanocomposites with poor dispersion and poor interfacial bonding.

Raman spectroscopy showed to be a powerful tool in identifying the surface chemistry of functionalized boehmite. This led to the development of the technique using Raman spectroscopy to characterise nano sized silicon dioxide (SiO_2) after its surface had been modified with silane z-6040. The addition of the silane coupling agent z-6040 showed a Raman epoxide peak develop at ~1250 cm^{-1}. This was seen to reach a maximum at 15% wt of silane.

Sonicated dispersions of treated SiO_2 showed far lower values of viscosity then that of the functionalized boehmite. This was believed to be due to excess amounts of silane present in the dispersions. Dispersions of untreated SiO_2 showed the highest viscosity between all epoxy systems studied; a consequence of the large interfacial area inherent to the particulates and by the addition of sonication in sample preparation methodology.

Electrical tests for treated SiO_2 nanocomposites showed an increase of 18% in breakdown strength at the α value (63% probability of breakdown) for 1%, 5% and 10% loaded samples. The β parameter increased dramatically at increased loadings. This was attributed to good dispersion and interfacial bonding. Further work using transmission electron microscopy would be needed to allow for further discussions on the dispersive nature the organo-modified fillers have on the epoxy matrix.

This work contributes methodologies that have been developed throughout the course of this research. These contributions are; Rheology on various systems and the limitations of the equipment, manufacture of epoxy composites/nanocomposite and lastly, surface modifications of inorganic particulates with the use of Raman spectroscopy.

References

[1] ULF W. Gedde. Polymer Physics, Kluwer Academic Publishers

[2] G. Bodor. Structural Investigation of Polymers. Chichester, UK: Ellis Horwood, 1991, pp 182-196

[3] Y. Zhao, A. S. Vaughan, S. J. Sutton, S. G. Swingler. On the Crystallization, Morphology and Physical Properties of a Clarified Propylene/Ethylene Copolymer. Polymer 2001, Vol. 42, pp 6587-6597

[4] Hull, Clyne. An Introduction to Composite Materials. Second Edition, Cambridge University Press

[5] A. Boudefel, P. Gonon. Dielectric Response of an Epoxy Resin when Exposed to High Temperatures. Journal of Materials Science: Materials in Electronics 2006, Vol. 17, pp 205-210.

[6] T. Tanaka. Recent progress in Electrical Insulation Systems and Prospects for the 21st Century. International Symposium on Electrical Insulating Materials 1998, Proceedings pp 29-34

[7] S. Okabe. Insulation Properties and Degradation Mechanism of Insulating Spacers in Gas Insulated Switchgear (GIS) for Repeated/Long Voltage Application. IEEE Transactions on Dielectric and Electrical Insulation 2007, Vol. 14, pp. 101-110

[8] G. T. Barnes, I. R. Gentle. Interfacial Science. Oxford University Press

[9] E. Mader, S. Melcher, J. W. Liu, S. L. Gao, A. D. Bianchi, S. Zherlitsyn, J. Wosnitza. Adhesion of PBO Fiber in Epoxy Composites. Journal of Material Science 2007, Vol. 42, pp 8047-8052

[10] S. J. Park, M. H. Kim, J. R. Lee, S. Choi. Effect of Fiber-Polymer Interactions on Fracture Toughness Behaviour of Carbon Fiber-Reinforced Epoxy Matrix Composites. Journal of Colloid and Interface Science 2000, Vol. 228, pp 287-291

[11] E. Mader. Study of Fiber Surface Treatments For Control of Interphase Properties in Composites. Composite Science and Technology 1997, Vol. 57, pp 1077-1088

[12] Z. Xu, L. Chen, Y. Huang, J. Li, X. Wu, X. Li, Y. Jiao. Wettability of Carbon Fibers Modified by Acrylic Acid and Interface Properties of Carbon Fiber/Epoxy. European Polymer Journal 2008, Vol. 44, pp 494-503

[13] M. I. Aranguren, E. Mora, J. V. DeGroot, Jr: C. W. Macosko. Effect of Reinforcing Fillers on the Rheology of Polymer Melts. Journal of Rheology 1992, Vol. 36, pp 1165-1182

[14] N. E. Marcovich, M. I. Aranguren, M. M. Reboredo. Modified Woodflour as Thermoset Filler. I. Effect of the Chemical Modification and Percentage of Filler om the Mechanical Properties. Polymer 2001, Vol. 42, pp 815-825

[15] M. Alexandre, P. Dubois. Polymer-Layered Silicate Nanocomposites: Preparation, Properties and Uses of a New Class of Materials. Materials Science and Engineering 2000, Vol. 28, pp 1-63

[16] J. E. Mark. Ceramic Reinforced Polymers and Polymer-Modified Ceramics. Polymer Engineering Science 1996, Vol. 36, pp 2905-2920

[17] E. Reynaud, C. Gauthier, J. Perez. Nanophases in Polymers. Review Metallurgie 1999, Vol. 96, pp 169-176

[18] N. Herron, D. L. Thorn. Nanoparticles. Uses and Relationships to Molecular Clusters. Advanced Materials 1998, Vol. 10, pp 1173-1184

[19] P. Calvert. Potential Applications of Nanotubes. T. W. Ebbessen (Ed.), Carbon Nanotubes, CRC Press, Boca Raton, FL, 1997, pp 277-292

[20] A. Usuki, Y. Kojima, M. Kawasumi, A. Okada, Y. Fukushima, O. Kamigaito. Synthesis of Nylon-6-Clay Hybrid. Journal of Material Research 1993, Vol. 8, pp 1179-1183

[21] Y. Kojima, A. Usuki, M. Kawasumi, A. Okada, Y. Fukushima, T. Kurauchi, O. Kamigaito. Mechanical Properties of Nylon-6-Clay Hybrid. Journal of Material Research 1993, Vol. 8, pp 1185-1189

[22] S. R. Sinha, K. Okamoto, M. Okamoto. Structure –property relationship in biodegradable ploly(butylene succinate)/layered silicate nanocomposites. Macromolecules 2003, Vol 36, pp 2355-67

[23] M. W. Noh, D. C. Lee. Synthesis and charcaterization of PS-clay nanocomposite by emulsion polymerization. Polymer Bulletin 1999, Vol. 42, pp 619-626

[24] M. Okamoto, S. Morita, Y. H. Kim, T. Kotaka, H. Tateyama. Dispersed structure change of smectic clay/poly(methyl methacrylate) nanocomposites by copolymerization with polar comonomers. Polymer 2001, Vol. 42, pp 1201-1206

[25] P. H. Nam, P. Maiti, M. Okamoto, T. Kotaka, N. Hasegawa, A. Usuki. A hierarchical structure and properties of intercalated polypropylene/clay nanocomposites. Polymer 2001, Vol. 42, pp 9633-9640

[26] X. Liu, Q. Wu. PP/clay nanocomposites prepared by grafting-melt intercalation. Polymer 2001, Vol. 42, pp 10013-10019

[27] S. S. Ray, P. Maiti, M. Okamoto, K. Yamada, K. Ueda. New Polyactide/Layered Silicate Nanocomposites. 1. Preparation, Characterization, and Properties. Macromolecules 2002, Vol. 35, pp 3104-3110

[28] P. Maiti, P. H. Nam, M. Okamoto. Influence of Crystallization on Intercalation, Morphology, and Mechanical Properties of Polypropylene/Clay Nanocomposites. Macromolecules 2002, Vol. 35, pp 2042-2049

[29] K. S. Seo, D. S. Kim. Curing Behaviour and Structure of an Epoxy/Clay Nanocomposite System. Polymer Engineering and Science 2006, pp 1318-1325

[30] S. C. Zunjarrao, R. P. Singh. Characterization of the Fracture Behaviour of Epoxy Reinforced with Nanometer and Micrometer sized Aluminium Particles. Composite Science and Technology 2006, Vol. 66, pp 2296-2305

[31] Y. Zheng, K. Chonung, G. Wang, P. Wei, P Jiang. Epoxy/Nano Silica Composites: Curing Kinetics, Glass Transition Temperatures, Dielectric, and Thermal-Mechanical Performances. Journal of Applied Polymer Science 2009, Vol. 111, pp 917-927

[32] V. Nigam, D. K. Setua, G. N. Mathur, K. K. Kar. Epoxy Montmorillonite Clay Nanocomposites: Synthesis and Characterization. Journal of Applied Polymer Science 2004, Vol. 93, pp 2201-2210.

[33] Y. Kojima, A. Usuki, M. Kawasumi, A. Okada, T. Kurauchi, O. Kamigaito. Synthesis of Nylon-6 Hybrid by Montmorillonite Intercalated with ε-Caprolactam. Journal of Polymer Science, Part A: Polymer Chemistry 1993, Vol. 31, pp 983-986

[34] S. S. Ray, K. Yamada, M. Okamoto, K. Ueda. New Polyactide-Layered Silicate Nanocomposites. 2. Concurrent Improvments of Material Properties, Biodegradability and Melt Rheology. Polymer 2003, Vol. 44, pp 857-866

[35] A. Blumstein. Polymerization of Adsorbed Monolayers. 2. Thermal Degradation of the Inserted Polymer. Journal of Polymer Science Part A: General Papers, 1965, Vol. 3, Issue 7, pp 2665-2672. Preparation of Clay-Polymer Complex. Journal of Polymer Science, Part A: General Papers 1965, Vol. 3, Issue 7, pp 2653-2664

[36] S. D. Burnside, E. P. Giannelis. Synthesis and Properties of New Poly(dimethylsiloxane) Nanocomposites. Chemistry of Materials 1995, Vol. 7, Issue 9, pp 1597-1600

[37] J. Zhu, A. B. Morgan, F. J. Lamelas, C. A. Wilkie. Fire Properties of Polystyrene-Clay Nanocomposites. Chemistry of Materials 2001, Vol. 13, pp 3774-3780

[38] M. Zanetti, G. Camino, R. Thomann, R. Mulhaupt. Synthesis and Thermal Behaviour of Layered Silicate-EVA Nanocomposites. Polymer 2001, Vol. 42, pp 4501-4507

[39] G. S. Sur, H. L. Sun, S. G. Lyu, J. E. Mark. Synthesis, Structure, Mechanical Properties, and Thermal Stability of Some Polysulfone/Organoclay Nanocomposites. Polymer 2001, Vol. 42, pp 9783-9789

[40] B. Lepoittevin, M. Devalckenaere, N. Pantoustier, M. Alexandre, D. Kubies, C. Calberg, R. Jerome, P. Dubois. Poly(ε-caprolactone)/Clay Nanocomposites Prepared by Melt Intercalation: Mechanical, Thermal and Rheological Properties. Polymer 2002, Vol. 43, pp 4017-4023

[41] B. Guo, D. Jia, C. Cai. Effects of Organo-Montmorillonite Dispersions on Thermal Stability of Epoxy Resin Nanocomposites. European Polymer Journal 2004, Vol. 40, pp 1743-1748

[42] Y. Sun, Z. Zhang, K. S. Moon, C. P. Wong. Glass Transition and Relaxation Behaviour of Epoxy Nanocomposites. Journal of Polymer Science, Part B: Polymer Physics 2004, Vol. 42, pp 3849-3858

[43] J. W. Gilman, C. L. Jackson, A. B. Morgan, R. Harris, Jr. Flammanility Properties of Polymer-Layered Silicate Nanocomposites. Polypropylene and Polystyrene Nanocomposites. Chemistry of Materials 2000, Vol. 12, pp 1866-1873

[44] J. W. Gilman. Flammability and Thermal Stability Studies of Polymer Layered Silicate (Clay) Nanocomposites. Applied Clay Science 1999, Vol. 15, pp 31-49

[45] K. Yano, A. Usuki, A. Okada. Synthesis and Properties of Polyimide-Clay Hybrid Films. Journal of Polymer Science, Part A: Polymer Chemistry 2000, Vol. 35 pp 2289-2294

[46] S. S. Ray, K. Yamada, M. Okamoto, A. Ogami, K. Ueda. New Polyactide/Layered Silicate Nanocomposites. 3. High Performance Biodegradable Materials. Chemistry of Materials 2003, Vol. 15, pp 1456-1465

[47] R. Xu, E. Manias, A. J. Snyder, J. Runt. New Biomedical Poly(urethane urea)-Layered Silicate Nanocomposites. Macromolecules 2001, Vol. 34, pp 337-339

[48] R. K. Bharadwaj. Modeling the Barrier Properties of Polymer-Layered Silicate Nanocomposites. Macromolecules 2001, Vol. 34, pp9189-9192

[49] R. A. Vaia, S. Vasudevan. W. Krawiec, L. G. Scanlon, E. P. Giannelis. New Polymer Electrolyte Nanocomposites: Melt Intercalation of Poly(ethylene oxide) in Mica Type Silicates. Advanced Materials 1995, Vol. 7, pp 154-156

[50] J. C. Hutchison, R. Bissessur, D. F. Shriver. Conductivity Anisotropy of Polyphosphazene-Montmorillonite Composite Electrolytes. Chemistry of Materials 1996, Vol. 8, pp 1597-1599

[51] K. E. Strawhecker, E. Manias. Structure and Properties of Poly(vinyl alcohol)/Na^+ Montmorillonite Nanocomposites. Chemistry of Materials, Vol. 12, pp 2943-2949

[52] J. A. Tetto, D. M. Steeves, E. A. Welsh, B. E. Powell. Biodegradable Poly(ε-caprolactone)/clay nanocomposites. ANTEC'99. pp 1628-1632

[53] Y. S. Song, J. R. Youn. Influence of Dispersion States of Carbon Nanotubes on Physical Properties of Epoxy Nanocomposites. Carbon 2005, Vol. 43, pp 1378-1385

[54] B. Guo, D. Jia, C. Cai. Effects of Organo-Montmorillonite Dispersion on Thermal Stability of Epoxy Resin Nanocomposites. European Polymer Journal 2004, Vol. 40, pp 1743-1748

[55] T. Lam, P. D. Kaviratna, T. J. Pinnavaia. Mechanisms of Clay Tactoid Exfoliation in Epoxy-Clay Nanocomposites. Chemical Materials 1995, Vol. 7, pp 2144-2150

[56] H. Wang, S. V. Hoa, P. M. Wood-Adams. New Method for the Synthesis of Clay/Epoxy Nanocomposites. Journal of Applied Polymer Science 2006, Vol. 100, pp 4286-4296.

[57] P. F. Luckham, M. A. Ukeje. Effect of Particle Size Distribution on the Rheology of Dispersed Systems. Journal od Colloid and Interface Science 1999, Vol. 220, pp 347-356

[58] T. P. Mohan, M. R. Kumar, R. Velmurugan. Rheology and Curing Characteristics of Epoxy-Clay Nanocomposites. Polymer International 2005, Vol. 54, pp 1653-1659

[59] R. Krishnamoorti, R. A. Vaia, E. P. Giannelis. Structure and Dynamics of Polymer Layered Silicate Nanocomposites. Chemistry of Materials 1996, Vol. 8, pp 1728-1734

[60] M. J. Solomon, A. S. Almusallam, K. F. Seefeldt, S. Somwangthanaroj, P. Varadan. Rheology of Polypropylene/Clay Hybrid Materials. Macromolecules 2001, Vol. 34, pp 1864-1872

[61] G. Galgali, C. Ramesh, A. Lele. A Rheological Study on the Kinetics of Hybrid Formation in Polypropylene Nanocomposites. Macromolecules 2001, Vol. 34, pp 852-858

[62] L. L. Pluart, J. Duchet, H. Sautereau, P. Halley, J. F. Gerard. Rheological Properties of Organoclay Suspensions in Epoxy Network Precursors. Applied Clay Science 2004, Vol. 25, pp 207-211

[63] http://en.wikipedia.org/wiki/Dielectric_spectroscopy, accessed November 2009

[64] J. K. Nelson, L. A. Utracki, R. K. Macrone, C. W. Reed. Role of the interface in Determining the Dielectric Properties of Nanocomposites. IEEE-CEIDP 2004, pp 314-317

[65] R. Sarathi, R. K. Sahu, P. Rajeshkumar. Understanding the Thermal, Mechanical and Electrical Properties of Epoxy Nanocomposites. Materials Science and Engineering A 2007, Vol. 445-446, pp 567-578

[66] T. Imai, Y. Hirano, H. Hirai, S. Kojima, T. Shimizu. Preparation and Properties of Epoxy-Organically Modified Layered Silicate Nanocomposites. IEEE-ISEI 2002, pp 379-383

[67] S. Singha, M. J. Thomas. Permittivity and Tan Delta Characteristics of Epoxy Nanocomposites in the Frequency Range of 1 MHz -1GHz. IEEE Transactions on Dielectrics and Electrical Insulation 2008. Vol. 15, No. 1, pp 1-11

[68] Y. Rao, J. M. Pochan. Mechanics of Polymer-Clay Nanocomposites. Macromolecules 2007, Vol. 40, pp 290-296

[69] G. J. Papakonstantopoulos, M. Doxastakis, P. F. Nealey, J. L. Barrat, J. J. de Pablo. Calculation of local mechanical properties of filled polymers. Physical Review E 2007, Vol. 75, pp 031803(1) – 038103(13)

[70] R. C. Picu, A. Rakshit. Dynamics of free chains in polymer nanocomposites. Journal of Chemical Physics 2007, Vol. 126, pp 144909(1) – 144909(6)

[71] J. Lewis. Nanometric Dielectrics. IEEE Transactions on Dielectrics and Electrical Insulation 1994. Vol. 1, No. 5, pp 812 - 825

[72] T. J. Lewis. Interfaces are the Dominant Feature of Dielectrics at the Nanometric Level. IEEE Transactions on Dielectrics and Electrical Insulation 2004, Vol. 11 No. 5, pp 739-753

[73] T. Tanaka, M. Kozako, N. Fuse, Y. Ohki. Proposal of a Multi Core Model for Polymer Nanocomposite Dielectrics. IEEE Transaction on Dielectrics and Electrical Insulation 2005, Vol. 12, No. 4, pp 669-681

[74] V. Singh, A. R. Kulkarni, T. R. Rama Mohan. Dielectric Properties of Aluminun-Epoxy Composites. Journal of Applied Polymer Science 2003, Vol. 90, pp 3602-3608

[75] J. C. Fothergil, J. K. Nelson, M. Fu. Dielectric Properties of Epoxy Nanocomposites Containing TiO_2, Al_2O_3 and ZnO Fillers, IEEE-CEIDP 2004, pp 406-409

[76] N. Tagami, M. Okada, N. Hirai, Y. Ohki, T. Tanaka, T. Imai, M. Harada, M. Ochi. Dielectric Properties of Epoxy/Clay Nanocomposites – Effects of Curing Agent and Clay Dispersion Method-. IEEE Transactions on Dielectrics and Electrical Insulation 2008, Vol. 15, No. 1, pp 24-32

[77] T. Imai, F. Sawa, T. Ozaki, T. Shimizu, R. Kido, M. Kozako, T. Tanaka. Influence of Temperature on Mechanical and Insulation Properties of Epoxy Layered Silicate Nanocomposites. IEEE Transactions on Dielectrics and Electrical Insulation 2006, Vol. 13, No. 1, pp 445-452

[78] C. Zilg, D. Kaempfer, R. Thomann, R. Muelhaupt, G. C. Montanari. Electrical Properties of Polymer Nanocomposites. IEEE-CEIDP 2003, pp 546-550

[79] G. C. Montanari, D. Fabiani, F. Palmieri. Modification of Electrical Properties and Performance of EVA and PP Insulation through Nanostructure by Organophilic Silicates. IEEE Transactions on Dielectrics and Electrical Insulation 2004. Vol. 11, No. 5, pp 754-762

[80] J. K. Nelson, Y. Hu, J. Thiticharoenpong. Electrical properties of TiO2 nanocomposites. IEEE-CEIDP 2003, pp 719-722

[81] M. Kozako, Y. Ohki, M. Kohtoh, S. Okabe, T. Tanaka. Preparation and Various Characteristics of Epoxy/Alumina Nanocomposites. IEEJ Transactions FM 2006, Vol. 126, No. 11, pp 1121-1127

[82] T. Tanaka. Dielectric Nanocomposites with Insulating Properties. IEEE Transactions on Dielectrics and Electrical Insulation 2005. Vol. 12, No. 5, pp 914-928

[83] V. Illingworth (editor). Dictionary of Physics, Second Edition, Penguin Publishing

[84] S. Pople. Advanced Physics Through Diagrams. Oxford University Press

[85] R. Muncaster. A-Level Physics, 4th Edition. Stanley Thornes (Publishers) Ltd.

[86] M. Clugston, R. Flemming. Advanced Chemistry. Oxford University Press

[87] P. K. Vinson, J. R. Bellare, H. T. Davis, W. G. Miller, L. E. Scriven. Direct Imaging of Surfactant Micelles, Vesicles, Discs, and Ripple Phase Structures by Cryo-Transmission Electron Microscopy. Journal of Colloid and Interface Science 1991, Vol. 142

[88] R. F. Kamrath, E. I. Franses. Thermodynamics of Mixed Micellization. Pseudo Phase Separation Models. Industrial and Engineering Chemistry Fundamentals 1983, Vol. 22, pp 230-239

[89] H. A. Barnes, J. F. Hutton, K. Walters. An Introduction to Rheology; Volume 3 of Rheology Series. Elsevier publishing 1989, pp 27

[90] D. R. Lide. CRC Handbook of Chemistry and Physics, 73rd edition. 1992-1993

[91] Z. Tadmor, C. G. Gogos. Principles of polymer processing. John Wiley and Sons publishing, 2006, pp 108-109

[92] G. C. Kalur, S. R. Raghaven. Anionic Wormlike Micellar Fluids that Display Cloud Points: Rheology and Phase Behavior. Journal of Physical Chemistry 2005, Vol. 109, No. 18, pp 8599-8604

[93] N. Pilpel. Viscoelasticity in Aqueous Soap Solutions. Journal of Physical Chemistry 1956. Vol. 60, pp 779-782

[94] M. E. Cates, S. J. Candau. Statistics and Dynamics of Worm-Like Surfactant Micelles. Journal of Physics: Condensed Matter 2 1990, Vol. 2, pp 6869-6892

[95] P. A. Hassan, S. R. Raghavan, E. R. Kaler. Microstructural Changes in SDS Micelles Induced by Hydotropic Salt. Langmuir 2002, Vol. 18, pp 2543-2548

[96] L. J. Magid, Z. Li, P. D. Butler. Flexibility of Elongated Sodium Dodecyl Sulfate Micelles in Aqueous Sodium Chloride: A Small Angle Neutron Scattering Study. Langmuir 2000, Vol. 16 pp 10028-10036

[97] S. Chandrasekhar. Hydrodynamics and Hydromagnetic Stability. Dover, New York, 1961

[98] G. I. Taylor. Stability of a Viscous Liquid Contained Between Two Rotating Cylinders. Philosophical Transactions for the Royal Society of London 1923, Vol. A 223, pp 289-343

[99] Hua-Shu Do, B. C. Khoo, K. S. Yeo. Energy Loss Distribution in the Plane Couette Flow and the Taylor-Couette Flow Between Concentric Rotating Cylinders. International Journal of Thermal Sciences 2007, Vol. 46, pp 262-275

[100] H. Schlichting. Boundary Layer Theory. Fourth Edition, McGraw-Hill series in Mechanical Engineering

[101] H. Faist, B. Eckhardt. Transition from Couette-Taylor System to the Plane Couette System. Physical Review E 2000, Vol. 61

[102] H.-S. Dou. Energy Gradient Theory of Hydrodynamic Instability. The Third International Conference on Nonlinear Science, Singapore, 30 June-2 July, 2004, Also H.-S. Dou, Mechanism of Flow Instability and Transition to Turbulence. International Journal of Non-Linear Mechanics. Vol. 41 (2006) pp 512-517.

[103] H.-S. Dou, B. C. Khoo, K. S. Yeo. Flow Transition in Plane Couette Flow. Technical Report of National University of Singapore, October 2003

[104] E. L. Koschmieder. Bénard Cells and Taylor Vortices. Cambridge University Press.

[105] R. H. F. Pao. Fluid Dynamics. Merrill Books, Inc., Columbus, Ohio

[106] D. Coles. Transition in Circular Couette Flow. Journal of Fluid Mechanics 1986, Vol. 164, pp 155-183

[107] H. Faisst, B. Eckhardt. Transition from the Couette-Taylor system to the Plane Couette System. Physical Review E 61 2000, 7227-7230

[108] Y. S. Song, J. R. Youn. Influence of Dispersion States of Carbon Nanotubes on Physical Properties of Epoxy Nanocomposites. Carbon 2005, Vol. 43, pp 1378-1385

[109] L. Quercia, F. Loffredo, G. Di Francia. Influence of Filler Dispersion on Thin Film Composites Sensing Properties. Sensors and Actuators B 2005, Vol. 109, pp 153-158

[110] Y. H. Lee, C. B. Park, M. Sain, M. Kontopoulou, W. Zheng. Effects of Clay Dispersion and Content on the Rheological, Mechanical Properties, and Flame Retardance of HDPE/Clay Nanocomposites. Journal of Applied Polymer Science 2003, Vol. 104, pp 1993-1999

[111] T. Ramanathan, S. Stankovich, D. A. Dikin, H. Liu, H. Shen, S. T. Nguyen, L. C. Brinson. Graphitic Nanofillers in PMMA Nanocomposites – An Investigation of Particle Size Dispersion and their Influence on Nanocomposite Properties. Journal of Polymer Science: Part B: Polymer Physics 2007. Vol. 45, pp 2097-2112

[112] J. Moczo, E. Fekete, K. Laszlo, B. Pukanszky. Arregation of Particulare Fillers: Factors, Determination, Properties. Macromolecules Symposium 2003, Vol. 194, pp 111-124

[113] G. Karlstrom. A New Model for Upper and Lower Criticle Solution Temperatures in Poly(ethylene oxide) Solutions. The Journal of Physical Chemistry 1985, Vol. 89, pp 4962-4964

[114] M. Malmsten, P. Linse, K. W. Zhang. Phase Behaviour of Aqueous Poly(ethylene oxide)/Poly(propylene oxide) Solutions. Macromolecules 1993, Vol. 26, pp 2905-2910

[115] S. Bekiranov, R. Bruinsma, P. Pincus. Solution Behaviour of Poly(ethylene oxide) in Water as a Function of Temperature and Pressure. Physical Review E 1997, Vol. 55, pp 577-585

[116] A. Matsuyama, F. Tanaka. Theory of Solvation-Induced Reentrant Phase Seperation in Polymer Solutions. Phsyical Review Letters 1990, Vol. 65, pp 341-344

[117] R. Kjellander, E. Florin. Water Structure and Changes in Thermal Stability of the System Poly(ethylene oxide)-Water. Journal of Chemistry Society: Faraday Transactions 1, 1981, Vol. 77, pp 2053-2077

[118] E. E. Dormidontova. Role of Competitive PEO-Waer and Water-Water Hydrogen Bonding in Aqueous Solution PEO Behaviour. Macromolecules 2002, Vol. 35, pp 987-1001

[119] E. E. Dormidontova. Influence of End Groups on Phase Behaviour and Properties of PEO in Aqueous Solutions. Macromolecules 2004, Vol. 37, pp 7747-7761

[120] G. D. Smith, D. Bedrov, O. Borodin. Molecular Dynamics Simulation Study of Hydrogen Bonding in Aqueous Poly(ethylene oxide) Solutions. Physical Review Letters 2000, Vol. 85, pp 5583-5586

[121] D. L. HO, B. Hammouda, S. R. Kline. Clustering of Poly(ethylene oxide) in Water Revisted. Journal of Polymer Science: Part B: Polymer Physics 2003, Vol. 41, pp 135-138

[122] K. Devanand, J. C. Selser. Asymptotic Behaviour and Long-Range Interactions in Aqueous Solutions of Poly(ethylene oxide). Macromolecules 1991, Vol. 24, pp 5943-5947

[123] Y. C. Bae, S. M. Lambert, D. S. Soanne, J. M. Prausnitz. Cloud-Point Curves of Polymer Solutions from Thermooptical Measurements. Macromolecules 1991, Vol. 24, pp 4403-4407

[124] S. Magazu. NMR, Static and Dynamic Light and Neutron Scattering Investigations on Polymeric Aqueous Solutions. Journal of Molecular Structure 2000, Vol. 523, pp 47-59

[125] H. Venohr, V. Fraaije, H. Strunk, W. Borchard. Static and Dynamic Light Scattering from Aqueous Poly(ethylene oxide) Solutions. European Polymer Journal 1998, Vol. 34, pp 723-732

[126] S. Kawaguchi, G. Imai, J. Suzuki, A. Miyahara, T. Kitano, K. Ito. Aqueous Solution Properties of Oligo-and Poly(ethylene oxide) by Static Light Scattering and Intrinsic Viscosity. Polymer 1997, Vol. 38, pp 2885-2891

[127] W. F. Polik, W. Burchard. Static Light Scattering from Aqueous Poly(ethylene oxide) Solutions in the Temperature Range 20-90 °C. Macromolecules 1983, Vol. 16, pp 978-982

[128] C. Branca, S. Magazu, G. Maidano, P. Migliardo, V. Villari. Conformational Distribution of Poly(ethylene oxide) in Molten Phase and in Aqueous Solution by Quasi-Elastic and Inelastic Light Scattering. Journal of Physics: Condensed Matter 1998, Vol. 10, pp 10141-10157

[129] T. W. M. Bieze, A. C. Barnes, C. J. M. Huige, J. E. Enderby, J. C. Leyte. Distribution of Water around Poly(ethylene oxide): A Neutron Diffraction Study. The Journal of Physical Chemistry 1994, Vol. 98, No. 26, pp 6568-6576

[130] S. Lusse, K. Arnold. The Interaction of Poly(ethylene glycol) with Water Studied by 1H and 2H NMR Relaxation Time Measurements. Macromolecules 1996, Vol. 29, pp 4251-4257

[131] M. M. Fares, J. Hacaloglu, S. Suzer. Characterization of Degradation Products of Polyethylene Oxide by Pyrolysis Mass Spectrometry. European Polymer Journal, 1994, Vol. 30, pp 845-850

[132] J. Schiers, S. W. Bigger, O. Delatycki. Characterizing the Solid-State Thermal Oxidation of Poly(ethylene oxide) Powder, Polymer, 1991, Vol. 30, pp 2014-2019

[133] M. M. Crowley, F. Zhang, J. J. Koleng, J. W. McGinity. Stability of Polyethylene Oxide in Matrix Tablets Prepared by Hot-Melt Extrusion. Biomaterials, 2002, Vol. 23, pp 4241-4248

[134] A. R. D. Almeida, M. L. Dias. Comparative Study of Shear Degradation of Carboxymethylcellulose and Poly(ethylene) Oxide in Aqueous Solution. Polymer Degradation and Stability, 1997, Vol. 56, pp 331-337

[135] J. Q. G. Maclaine, C. Booth. Effect of Molecular Weight on Crystallization Isotherms of High Molecular Weight Poly(ethylene oxide) Fractions. Polymer, 1975, Vol. 16, pp 680-684

[136] G. N. Malcolm, J. S. Rowlinson. The Thermodynamic Properties of Aqueous Solutions of Polyethylene Glycol, Polypropylene Glycol and Dioxane. Transactions of the Faraday Society 1957, Vol. 53, pp 921-931

[137] K. Sasahara, M. Sakurai, K. Nitta. Volume and Compressibility Changes for Short Poly(ethylene glycol)-Water Systems at Various Temperatures. Colloid & Polymer Science 1998, Vol. 276, pp 643-647

[138] H. Gheng, R. Rosen, B. Zheng, H. Shimoda, L. Flemming, J. Liu, O. Zhou. Fabrication and Properties of Composites of Poly(ethylene oxide) and Functionalized Carbon Nanotubes. Advanced Materials, 2002, Vol. 14, pp 1387-1390

[139] E. Hackett, E. Mantas, E. P. Giannelis. Computer Simulation Studies of PEO/Layer Silicate Nanocomposites. Chemistry of Materials, 2000, Vol. 12, pp 2161-2167

[140] V. Kuppa and E. Manias. Computer Simulation of PEO/Layered-Silicate Nanocomposites: 2. Lithium Dynamics in PEO/Li+ Montmorillonite Intercalates. Chemistry of Materials, 2002, Vol. 14, pp 2171-2175

[141] K. E. Strawhecker, E. Manias. Crystallization Behaviour of Poly(ethylene oxide) in the presence of Na^+ Montmorillonite Fillers. Chemical Materials, 2003, Vol. 15, pp 844-849

[142] M. Y. Hikosaka, S. H. Pulcinelli, C. V. Santilli, K. Dahmouche, A. F. Craievich. Montmorillonite (MMT) Effect on the Structure of Poly(oxyethylene) (PEO)-MMT Nanocomposites and Silica-PEO-MMT Hybrid Materials. Journal of Non-Crystalline Solids, 2006, Vol. 352, pp 3705-3710

[143] K. Ratanarat, M. Nithitanakul, D. C. Martin, R. Magaraphasn. Polymer-Layered Silicate Nanocomposites: Linear PEO and Highly Branched Dendrimer for Organic Wastewater Treatment. Reviews on Advance Materials Science, 2003, Vol. 5, pp 187-192

[144] R. A. Vaia, B. B. Sauer, O. K. Tse, E. P. Giannelis. Relaxations of Confined Chains in Polymer Nanocomposites: Glass Transition Properties of Poly(ethylene oxide) Intercalated in Montmorillonite. Journal of Polymer Science: Part B: Polymer Physics, 1997, Vol. 35, pp 59-76

[145] H. J. Choi, S. G. Kim, Y. H. Hyun, M. S. Jhon. Preparation and Rheological Characteristics of Solvent Cast Poly(ethylene oxide)/Montmorillonite Nanocomposites. Macromolecules Rapid Communications, 2001, Vol. 22, pp 320-325

[146] Y. H. Hyun, S. T. Lim, H. J. Choi, M. S. Jhon. Rheology of Poly(ethylene oxide)/Organoclay Nanocomposites. Macromolecules, 2001, Vol. 34, pp 8084-8093

[147] N. Ogata, S. Kawakage, T. Oglihara. Structure and Thermal/Mechanical Properties of Poly(ethylene oxide)-Clay Mineral Blends. Polymer, 1997, Vol. 38, pp 5115-5118

[148] W. Loyens, P. Jannasch, F. H. J. Maurner. Effect of Clay Modifier and Matrix Molar Mass on the Structure and Properties of Poly(ethylene oxide)/Cloisite Nanocomposites via Melt-Compounding. Polymer, 2005, Vol. 46, pp 903-914

[149] J. Wu, M. M. Lerner. Structural, Thermal, and Electrical Characterization of Layered Nanocomposites Derived from Na-Montmorillonite and Polyethers. Chemistry of Materials, 1993, Vol. 5, pp 835-838

[150] J. Bujdak, E. Hackett, E. P. Giannelis. Effect of Layer Charge on the Intercalation of Poly(ethylene oxide) in Layered Silicates: Implications on Nanocomposite Polymer Electrolytes. Chemistry of Materials, 2000, Vol. 12, pp 2168-2174

[151] S. Wong, R. A. Vaia, E. P. Giannelis, D. B. Zax. Dynamics in a Poly(ethylene oxide)-Based Nanocomposite Polymer Electrolyte Probed by Solid State NMR. Solid State Ionics, 1996, Vol. 86-88, pp 547-557

[152] H. A. Baghdadi, H. Sardinha, S. R. Bhatia. Rheology and Gelation Kinetics in Laponite Dispersions Containing Poly(ethylene oxide). Journal of Polymer Science: Part B: Polymer Physics, 2005, Vol. 43, pp 233-240

[153] J. Zebrowski, V. Prasad, W. Zhang, L. M. Walker, D. A. Weitz. Shake-Gels: Shear-Induced Gelation of Laponite-PEO Mixtures. Colloids and Surfaces A: Physiochemical Engineering Aspects, 2003, Vol. 213, pp 189-197

[154] C. B. Arias, A. A. Zaman, J. Talton. Rheological Behaviour and Wear Abrasion Resistance of Polyethylene Oxide/Laponite Nanocomposites. Journal of Dispersion Science and Technology, 2007, Vol. 28, 247-254

[155] D. C. Pozzo, L. M. Walker. Reversible Shear Gelation of Polymer-Clay Dispersions. Colloids and Surfaces A: Physiochemical Engineering Aspects, 2004, Vol. 240, pp 187-198

[156] G. Schmidt, A. I. Nakatani, D. Butler, C. C. Han. Small-Angle Neutron Scattering from Viscoeleastic Polymer-Clay Solutions. Macromolecules, 2002, Vol. 35, pp 4725-4731

[157] Q. Zhang, L. A. Archer. Poly(ethylene oxide)/Silica Nanocomposites: Structure and Rheology. Langmuir, 2002, Vol. 18, pp 10435-10442

[158] C-S. Liao, W-B. Ye. Structure and Conductive Properties of Poly(ethylene oxide)/Layered Double Hydroxide Nanocomposite Polymer Electrolytes. Electrochemica Acta, 2004, Vol. 49, pp 4993-4998

[159] H. A. Stretz, D. R. Paul, R. Li, H. Keskkula, P. E. Cassidy. Intercalation and Exfoliation Relationships in Melt Processed Poly(styrene-co acrylonitrile)/Montmorillonite Composites. Polymer, 2005, Vol. 46, pp 2621-2637

[160] H. R. Dennis, D. L. Hunter, D. Chang, S. Kim, J. L. White, J. W. Cho, D. R. Paul. Effect of Melt Processing Conditions on the Extent of Exfoliation in Organoclay-Based Nanocomposites. Polymer, 2001, Vol. 42, pp 9513-9522

[161] Y. Liu, J. Y. Lee, L. Hong. Morphology, Crystallinity, and Electrochemical Properties of the In-Situ Formed Poly(ethylene oxide)/TiO_2 Nanocomposite Polymer Electrolyte. Journal of Applied Polymer Science, 2003, Vol. 89, pp 2815-2822

[162] S. X. Ma, S. L. Cooper. Shear Thickening in Aqueous Solutions of Hydrocarbon End Capped PEO. Macromolecules, 2001, Vol. 34, pp 3294-3301

[163] M. C. Khan. Aggregate Formation in Poly(ethylene oxide) Solutions. Journal of Applied Polymer Science, 2006, Vol. 102, pp 2578-2583

[164] M. Ortiz, D. De Kee, P. J. Carreau. Rheology of Concentrated Poly(ethylene oxide) Solutions. Journal of Rheology, 1994, Vol. 38, Part 3, pp 519-539

[165] J. Smanalieva, B. Senge. Analytical and Rheological Investigations into Selected Unifloral German Honey. European Food Research and Technology, 2009, Vol. 229, pp 107-113

[166] S. Vandresen, M. G. N. Quadri, J. A. R. de Souza, D. Hotza. Temperature Effect on the Rheological Behaviour of Carrot Juices. Journal of Food Engineering, 2009, Vol. 92, pp 269-274

[167] E. Alveraz, M. A. Cancela, N. Delgado-Bastidas, R. Maceiras. Rheological Characterization of Commercial Baby Fruit Purees. International Journal of Food Properties, 2008, Vol. 11, pp 321-329

[168] F. Febrianto, M. Yoshioka, Y. Nagai, M. Mihara, N. Shiraishi. Composites of Wood and Trans-1,4-Isoprene rubber I: Mechanical, Physical and Flow Behaviour. Journal of Wood Science, 1999, Vol. 45, pp 38-45

[169] I. A. Kinloch, S. A. Roberts, A. H. Windle. A Rheological Study of Concentrated Aqueous Nanotube Dispersions. Polymer, 2002, Vol. 43, pp 7483-7491

[170] P. J. Carreau, D. C. R. De Kee, R. P. Chhabra. Rheology of Polymeric Systems: Principles and Applications. Hanser Publishing 1997

[171] D. De Kee, P. J. Carreau. A Constitutive Equation Derived from Lodge's Network Theory. Journal of Non-Newtonian Fluid Mechanics, 1979, Vol. 6, pp 127-143

[172] A. S. Vaughan, S. G. Swingler, Y. Zhang. Polyethylene Nanodielectrics: the Influence of Nanoclays on Structure Formation and Dielectric Breakdown. IEEJ Transactions on Fundamentals and Materials, 2006, Vol. 126, pp 1057-1063

[173] P. Maiti, P. H. Nam, M. Okamoto, N. Hasegawa, A. Usuki. Influence on Crystallisation on Intercalation, Morphology and Mechanical Properties of Polypropylene/Clay Nanocomposites. Macromolecules, 2002, Vol. 35, pp 2042-2049

[174] T. G. Gopakumar, J. A. Lee, M. Kontopoulou, J. S. Parent. Influence of Clay Exfoliation on the Physical Properties of Montmorillonite/Polyethylene Composites. Polymer, 2002, Vol. 43, pp 5483-5491

[175] D. M. Lincoln, R. A. Vaia, R. Krishnamoorti. Isothermal Crystallization of Nylon-6/Montmorillonite Nanocomposites. Macromolecules, 2004, Vol. 37, pp 4554-4561

[176] X. Hu, A. J. Lesser. Non-Isothermal Crystallization of Poly(trimethylene terephthalate) (PTT)/Clay Nanocomposites. Macromolecular Chemistry and Physics, 2004, Vol. 205, pp 574-580

[177] R. Nowacki, B. Monasse, E. Piorkowska, A. Galeski, J. M. Haudin. Spherulite Nucleation in Isotacic Polypropylene Based Nanocomposites with Montmorillonite under Shear. Polymer, 2004, Vol. 45, pp 4877-4892

[178] J. K. Nicholson. The Chemistry of Polymers 2nd edition. RSC Paperbacks

[179] P. F. Bruins. Epoxy Resin Technology. Interscience Publishers

[180] C. Ramirez, M. Rico, J. Lopez, B. Montero, R. Montes. Study of an Epoxy System Cured with Different Diamines by Differential Scanning Calorimetry. Journal of Applied Polymer Science, 2007, Vol. 103, pp 1759-1768

[181] V. L. Zvetkov. Comparative DSC Kinetics of the Reaction of DGEBA with aromatic Diamines. II. Isothermal Kinetic Study of the Reaction of DGEBA with *m*-Phenylene Diamine. Polymer, 2003, Vol. 43, pp 1069-1080

[182] L. Nunez-Regueira, C. A. Gracia-Fernandez, S. Gomez-Barreiro. Use of Rheology, Dielectric Analysis and Differential Scanning Calorimetry for Gel-Time Determination of a Thermoset. Polymer, 2005, Vol. 46, pp 5979-5985

[183] K. Okada, T. Nagashima, Y. Kameshima, A. Yasumori, T. Tsukada. Relationship between Formation Conditions, Properties, and Crystallite Size of Boehmite. Journal of Colloid and Interface Science, 2002, Vol. 253, pp 308-314

[184] H- L. Wen, F- S. Yen. Growth Characteristics of Boehmite-Derived Ultrafine theta and alpha-alumina particles during phase transformation. Journal of Crystal Growth, 2000, Vol. 208, pp 696-708

[185] T. Tsukada, H. Segawa, A. Yasumori, K. Okada. Crystallinity of Boehmite and its Effect on Phase Transition Temperature of Alumina. Journal of Materials Chemistry, 1999, Vol. 9, pp 549-553

[186] Z. R. Ismagilov, R. A. Shkrabina, N. A. Koryabkina. New Technology for Production of Spherical Alumina for Fluidized Bed Combustion. Catalysis Today, 1999, Vol. 47, pp 51-71

[187] M. L. Guzman-Castillo, X. Bokhimi, , A. Toledo-Antonio, J. Salmones-Blasquez, F. Hernandez-Beltran. Effect of Boehmite Crystallte Size and Steaming on Alumina Properties. Journal of Physical Chemistry: Part B, 2001, Vol. 105, pp 2099-2106

[188] X. Bokhimi, J. A. Toledo-Antonio, M. L. Guzman-Castillo, F. Hernandez-Beltran. Relationship between Crystallite Size and Bond Lengths in Boehmite. Journal of Solid State Chemistry, 2001, Vol. 159, pp 32-40

[189] J. J. Fitzgerald, G. Piedra, S. F. Dec, M. Seger, G. E. Maciel. Dehydration Studies of a High-Surface-Area Alumina (Pseudo-Boehmite) Using Solid State ^{1}H and ^{27}Al NMR. Journal of the American Chemical Society, 1997, Vol. 119, pp 7832-7842

[190] Y. Nakazaki, M. Inoue. Computational Approach to Estimate Layer Structures of Organic Derivatives of Boehmite. Journal of Physics and Chemistry of Solids, 2004, Vol. 65, pp 429-434

[191] E. M. Moroz, K. I. Shefer, D. A. Zyuzin, A. S. Ivanova, E. V. Kulko, V. V. Goidin, V. V. Molchanov. Local Structure of Pseudoboehmites. Reaction Kinetics and Catalysis Letters, 2006, Vol. 87, No. 2, 367-375

[192] E. Tuncer, I. Sauers, D. R. James, A. R. Ellis, M. P. Paranthaman, T. Aytug, S. Sathyamurthy, K. L. More, J. Li, A. Goyal. Electrical Properties of Epoxy Based Nanocomposites. Nanotechnology, 2007, Vol. 18,

[193] H. D. Ruan, R. L. Frost, J. T. Kloprogge. Comparison of Raman Spectra in Characterizing Gibbsite, Bayerite, Diaspore and Boehmite. Journal of Raman Spectroscopy, 2001, Vol. 32, pp 745-750

[194] S. Bocchini, S. Morlat-Therias, J- L. Gardette, G. Camino. Influence of Nanodispersed Boehmite on Polypropylene Photooxidation. Polymer Stability and Degradation, 2007, Vol. 92, pp 1847-1856

[195] J. M. Alia, H. G. M. Edwards, B. M. Kiernan. Raman Spectroscopy of Benzensulfonic and 4-Toluenesulfonic Acids Dissolved in Dimethylsulfoxide. Spectrochimica Acta Part A, 2006, Vol. 60, pp 1533-1542

[196] X. Kornmann, H. Lindberg, L.A. Berglund. Synthesis of Epoxy-Clay Nanocomposites: Influence of the Nature of the Clay on Structure. Polymer, 2001, Vol. 42, pp 1303-1310

[197] B. R. Baker, R.M. Pearson. Water Content of Pseudoboehmite: A New Model for its Structure. Journal of Catalysis, 1974, Vol. 33, pp 265-278

[198] A. S. Vaughan, S. G. Swingler, Y. Zhang. Polyethylene Nanodielectrics: The Influence of Nanoclays on Structure Formation and Dielectric Breakdown. IEEJ Transactions on Fundamentals and Materials, 2006, Vol. 126, pp 1057-1063

[199] J. K. Nelson, J. C. Fothergil. Internal Charge Behaviour of Nanocomposites. Nanotechnology, 2004, Vol. 15, pp 586-595

[200] C. V. Raman. Diffraction by Molecular Clusters and the Quantum Structure of Light. Nature, 1922, Vol. 109, pp 444-445; reprinted in The Scientific Papers of C. V. Raman: The Scattering of Light (Bangalore: The Indian Academy of Sciences, 1978) pp 149-151

[201] A. Anderson. The Raman Effect. Volume 1: Principles, Marcel Dekker, Inc. 1971

[202] M. L. Myrick, S. M. Angel, R. E. Lyon, T. M. Vess. Epoxy Cure Monitoring using Fibre-Optic Raman Spectroscopy. Society for the Advancement of Materials and Process Engineering, 1992, Vol. 28, pp 37-42

[203] J. D. Anastassopoulou, M. Berjot, J. Marx, C. M. Paleos, T. Theophanides, A. J. P. Alix. Raman Spectra and Conformational Analysis of Long-Methylene-Chain-Diamine-Copper Complexes. Journal of Molecular Structure, 1997, Vol. 415, pp 225-237

[204] E- S. Lee, S- M. Lee, W. Roger Cannon, D. J. Shanefield. Improved Dispersion of Aluminium Nitride Particles in Epoxy Resin by Adsorption of Two-Layer Surfactants. Colloids and Surfaces A: Physiochemical and Engineering Aspects, 2008, Vol. 316, pp 95-103

[205] H. Ismail, S. Shuhelmy, M. R. Edyham. The Effects of a Silane Coupling Agent on Curing Characteristics and Mechanical Properties of Bamboo Fibre Filled Natural Rubber Composites. Euro[pean Polymer Journal, 2002, Vol. 38, pp 39-47

[206] E. P. Plueddemann. Silane Coupling Agents. Plenum Press, New York and London, 1982, pp 186

[207] M. J. Marmo, M. A. Mostafa. Acid-Base Interactions in a Filler-Matrix System. Industrial and Engineering Chemistry Product Research and Development, 1976, Vol. 15, pp 206-211

[208] R. S. Drago, L. B. Parr, C. S. Chamberlain. Solvent Effects and Their Relationship to the E and C Equation. Journal of the American Chemical Society, 1977, Vol. 99, pp 3203-3209

[209] C. D. Green, A. S. Vaughan, G. R. Mitchell, T. Liu. Structure Property Relationships in Polyethylene/Montmorillonite Nanodielectrics. IEEE Transactions on Dielectrics and Electrical Insulation, 2008, Vol. 15, pp 134-143